Ministry of Higher Education &
Scientific Research
Al-Nahrain University
College of Engineering

DESIGN OF EFFICIENT POINT-TO-MULTIPOINT OPTICAL NETWORK ARCHITECTURES TO SUPPORT 5G AND BEYOND SERVICES

A Thesis

Submitted to the College of Engineering of
Al-Nahrain University in Partial Fulfillment
of the Requirements for Degree of Master of Science

in
Computer Engineering

by

Ali Saadi Abed

(B.Sc. in Computer Engineering 2016)

Safar 1444

September 2022

Supervisor Certification

I certify that this thesis entitled **"Design of Efficient Point-to-Multipoint Optical Network Architectures to Support 5G and Beyond Services"** was prepared under my supervision at College of Engineering / Al-Nahrain University in partial fulfillment of the requirement for the degree of **Master of Science in Computer Engineering.**

Prof. Dr. Raad Sami Fyath

Supervisor

10 /10 / 2022

In view of the available recommendation, I forward this thesis for debate by the **Examining Committee**.

Dr. Atheel Nowfal Alkhayyat

Head of the Computer Engineering Department

13 / 10 / 2022

Committee Certificate

We certify, as an Examining Committee, that we have read this thesis entitled **"Design of Efficient Point-to-Multipoint Optical Network Architectures to Support 5G and Beyond Services"** and examined the student **" Ali Saadi Abed"** in its content and what related to it, and found it adequate for the standard of a thesis for the degree of **Master of Science in Computer Engineering.**

Prof. Dr. Abdulkareem A. Kadhim
(Chairman)
10 / 10 / 2022

Asst. Prof. Dr. Bilal R. Al-Kaseem
(Member)
10 / 10 / 2022

Dr. Israa Badr Al-Mashhadani
(Member)
10 / 10 / 2022

Prof. Dr. Raad Sami Fyath
(Supervisor and Member)
10 / 10 / 2022

Approved by the College of Engineering / Al-Nahrain University

Prof. Dr. Basim O. Hasan
Dean of the College of Engineering
13 / 10 / 2022

ABSTRACT

The fifth generation (5G) and beyond mobile networks support increasing number of users with increasing bit rate per users. This encourages researcher to proposed coherent digital subcarrier multiplexing point-to-multipoint (P2MP) architecture to reduce the cost and complexity of optical transport network, particularly in the metro aggregation scenario. However, the coherent optical receiver is more cost and far-reachable compared with direct-detection (DD) counterpart due to the use of the synchronized local laser. The main problem facing the researchers in this field is how to redesign the optical P2MP networks using low-complexity and high-flexibility artiticers. This thesis proposes the use of intensity modulation/direct-detection (IM/DD) technique to resolve the issue.

Different P2MP architectures are designed using digital RF multisubcarrier (MSC) waveform that embedded on the intensity of continuous-wave (CW) laser beside direct-detection scheme. The design covers C- and O-band operation using a single optical channel and then extended to a wavelength-division multiplexing (WDM) architecture. Further, both single- and double-polarization (SP and DP) versions are reported for each type of the networks. The DP architectures allows doubling the transmitted bit rate compared with the SP counterpart. The above architectures are built in a Optisystem environment and simulated for different network parameters. Among these parameters are number of MSC channels N_{sc}, number of WDM channels, and different M-quadrature amplitude modulation (QAM) formats. Under the assumption of 25 Gbps per subcarrier data rate. The main performance measures are maximum rout reach L_{max} and bit rate-distance product (BDP). The simulation results indicate that DD networks can replace the coherent counterpart when N_{sc} is 4. In addition to that, the O-band P2MP networks offer high values of maximum reach and BDP than the C-band counterparts.

List of Contents

Notations

Symbols		Notations
B_{mo}	=	Optical message bandwidth
B_{me}	=	Electrical message bandwidth
D	=	Group-velocity dispersion
Δf_{sc}	=	Subcarrier frequency spacing
Δf_{ch}	=	Optical channel frequency spacing
L_{DCF}	=	Length of DCF
L_{max}	=	Maximum transmission reach
L_{SMF}	=	Length of the single mode fiber
L_i	=	Length of whole route
L_s	=	Length of the common link
L_{bi}	=	Length for each subcarrier link
M	=	Order of the QAM modulation
N_{ch}	=	Number of WDM channels
N_{sc}	=	Number of subcarriers
R_b	=	Bit rate per subcarrier
R_{bt}	=	Total bit rate
R_s	=	Symbol rate
r	=	Raised-cosine roll-off factor
S	=	Dispersion slope
α_{SMF}	=	Attenuation of SMF
α_{DCF}	=	Attenuation of DCF
λ	=	Optical wavelength

Abbreviations

4G = Fourth Generation

5G = Fifth Generation

6G = Sixth Generation

ADC = Analog-to-Digital Converter

AI = Artificial Intelligence

ASK = Amplitude Shift Keying

B5G = Beyond Fifth Generation

BBU = Baseband Unit

BDP = Bit Rate-Distance Product

BER = Bit Error Rate

BER_{th} = Bit Error Rate Threshold

CD = Chromatic Dispersion

CW = Continuous-Wave

DCF = Dispersion Compensation Fiber

DEMUX = Demultiplexer

DP = Dual-Polarization

DSP = Digital Signal Processing

EDFA = Erbium-Doped Fiber Amplifier

GVD = Group-Velocity Dispersion

HD = Hard Decision

IM/DD = Intensity Modulation/Direct Detection

IoT = Internet of Things

KPI = Key Performance Indicator

LO = Local Oscillator

LSB = Lower-Sideband

MUX = Multiplexer

MZM = Mach-Zander modulator

MSC = Multisubcarrier

OA = Optical Amplifier

OLT = Optical Line Terminate

ON = Optical Network

ONT = Optical node terminate

ONU = Optical Network Unit

OSD = Optical Sideband Demultiplexer

P2MP = Point-to-Multipoint

P2P = Point-to-Point

PD = Photodiode

PON = Passive Optical Network

Q = Quadrature

QAM = Quadrature Amplitude Modulation

QPSK = Quadrature Phase Shift Keying

RF = Radio Fiber

SC = Subcarrier

SCM = Subcarrier Multiplex

SMF = Single-Mode Fiber

SP = Single-polarization

USB = Upper-Sideband

WDM = Wavelength-Division Multiplexing

List of Tables

List of Figures

CHAPTER ONE

Introduction

1.1 Motivation

Optical networks are vital for assisting the fifth generation (5G) cellular networks through presenting the connectivity to remote units, distribute units, central units, and the core network. In addition, optical networks connect broadly deployed data centers, which offer services computation and storage functions, as well as content the generation and the routing functions. The 5G represents a great evolution from the preceding generations of the cellular networks through assembly the record information needs for lots use cases under three major utilities [1]

i- Enhanced the mobile broadband, which enables the applications such as the ultra-high-definition video, three-dimensional (3D) video, cloud-based work and play, and augmented and virtual reality (AR/VR).

ii- Ultra-reliable and low-latency communications for self-driving vehicles and drones, industry automation, remote medical treatments, and other mission-critical applications.

iii- Massive machine type communications which provide applications such as smart home, smart building, smart city and internet of things (IoT).

This developing demand has led to the next-generation wireless communication technology, sixth-generation (6G) mobile technology, which anticipates offering 1 Tbps data rates [2]. Figure. 1-1 summarizes growth of the wireless access technologies with emphasis on key enabling technologies,

modulation schemes, achievable data rates, and applications throughout [3]. The applications that supported by 6G are expected to be more diverse and more far-reaching than ever, with unprecedented demand and requirements for higher data rate and ultra-low delay. The intelligent communication powered by artificial intelligence (AI) including machine-learning technologies are expected to play key roles in realizing verticals such as digital twins, holographic communications, industrial automation, remote surgery, space exploration, communication, and much more. 6G will therefore need to optimize multiple performance metrics in an increasingly complex and extremely heterogeneous network environment [4].

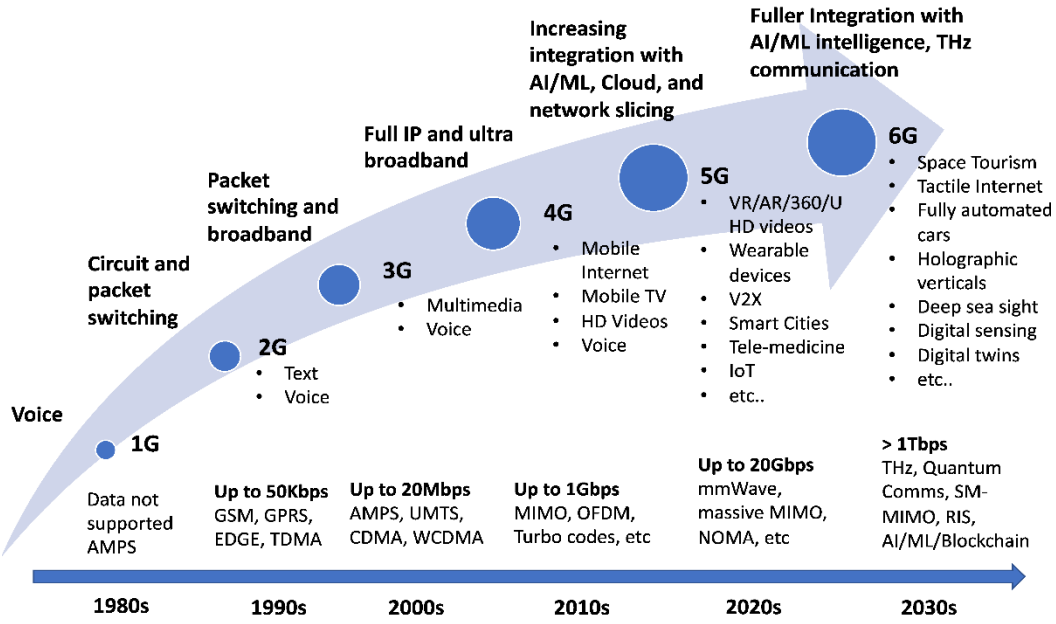

Figure 1-1: Overview of the evolution of wireless access technologies from 1G to 6G [4]. AMPS: Advance mobile phone system. GSM: Global system for mobile communications. EDGE: Enhanced data rates for GSM evolution UMTS: Universal mobile terrestrial/telecommunication system. MIMO: Multiple input multiple output. IP: Internet protocol. CDMA: Code division multiple access.

Table 1-1 suggests a contrast of 6G with the 4G and 5G communication systems. It is predicted that 6G would require a brand new key performance

indicator (KPI) drivers except the KPIs of 5G communication systems. Many KPIs of the 5G devices may be additionally legitimate for 6G. However, the 5G KPIs have to be reviewed and new KPIs have to be taken into consideration for 6G. There are numerous KPI lessons which are presently hard to outline for 6G and anticipated to be finalized through future investigations [5].

Table 1-1: Comparison of 6G with the 4G and 5G communication systems [5].

Issue	4G	5G	6G
Per Device Peak Data Rate	1 Gbps	10 Gbps	1 Tbps
End-to-end (E2E) latency	100 ms	10 ms	1 ms
Maximum Spectral Efficiency	15 bps/Hz	30 bps/Hz	100 bps/Hz
Mobility Support	Up to 350 km/hr	Up to 500 km/hr	Up to 1000 km/hr
Satellite Integration	No	No	Fully
Artificial Intelligent (AI)	No	Partial	Fully
Autonomous Vehicle	No	Partial	Fully
THz Communication	No	Very limited	Widely
Service Level	Video	VR, AR	Tactile
Architecture	MIMO	Massive MIMO	Intelligent surface
Maximum Frequency	6 GHz	90 GHz	10 THz

High speed digital subcarrier multiplex (SCM) has been proposed to support 5G and beyond services where multiple RF subcarriers are carried in single optical wavelength [6]. It is worthy to denote that the type of detection that used in the receiver side is essential. Using coherent detection technique in the user receiver side to deal with high data in point-to-multipoint (P2MP) has attracted interest in recent years [7]. The scan of literature reveals that the proposed P2MP optical networks use coherent detection scheme. P2MP optical network using intensity-modulation and direct-detection (IM/DD) technique is addressed in this thesis. The high-speed IM/DD optical systems offer the advantages of low cost, low-power

consumption, and small receiver footprint [8] and [9]. IM/DD technique (i.e., noncoherent technique) is strongly recommended for implementing these advanced interconnects over coherent techniques. The main characteristics of IM/DD technique are firstly, intensity modulation can be applied efficiently using directly modulated laser (DML) [10]. Secondly, DD needs one single-end photodiode (PD) and one analog-to-digital converter (ADC) [11]. In contrast, the coherent receiver requires complex hardware including local laser (to act as a local oscillator and should be synchronized with the transmitter laser), balanced PDs, and more than one ADC [12].

1.2 Point-to-Multipoint Optical Networks

A point-to-multipoint (P2MP) structure offers an advanced answer for the aggregation networks inclusive of 5G-Xhaul and passive optical networks (PONs). The P2MP structure replaces the numerous low-ability hub transceivers with one high-ability transceiver enabled with the aid of using virtual subcarrier multiplexing (SCM). Compared with a conventional point-to-point (P2P) structure, the P2MP structure has the benefits of flexibility, low value and low power consumption [13]. Figure 1-2 exhibits P2MP optics which lets in hub sites to leverage higher-rate ports. At the same time, the smaller intermediate nodes might also additionally use lower-rate ports. This minimizes the cost per bit transported in all node types. With P2MP transceivers, the top-quality rate port may be chosen, independent of its neighboring sites [14].

Capital expenditures (CAPEX) examination has indicate thet the extensive financial savings became accomplished over a 5-year length using P2MP pluggable optics for a reference set of metro network chains and hub-and-spoke

traffic [14]. This is true under the assumption of constant transponder costs. While the prices of the capacity planning solution using P2MP pluggable optics in evaluation with simplest P2P transponders and a combination, for exclusive relative transponder costs. The results imply that the massive CAPEX financial savings may be performed with the P2MP and hybrid solutions when the costs of P2MP transponders are as much as 50% better than P2P [8]

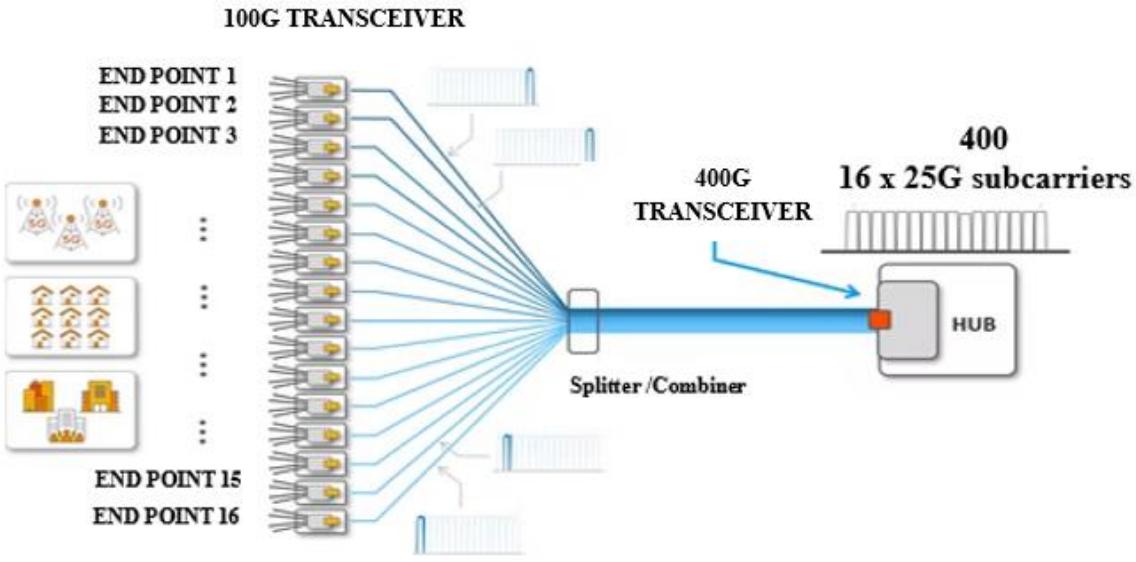

Figure 1-2: 16 Digital subcarriers enable point-to-multipoint transmission [14].

The P2MP transponders dramatically reduces the variety of gadgets, that could result in area and electricity financial savings. Since the P2MP are nonetheless now no longer commercial, a parameter α has been introduce to version their fees, various α in range [1,3] in increments of 0.5. This permits use to be research for which relative cost, deploying P2MP device will become worthwhile. Figure 1-3 displays the overall costs and variety of devices according to transponder kind for various α values for the P2MP in evaluation to P2P. According to it, the figure 1-3 suggests that as α increases, the multipoint characteristic remains worthwhile for better charge transponders however many

100G P2MP transponders are changed with the multiple decrease rate 25G P2P transponders [9].

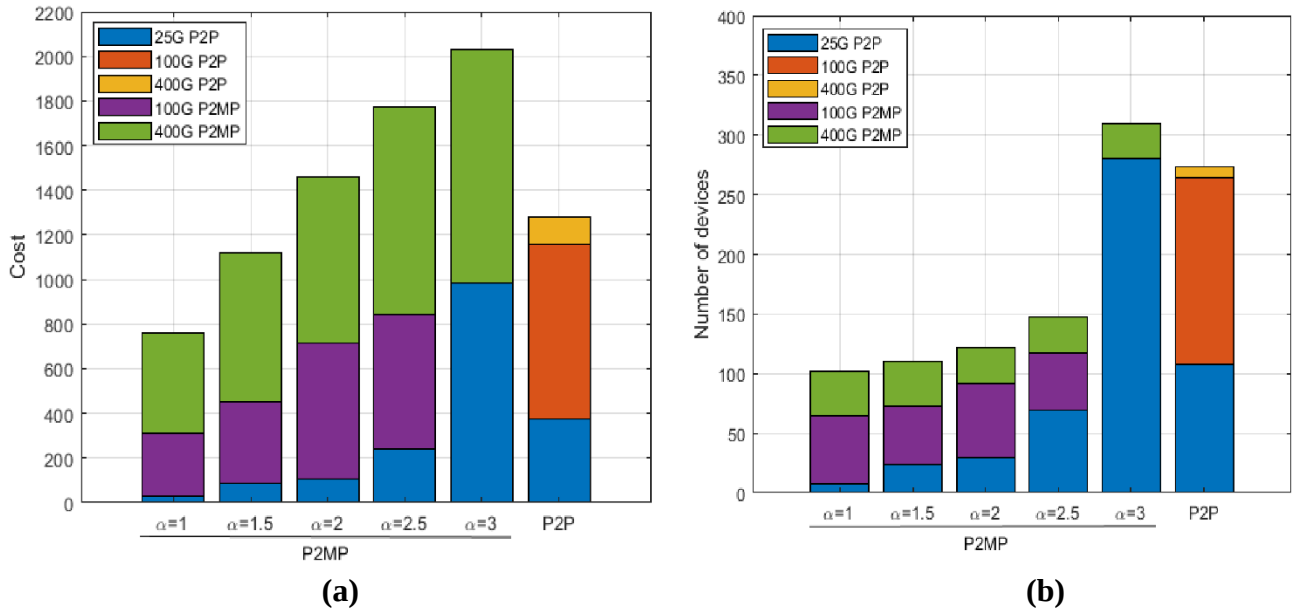

Figure 1-3: The (a) costs and (b) number of devices in the P2MP scenario (for varying α) in comparison to the P2P scenario [9].

The main limitations of P2P networks are using large number of devices, higher cost, and there is no obvious value of traffic to the end customer [15]. The main benefits of P2MP networks are the need number of devices less than P2P, lower cost than P2P, and exploit the band, thus reduce the capacity per byte. However, the P2MP suffer from various issues such as [15]

i. The aggregation function is removed when aggregation devices are taken out of the network. Routers are feature-rich devices and the operators use them for a variety of functions

ii. Reliability, decreasing the number of pluggable optics in the hub sites will enhance the network uptime, operators need to ensure that the effect of a failure is contained. Compared to P2P, a P2MP hub optic failure will take

down more traffic and affect connectivity to various nodes; this can be addressed by using protection or restoration.

iii. Light paths from a single hub to numerous edge transceivers may include a wide range of losses, necessitating power balancing so that the SCs arrive at the hub with nearly the same power. The envision that the edge P2MP optics will have a wide-range adjustable transmit output power and that a power control loop between the hub and each edge transceiver will be used to equalize the SC powers.

Figure 1-4 (a) illustrates a common and simplified metro/access network architecture, where the transceivers of N endpoints (leaves) (5G antennas, curb aggregation boxes, etc.) communicate with those at the electrical aggregation stage [16]. N low-data rate transceivers are needed on each side, i.e., $N \times 2$ transceivers, plus 2 additional high-speed ones. Figure 1-4 (b) shows the impact of implementing the proposed P2MP architecture in the same typical metro aggregation network of Figure 1-4 (a). Here, the electrical aggregation stage of Figure 1-4 (a) has been replaced by a simple 1 : N passive optical combiner. The number of devices and stages needed to be aggregated and the traffic speed that transported to the next hub is greatly reduced [16].

1.3 Techniques Supporting P2MP Optical Networks

This section summarizes the main techniques which supporting the operating of P2MP optical networks as related to the mobile access services.

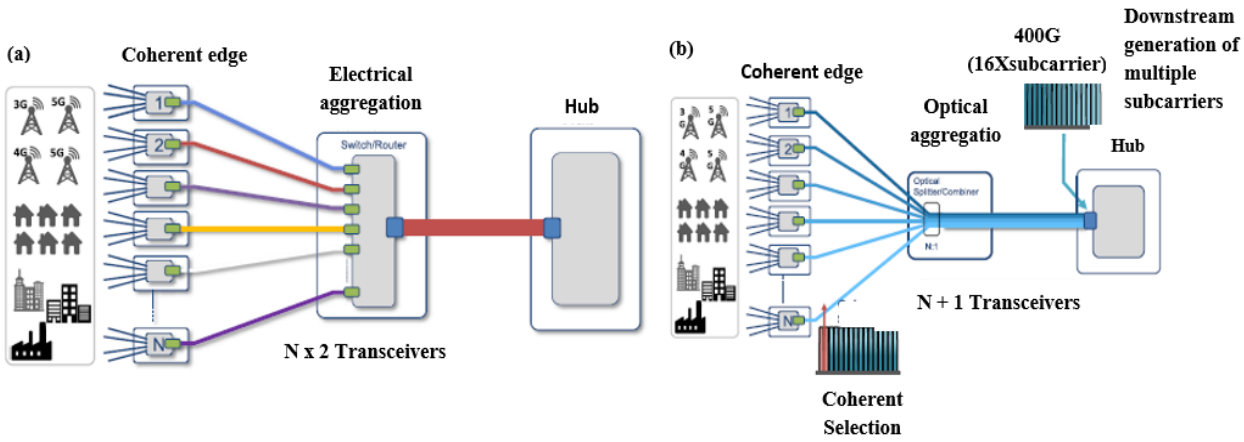

Figure 1-4: (a) P2P (b) P2MP Architectures [16].

1.3.1 Subcarrier Multiplexing

Digital subcarrier multiplexing (SCM) support both P2MP and P2P applications. In a P2MP application, digital SCM facilitates savings by the eliminating intermediate aggregation routers/switches and associated transceivers that are otherwise required to multiplex P2P links. furthermore, digital subcarriers do not compromise the reach of the transceiver, rather they enable the optimized network utilization by selectively adapting/loading those parts of the spectrum that can transmit more capacity or are subjected to strong filter penalties [17]. A subcarrier-multiplexed radio over fiber (ROF) system using optical modulation has been proposed in the literature [18]. SCM is a technique that used to transmit multiple radio frequency (RF) signals through the same optical fiber to exploit its large bandwidth. This technique is very relevant in the emerging 5G standards which require accesses of multiple standards simultaneously (5G, LTE, and Wi-Fi). In SCM, the multiple microwave carriers which are well divided in frequency are used for transmitting data. Each such channel is capable of carrying data of multiple applications at different rates. These RF subcarriers are joint together and

modulated on to an optical carrier which is spread through optical fiber, as shown in Fig. 1-5 [18].

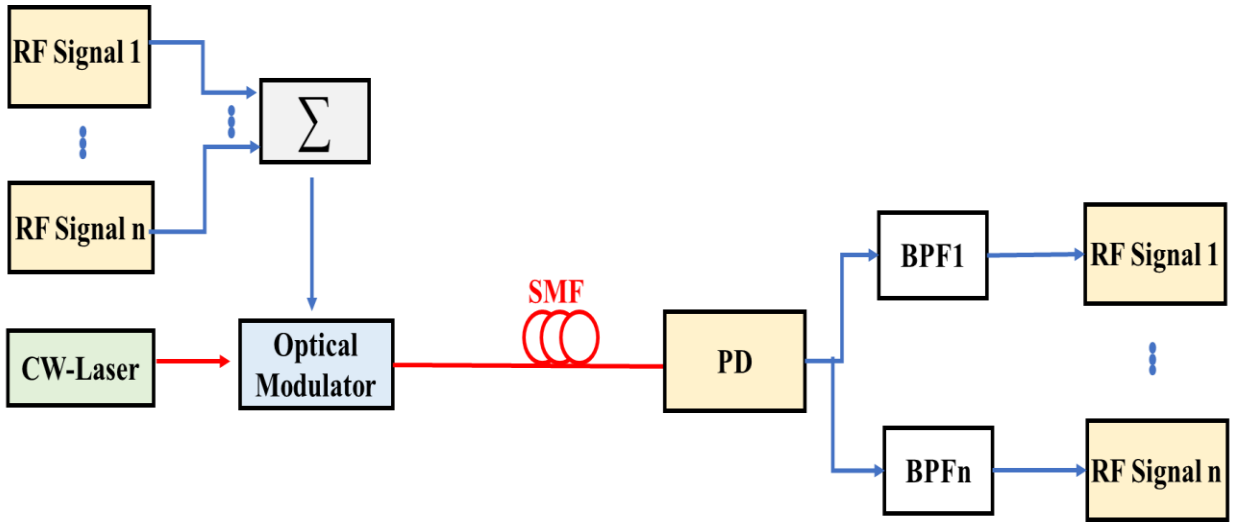

Figure. 1-5: RF subcarrier multiplexing based optical network. PD: Photodiode. BPF: Bandpass filter [18].

1.3.2 Wavelength-Division Multiplexing

Wavelength-division multiplexing (WDM) has an important role in the development of the optical communications. WDM has gave the flexibility to the network and easy to work with the network design. It helps the improvement of the network capacity by transferring many wavelengths over a single fiber [19]. An elementary WDM RoF system is shown in Fig. 1-6 [19]. The electrical data that received from an individual sensor is fed into the transmitter (present at the central station), which consists of an RF modulator, a continuous-wave (CW) laser, and Mach-Zehnder modulator (MZM). After that, it is fed to the multiplexer; similarly, all transmitters feed $\lambda_1 \ldots \lambda_N$ into the multiplexer. The multiplexer then gathered all wavelengths and at forward it on the optical fiber to the demultiplexer. The demultiplexer spreads all the wavelengths and passes them to the receiver

base station (BS). The BS consists of a photodiode and a filter. The signal is then spread through an antenna to other mobile stations [19].

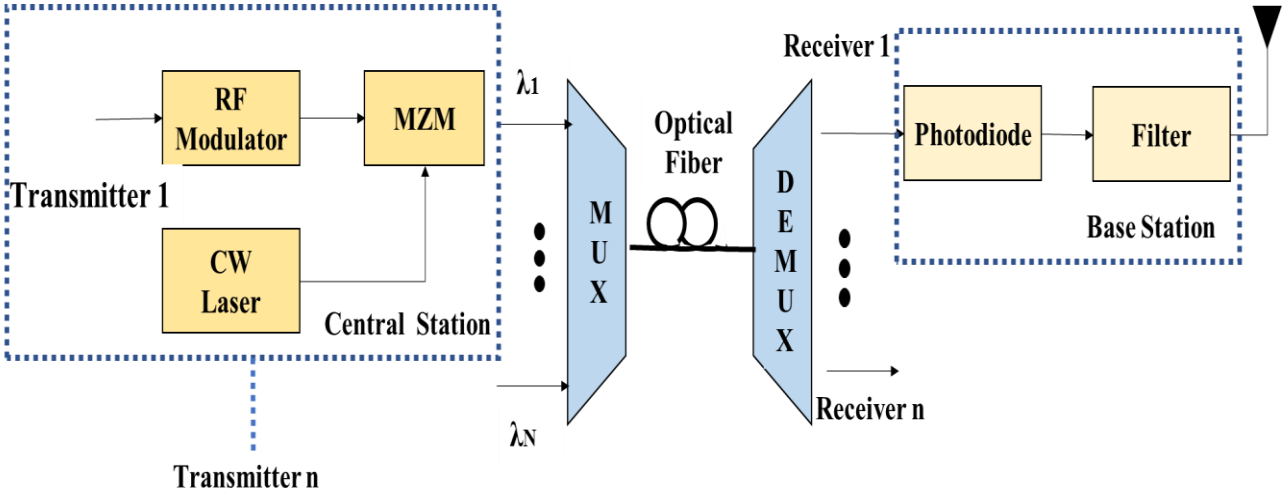

Figure 1-6: Wavelength Division Multiplexing configuration [19].
N: Number of multiplexed optical channels

1.3.3 Radio-over-Fiber

ROF grown over the last three decades with the original focus on backhaul transport to current focus of mobile fronthaul. Despite the large available bandwidth, the high spread losses of millimeter (mm) wave wireless signals limit the wireless signals transmission distance. With the introduction of RoF technology, it possible to extend the reach of the mm- wave wireless signals to service areas, that would not possibly base on free-space transmission. Optical fiber organization with its inherent characteristics of low loss, high bandwidth, and immunity to electromagnetic interference is able to deliver the much-needed capacity to distribute these ultrabroadband mm-wave wireless signals. Furthermore, the single configuration of RoF architecture as shown in Fig. 1-7 enables centralized-control implementation that favors the optical generation and distribution of mm-wave wireless signals[20].

The main advantages of ROF are [21]

i- Supporting very high-frequency wireless signals transport.

ii- Providing a large bandwidth medium for the transport of high wireless signals

iii- Extending the propagation distance of high-frequency wireless signal.

While, the main drawbacks of ROF are [22]

i- Severely impacted by the nonlinearity of the optical stage.

ii- Effected by Fiber chromatic dispersion.

iii- Low conversion efficiency between the optical and the RF domain.

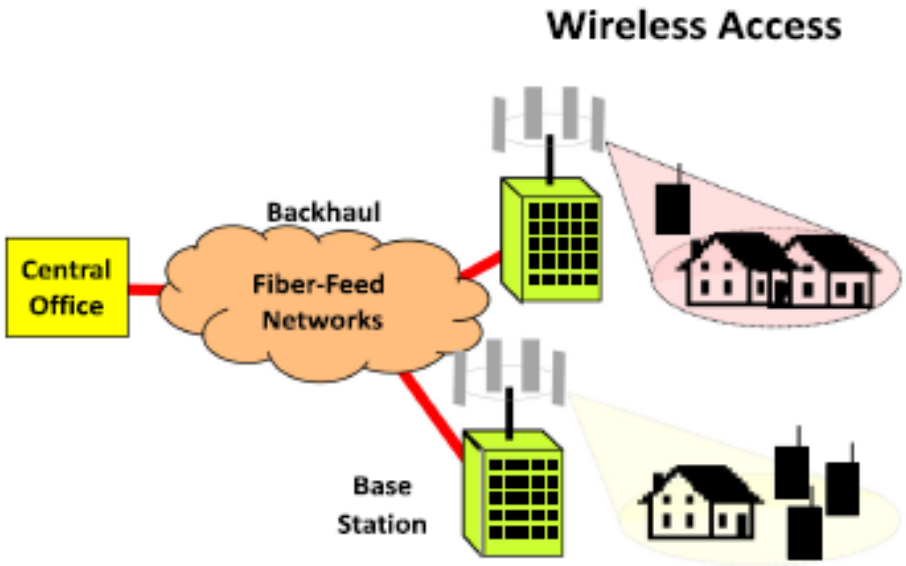

Figure. 1-7: Generic radio-over-fiber style [20].

1.4 Literature Survey

In 2017, Krause et al. [24] demonstrated the idea of digital MSC coherent optical modulation to compensate large dispersion and at the same time mitigation Kerr nonlinearity effect. The advantages of MSC with different modulation

formats is to achieve efficient spectral. The system used 4 SCs with different modulation format (QPSK, 8-QAM, and 16-QAM) by using coherent detection scheme over fiber length 8700 km.

In 2020, Ren et al. [13] proposed power optimization for P2MP structure based on coherent multi-subcarrier technique. The results reveal that 2-3 dB power was gained experimentally with 8 SCs and 4G baud in each , 16-QAM, 4GHz band in each SC and transmission link of 24 km.

In 2020, Zhang et al. [25] proposed rate-flexible single-wavelength for 100 GHz time- and frequency-division multiplexing QPSK coherent PON architecture based on digital subcarrier multiplexing technology. The architecture implementation with 4 SCs is demonstrated, reaching -38 dB sensitivity after 50 km fiber transmission.

In 2021, Neves et al. [26] demonstrated that it is possible to overcome the laser phase noise and nonlinear phase noise in SCM technique by using dual- stage join processing. This process is combined of two steps: the pilot-based carrier-phase estimation and the blind phase search. The results showed that this would improve the performance of symbol rate per SC. Also, signal-to-noise ratio gain of about 1 dB was achieved. Though join SC carrier phase estimation processing in a shorter reach link, the results illustrate that gain would reduce by 0.5 dB after 3000 km transmission link

In 2021, Welch et al. [16] introduced and demonstrated the architecture of P2MP optical networks using coherent digital MSC technique. Performance comparison with the P2P approach was performed. The results indicated that proposed approach offers significant evolution of traffic from endpoint-to-

endpoint to current hub-and-spoke patterns, at least in the parts of the network experiencing the fastest growth. Experimental results revealed that when the hub is equipped with a 400G P2MP transceiver operated in multiples of 25G, it was capable of transmitting up to 16 SCs each with 4 GHz bandwidth employing 16-QAM modulation. An EDFA was used to compensate the loss of the 25 km SMF.

In 2022, Fan et al. [8] proposed low cost P2MP coherent architecture by using PAM 4 modulator with 2 SCs, and 10 Gbps bit rate for each subcarrier with 10 km transmission distance.

In 2022, Napoli et al. [27] proposed a model that combining P2MP coherent architecture with reconfigurable optical add/drop multiplexer (ROADM)/filterless line using 16-QAM 25 Gbps and 100 Gbps for 16 SCs and 4 SCs, respectively with transmission distance 25 km.

In 2022, Zhou et al. [29] demonstrated the multipoint to point network by using 16-QAM, 3 SCs, 4.29 Gbps bit rate for each subcarrier with transmission distance of 25 km.

Table 1-2 lists the key parameters of the preceding literature survey. It is clear that all the work was related to coherent-detection scheme for both P2P and P2MP architectures. The used modulation formats are limited to QPSK, PAM-4, and 16-QAM to support P2MP architecture. According to this, the aim of this thesis is to propose a new system that use direct detection scheme for MSC-P2MP optical networks to reduce the complexity of the SC optical receiver serving the end user. Further, higher order QAM modulation formats (such as 64- and 128-QAM) are used to increase the spectral efficiency.

Table 1-2: Main parameters of the scanned literature survey. The results have been reported for coherent-detection single-optical channel networks.

Reference	Polarization	Modulation format	Bit rate per subcarrier (Gbps)	Number of subcarriers	Distance (km)
Krause et al. [24] 2017	SP	Q-PSK 8-QAM 16-QAM	2.7	4	8700
Ren et al. [14] 2020	SP	16-QAM	16	8	24
Zhang et al. [25] 2020	DP	Q-PSK	25	4	50
Neves et al. [26] 2021	SP	16-QAM	48 24 12 8	2 4 8 12	400 300 200 100
Welch et al. [16] 2021	SP	16-QAM	25	16	25
Fan et al. [8] 2022	SP	PAM 4	16	2	10
Napoli et al. [27] 2022	SP	16-QAM	25	4	35
Zhou et al. [28] 2022	SP	16-QAM	4.3	3	29

1.5 Aim of Thesis

The aim of this thesis is to propose and investigate the performance of low cost, flexible, and scalable point-to-multipoint (P2MP) optical networks to support 5G and beyond mobile services. The aim may be achieved through the following steps

i- Design of intensity-modulation/direct-detection (IM/DD) P2MP optical networks incorporating digital RF subcarrier multiplexing technique. This is useful to replace the relatively cost coherent-detection counterparts proposed in the literature where each user receiver has a local laser synchronized with the transmitter laser.

ii- Enhancing the capacity of the designed IM/DD P2MP networks by incorporating both polarization-division multiplexing and wavelength-division multiplexing techniques.

iii- The design reported in steps i and ii should cover both C- and O-band operation.

iv- Addressing the transmission performance of the designed P2MP networks as a function of number of WDM channels, number of RF subcarriers per optical channel, and the order of modulation formats.

1.6 Thesis Outline

The work in the thesis is presented in five chapters including the introduction chapter (Chapter one). Chapter two gives the related theoretical background for P2P and P2MP network with a brief description of PON. Chapter three introduced, the proposed design issues for P2P and P2MP networks supporting 5G and beyond 5G (B5G) services. Simulations results of the designed P2P and P2MP networks are reported in Chapter four. Chapter five gives a summary of the main conclusions drawn from this study with suggestions for future work.

CHAPTER TWO

Theoretical Background for P2P and P2MP Optical Networks

2.1 Introduction

The basic concepts of P2P and P2MP networks are described in this chapter along with the passive optical network (PON) that presented with its architecture. Further, WDM is inserted in each design (P2P, P2MP, and PON) to support high capacity. In addition, the intensity modulation/direct detection (IM/DD) is illustrated in this chapter for the receiver detection.

2.2 Basic Concepts of P2P Optical Network

This section introduces the main concepts of a single-optical channel P2P networks incorporating optical fiber transmission links. The data is transferred completely from the transmitter side to the receiver side which uses a single-optical receive to recover the data. Figure 2.1 shows a simplified block diagram of a P2P fiber network that consists mainly of an optical transmitter, a transmission link, and optical receiver. The network operates at either around 1550 nm (C band) or around 1310 nm (O band) [29].

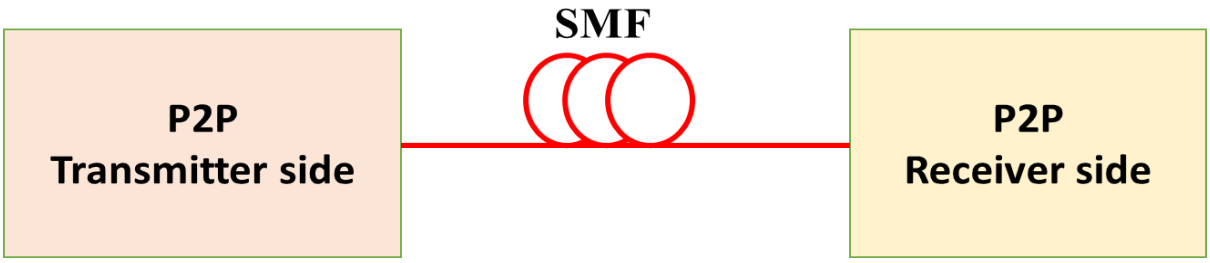

Figure 2-1: P2P optical network.

2.2.1 Transmitter Side

The optical transmitter uses a single-mode semiconductor laser which operating in continuous-wave (CW) mode after driving it with a constant bias current that is greater than its threshold current. The laser emits an optical waveform which acting as an optical carrier from communication point of view. The optical carrier has a time-varying electric field whose one or more of its parameters (mainly amplitude and phase) is (are) varied according to the analog or digital input data [30].

For a noiseless semiconductor laser, the emitted electric field $e_c(t)$ in CW operation can expressed as [31]

$$e_c(\mathrm{t}) = E_c \cos(\omega_c \mathrm{t} + \theta_c) \qquad (2.1)$$

where E_C, ω_C, and θ_c are the amplitude, radial frequency, and phase of the electric field, respectively. Note that $e_c(\mathrm{t})$ presents the unmodulated optical carrier whose parameter E_C, ω_C, and θ_c are constant independent of time. Further, $\omega_c = 2\pi f_c = 2\pi c/\lambda_c$ where f_c is the frequency measured in Hertz (H_Z), λ_c is the wavelength, and $c = 3 \times 10^8\, m/s$ is the speed of light in free space. The optical power intensity of the field I_{int} (measured in W/μm^2) is proportional to $|E_c|^2$.

The optical modulator embedded the input data on the amplitude and/or phase of the electric field. The electric field of the modulated optical carrier is expressed generally as [32]

$$e_{cm}(\mathrm{t}) = E_m \cos(\omega_c \mathrm{t} + \theta_m(\mathrm{t})) \qquad (2.2)$$

where the subscript m denotes the parameter of the modulated optical carrier and the initial phase θ_c is set to zero.

In the analog modulation, the intensity $I_{int}(t)$ of modulated optical carrier, which is proportional to $|E_m(t)|^2$, is usually varied with the modulating (information) signal x(t). Thus, the optical power of the modulated output can be expressed as [31]

$$P(t) = [1 + m_i\, x(t)]\, P_c \qquad (2.3)$$

where P_c is the power of the CW laser, m_i is the modulation index, and $x(t)$ with $|x(t)| \leq 1$ is the analog information signal. On the other hand, for the digital optical modulation, the input data is expressed as a sequence of binary bits (**logic 0** and **logic 1**). The input data is grouped to m-bit blocks (i.e., m-bit subsequence). This yields $M=2^m$ symbols (states) according to the various arrangement of **0** 's and **1**'s in the subsequence. This leads to M-ary digital modulation which is generally classified as follow [33]

i. M-ASK

In M-ary amplitude shift keying (M-ASK), the phase of the electric field of the modulated optical carrier is kept constant while its amplitude takes one of M-discrete value according to the symbol state.

ii. M-PSK

In M-ary phase shift keying (M-PSK), the electric field amplitude of the modulated optical carrier is kept constant while its phase takes M-discrete values according to the modulating state. The phase differences between succussing state equals to 360°/M.

iii. M-QAM

In M-ary quadrature amplitude modulation (M-QAM), both the amplitude and the phase of the carrier electrical field are varied with the modulating state. The M states are presented by M pairs of discrete field amplitudes and phases. The electric field corresponding to the i^{th} modulating state can be expressed, according to equ. 2.2 by equ. 2.4

$$e_{cmi}(t) = E_{mi}\cos(\omega t + \theta_{mi}) \quad (2.4)$$

where the amplitude and the phase are fixed for each state.

It is worth to mention here that equ. 2.4 can be rewritten in the following form

$$e_{cm}(t) = i(t)\cos\omega_c t + q(t)\sin\omega_c t \quad (2.5a)$$

where

$$i(t) = E_m(t)\cos[\theta_m(t)] \quad (2.5b)$$

$$q(t) = E_m(t)\sin[\theta_m(t)] \quad (2.5c)$$

Note that equ.2.5a indicates that the QAM signal consists of two ASK signals, one uses the in-phase (I) carrier component, $\cos\ \omega_c t$, and the other use quadrature (Q) carrier component, $\sin\omega_c t$. The QAM signal is usually generated as the sum of I-ASK and Q-ASK signals, using IQ optical modulator [32].

Figure 2.2 shows the constellation diagrams corresponding to the binary PSK (BPSK), quadrature PSK (QPSK), 16-QAM, and 64-QAM signaling. Each signal state is presented by a point in the I-Q plane. The vector from the origin to the point of the i^{th} state has E_{mi} length and θ_{mi} angle. In M-ary signaling, the number of i^{th} symbol bits carried by each symbol is equal to $\log_2 M$. Thus, the

symbol carries 1, 2, 4, and 6 bits in BPSK, QPSK, 16-QAM, and 64-QAM, respectively.

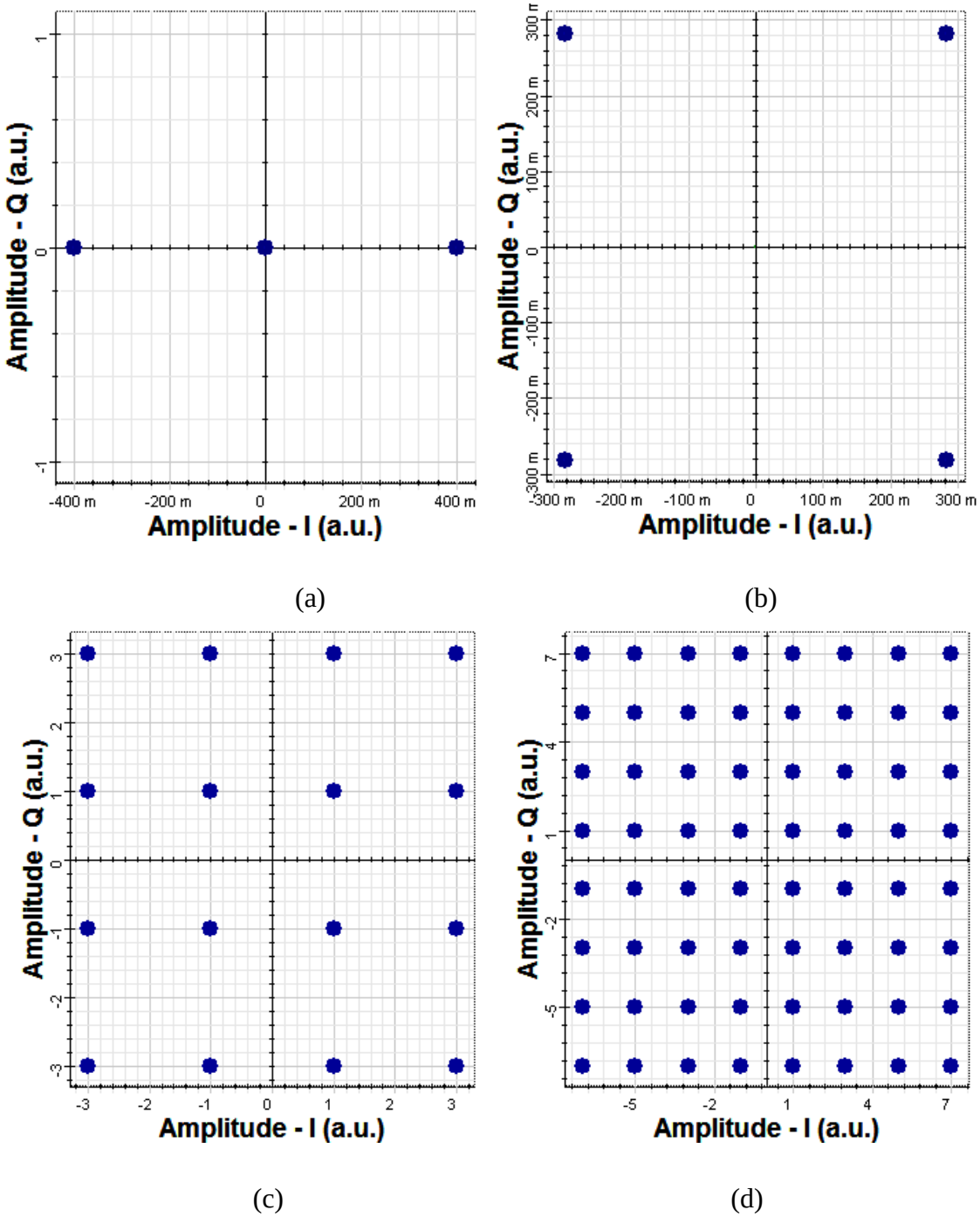

Figure. 2-2: Constellation diagrams of (a) BPSK. (b) QPSK. (c) 16-QAM. (d) 64-QAM.

2.2.2 Transmission link

The transmission link consists of a single or multispan of a single-mode fiber (SMF) with an optical amplifier is inserted at the end of each span to compensate the span loss. The propagation of optical pulses along the SMF is affected mainly by fiber linear mechanisms (attenuation and dispersion) and fiber nonlinear mechanisms which essentially arise from the defense of the fiber core refractive index on the intensity of the optical signal intensity. The modulate optical pulse contains frequency spectrum around the optical carrier frequency. The propagation of each optical frequency component ω along the fiber can be described by [34]

$$e(t,z) = E_0\, e^{-(\alpha/2)}\cos(\omega t + \beta z) \qquad (2.6)$$

where the fiber is assumed to be extended on the z axis. In equ. 2.6, $e(t,z)$ is the electric field at adistance z, E_0 is the field amplitude at z = 0 (transmitter side), $(\alpha/2)$ is the field amplitude attenuation coefficient (i.e., α is the power attenuation coefficient (dB/km)), and β is the propagation constant which is a function of signal frequency ω and optical intensity inside the fiber I_{int}.

The fiber loss is usually measured in dB/km and it is equal to (4.34α) where α in k_m^{-1} [29]. The propagation constant β depends on a fiber core refractive index n which is a function of ω and I_{int} (i.e., Kerr effect) [34,35] .

$$n(\omega, I_{int}) = n_0(\omega) + n_2(\omega_c) I_{int} \qquad (2.7)$$

where $n_0(\omega)$ is fiber core refractive index at low intensity (background refractive index) and n_2 is the nonlinear refractive index coefficient. Equation 2.7 indicates that the frequency components of the modulation optical pulse is travel at different

phase velocities $v(\omega) = c/n(\omega)$. Further, Equ. 2.7 assumes that $n_2(\omega_c)$ is a frequency independent across the spectrum of the optical pulses. This assumption is valid since optical pulse is used as symbol in communication system whose spectrum is usually much narrow then the optical carrier frequency ω_c. According to Equ.2.7, the propagation constant β becoming frequency and intensity dependence [35]

$$\beta(\omega, I_{int}) = \frac{2\pi n(\omega, I_{int})}{\lambda} = \frac{n(\omega, I_{int})\omega}{c} \tag{2.8}$$

where λ is the signal wavelength (λ = c/f = 2πc/ω). Equ. 2.8 can be written as sum of linear part β_l and nonlinear part β_{nl}

$$\beta(\omega) = \beta_l(\omega) + \beta_{nl}(\omega_c) \tag{2.9a}$$

where

$$\beta_l(\omega) = \frac{n(\omega)\omega}{c} \tag{2.9b}$$

$$\beta_{nl}(\omega_c) = \frac{n_2 I_{int}\omega_c}{c} \tag{2.9c}$$

It is useful to expand $\beta_l(\omega)$ in a Taylor sereies around the carrier frequency ω_c [34]

$$\beta_l(\omega) = \beta_0 + (\omega - \omega_c)\beta_1 + \frac{1}{2}(\omega - \omega_c)^2\beta_2 + \frac{1}{6}(\omega - \omega_c)^3\beta_3 + \cdots \tag{2.10a}$$

where $\beta_0 \equiv \beta_l(\omega_c)$ and

$$\beta_m = \left(\frac{d^m\beta_l}{d\omega^m}\right)_{\omega=\omega_c} \tag{2.10b}$$

Different spectral components of the modulated optical pulses travel at different velocities through the fiber leading to pulse boarding in the time domain

(i.e., dispersion). A specific spectral component of an angular frequency ω will arrive at the fiber end of length L after a time delay τ_g, known as group delay, [29]

$$\tau_g = \frac{L}{v_g} = L\frac{d\beta_L}{d\omega} = -L\frac{\lambda^2}{2\pi c}\frac{d\beta_L}{d\lambda} \tag{2.11}$$

where $v_g = (\frac{d\beta}{d\omega})^{-1} = \beta_1^{-1}$ is the group velocity, the speed at which the energy of the optical pulses travel. The optical pulses disperse after travelling a certain distance due to the differences in the time delay caronym the pulse spectrum. The pulse broadening is characterized by

$$\Delta\tau_g = \frac{d\tau_g}{d\omega}\Delta\omega = \frac{d\tau_g}{d\lambda}\Delta\lambda = LD\,\Delta\lambda \tag{2.12}$$

where $\Delta\lambda$ and $\Delta\omega$ represents the wavelength bandwidth and the frequency bandwidth, respectively, both of the optical pulses. Further, *D* (measured in ps/(nm.km)) represent the group velocity dispersion (GVD)

$$D = \frac{-2\pi c}{\lambda^2}\beta_2 \tag{2.13}$$

Higher-order dispersion effect still exists when operating at zero-GVD wavelength (i.e., *D* = 0) and then effect is grouped by the dispersion slop S [34]

$$S = \frac{dD}{d\lambda} = \frac{4\pi c}{\lambda^3}\beta_2 + \frac{2\pi c}{\lambda^2}\beta_3 \tag{2.14}$$

The dispersion slop parameter is also useful in WDM system which enables the system to predict *D* at different channel wavelengths if the GVD and S are know at a reference wavelength.

The standard SMF (SSMF) is characterized by ≈ 17 ps/(nm.km) GVD and ≈ 0.2 dB/km loss in C band (around 1550 nm). The values of their two parameters

are changes to $D \approx$ zero and $\alpha \approx 0.35$ dB/km when the system operates in O band (around 1310 nm). The 1550 nm and 1310 nm represent, respectively, the minimum-loss wavelength and zero GVD-wavelength of the SSMF [30].

2.2.3 Optical Receiver

The receiver used in optical networks can be classified into direct detection and coherent detection schemes as shown in Fig. 2.3. Generally, the first stage of the optical receiver is a photodiode(s)-based optical-to-electrical (OEC) convertor which yields a photocurrent proportional to the power of the received optical signal. The generated photocurrent is amplified using a low-noise electrical amplifier before applying it to the electrical receiver that is used to extract data and according to this, it was designed the modulation format that used in the transmission side [29]. In digital modulation, digital signal processing (DSP) may be used at the receiver side to perform different operation, based on the generated photocurrent such as carrier recovery, symbol rate recovery, and GVD compensation [36].

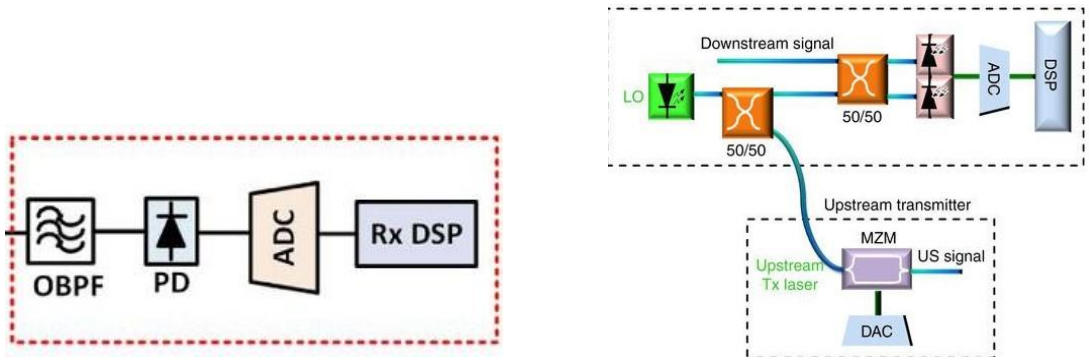

(a) Direct detection (b) Coherent detection.

Figure 2-3: Receiver optical networks [33].

For intensity modulation (IM)/direct-detection (DD) optical receiver, the EOC uses only a single photodiode (PD) to produce a photocurrent $i_{ph}(t)$ proportional to the received optical signal $P_s(t)$ [32]

$$i_{ph}(t) = \mathcal{R}P_s(t) \tag{2.15a}$$

$$\mathcal{R} = \eta_{PD}q/hf_s \tag{2.15b}$$

where $\mathcal{R}$ measured in A/W and denotes PD resposivety, η_{PD} is the PD quantum efficient, q is the electron charge, h is the Planck's constant, and f_s is the optical (carrier signal) frequency. Note that hf_s is the energy of the received signal photon.

When digital optical modulation is used such as ASK, PSK, and QAM, the data is digitally embedded on the optical carrier the coherent optical receiver is generally used to extract the data. This receiver uses coherent detection where the EOC has a local CW-laser to act as an optical local oscillate (LO) [33]. The electric field of the received signal $e_s(t)$ is summed with the electric field of the LO $e_{LO}(t)$ and the resultant field is then applied to a pair of balanced PDs to generate photocurrent. A coherent detection requires a polarization-control process for making the state of the polarization (SOP) of the LO field that should matches the received signal [31]. In addition, coherent detection has classified into two categories, heterodyne and homodyne detection [29,33]. In heterodyne detection, the frequency of LO field ω_{LO} should be traced the transmitter CW laser frequency ω_s where the different between them $\omega_{IF} = |\omega_s - \omega_{LO}|$ is kept constant during the operation. In this case the photocurrent contains the modulation spectrum centred around the intermediate frequency (IF). Therefore, an additional detection process (called demodulation) is required to down the frequency and convert the

spectrum from the IF to baseband before extractors the data. In contrast, homodyne detection operators with $\omega_{IF} = 0$ requires perfect frequency matching between the LO field and the transmitter CW-laser field. Here, the photocurrent contains the spectrum of the modulation signal directly in the baseband.

The mixing of the received signal field with the local oscillator field can improve the receiver performance. To illustrate this, the optical signal field and LO field are expressed, respectively, as [37]

$$e_s(t) = E_s \cos(\omega_s + \theta_s) \tag{2.16}$$

$$e_{LO}(t) = E_{LO} \cos(\omega_{LO}(t) + \theta_{LO}) \tag{2.17}$$

where E_{LO}, ω_{LO}, and θ_{LO} represent the amplitude, frequency, and phase of the local oscillator, respectively. Assuming that the two fields are identically polarized and incident at the photodetector, the photocurrent is given by [36]

$$P = \mathcal{R}/(e_s + e_{LO})^2 \tag{2.18a}$$

$$P(t) = P_s + P_{LO} + 2\sqrt{P_s P_{LO}} \cos(\omega_{IF} + \theta_S - \theta_{LO}) \tag{2.18b}$$

$$P_s = \frac{\mathcal{R} e_s}{P_{LO}} = \mathcal{R} E_{LO}^2 \tag{2.18c}$$

From equ. 2.17, the photocurrent is given by [37]

$$I(t) = \mathcal{R}(P_s + P_{LO}) + 2\mathcal{R}\sqrt{P_s P_{LO}} \cos(\omega_{IF} + \theta_s - \theta_{LO}) \tag{2.21}$$

Typically, $P_{LO} \gg P_s, and\ P_s + P_{LO} \approx P_{LO}$

The last term contains the information that transmitted and is used by the decision circuit. In homodyne detection technique, the LO frequency ω_{LO} is select to coincide with the signal-carrier frequency ω_s so that $\omega_{IF} = 0$

Consider the case in which the LO phase is locked to the signal phase so that $\theta_s = \theta_{LO}$. The homodyne signal is then given by

$$I_{ph}(\mathrm{t}) = 2\mathcal{R}\sqrt{P_s P_{LO}} \tag{2.22}$$

2.3 Optical Network Architectures Supporting Multiuser Services

This section presents brief description of multiuser-optical network architectures which used mainly to distribute mobile service and based on the fiber networking or hybrid fiber-wireless networking.

2.3.1 Passive Optical Network

The passive optical network (PON) is based on passive fiber infrastructure to support fiber-to-home services [38]. The network does not use active devices such as routers and switches for service distributing to the users. Figure 2-3 shows a schematic of PON where the data of the optical line terminal (OLT) located at the central office is transferred to a passive 1: N optical splitter via a SMF. Each one of N splitter outputs services one optical node terminal (ONT), i.e., one user end. The fiber splitter is compact, inexpensive and requires no DC voltage source [39]. Unfortunately, the splitter introduces an insertion loss equal to 10logN. For N = 8 and 16, the insertion loss of the splitter is 9 and 12 dB, respectively. Note that in

the PON that shown in Fig 2-4, all the users get the same data and share the same main SMF section.

Fiber splitting may be arranged in multiple stages to optimize the transmission plant when ONTs are clustered in several separate area [40]. Figure 2-5 illustrates the two-stage fiber split configuration that serving 16 ONT in four clusters.

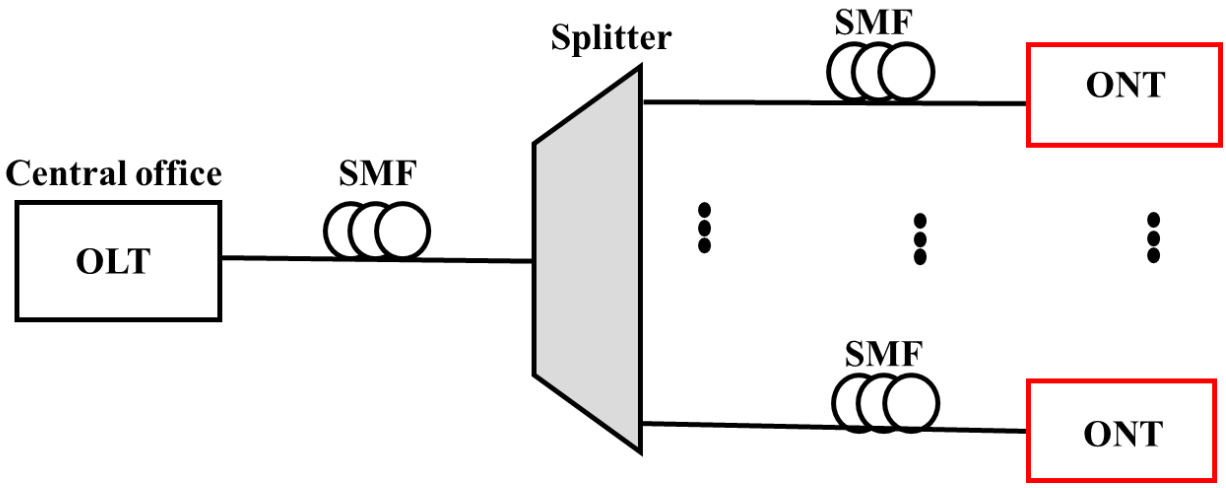

Figur 2-4: Basic structure for passive optical network (PON).

2.3.2 Wave Division Multiplexing-Passive Optical Network

Wavelength-division multiplexing (WDM) technique may support the operation of PONs. In this case the OLT guard a WDM optical signal by embedded different data source in different optical carriers (lasers). Each optical carrier has its own wavelength and carries one data source. A WDM demultiplexer (spectrally selective device) is used to replace the optical splitter used in conventional PON as illustrated in Fig. 2.6. Each output port of the demultiplexer is corresponds to

one which used wavelengths (channels) and forward it to the ONT. Note that each ONT has assigned separated wavelength. The WAM-PON may use either, direct-detection [41] or coherent-detection schemes [42].

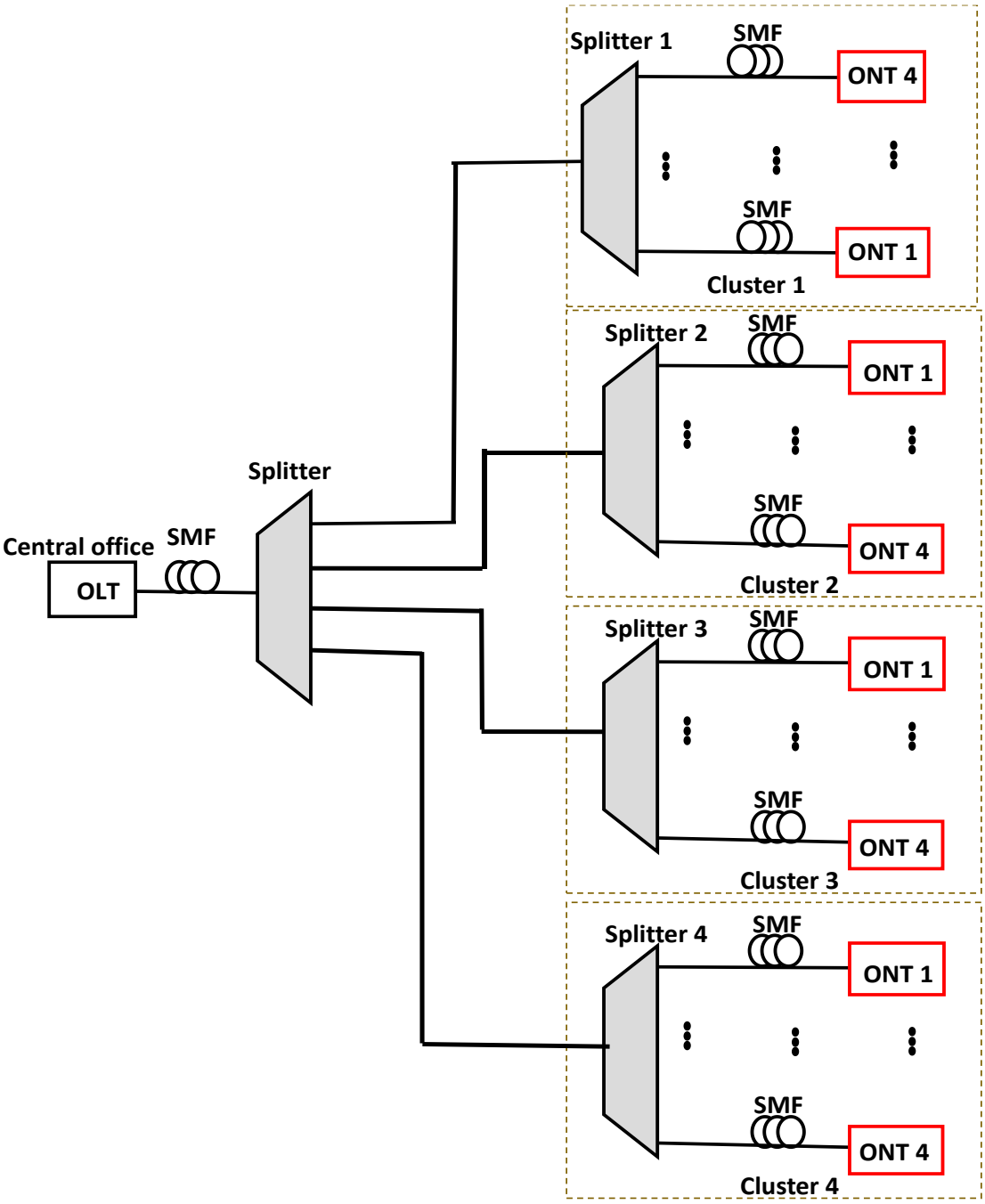

Figure 2-5: PON with two stages serving 16 subscribers in 4 clusters.

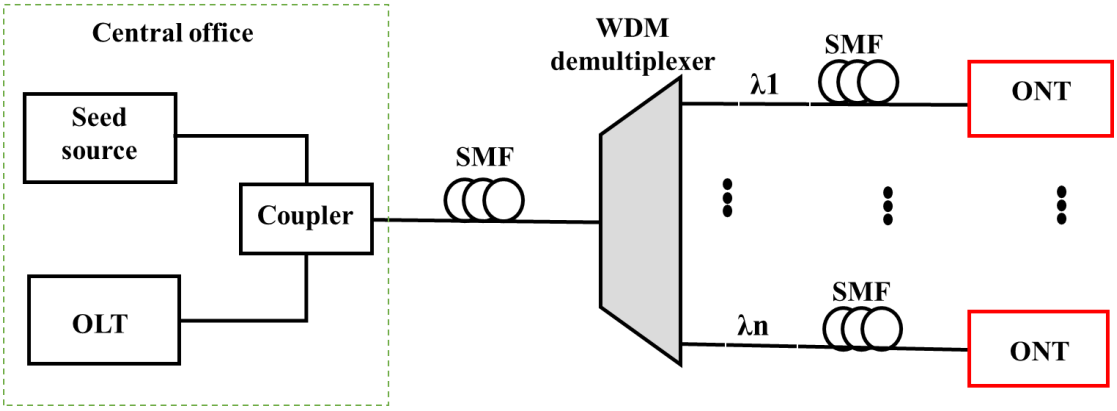

Figure 2-6: WDM-PON with duplex transmission to each user at the same wavelength.

The main advantages of WDM-PON are [43]

i. Lower loss in WDM that has about (3-6) dB than splitter.
ii. Full capacity of OLT can the user access and working at his wavelength.
iii. No time division multiplexing (TDM), all equipment is simpler.
iv. No access from un authorized user this procedure improves the security.
v. There is proportional increased in PON capacity to number of wavelengths.
vi. Different type of equipment can used in single WDM-PON.
vii. Individual fiber loop can be rented to several operators.

The demand for higher-space PON has been increasing to meet 5G and beyond mobile services. Figure. 2-7 illustrated the bandwidth demand, for forth coming 5G mobile front-haul (MFH) and back-haul networks based on WDM-PON [44]. For this network the peak data rate is assumed to be 20 G bps in each sector, the integrated remote radio head (RRH) covering three sectors in a small cell.

2.3.3 Point-to-Point and Point-to-Multipoint Networks

This section introduces the main concepts of P2P and P2MP architectures to support optical transport network.

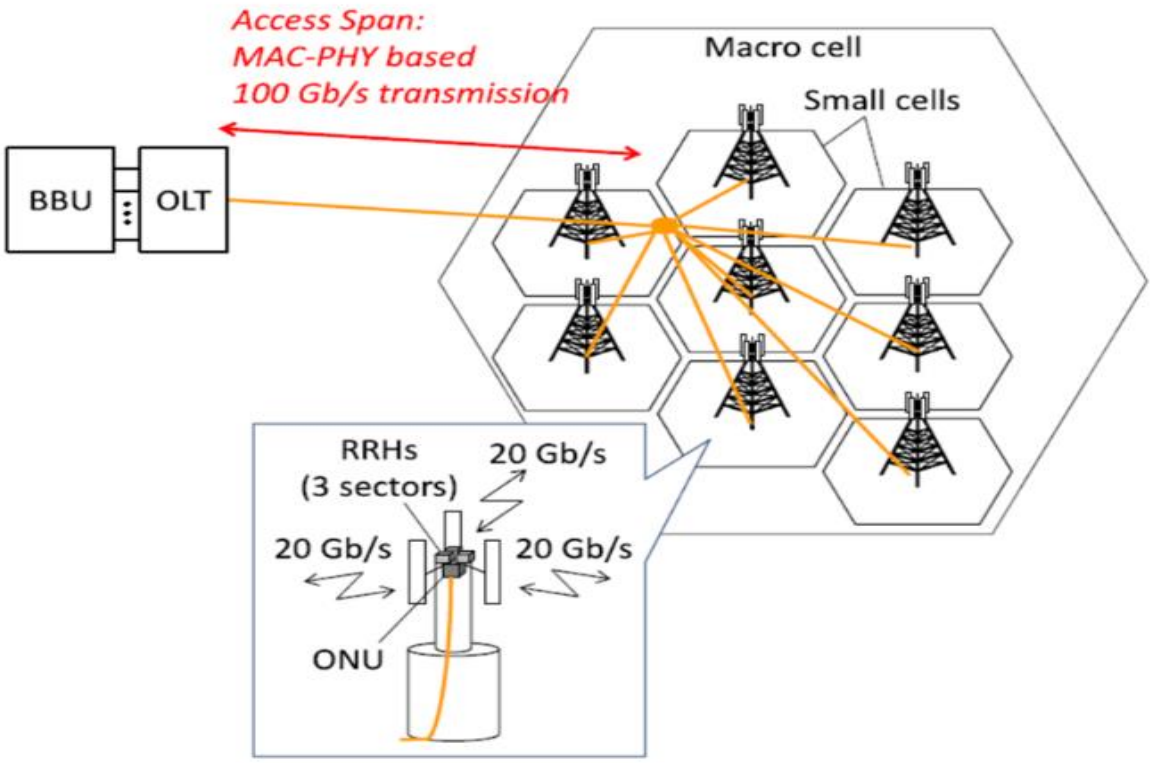

Figure 2-7: Bandwidth demand for 5G MFH/MBF-based PON technology [43].

A- Point-to-Point Optical Network

The P2P architecture is more complex than PON, the core switch at the central office connects over the optical fiber cables to an autonomous system (AS) at the distributed point, typically located at the street corner. Figure 2-8 illustrates the PON and P2P architectures. The ASs has many fiber ports and each port is directly connected to an ONT. Table 2-1 describe the strengths and weaknesses of

P2P and PON architecture and it rewritten from the information reported in Ref. [44]. Recently, a hybrid network in architecture has been proposed which uses PON operating with P2P sub architecture to increase the flexibility of service distribution for advance mobile communication networks [45].

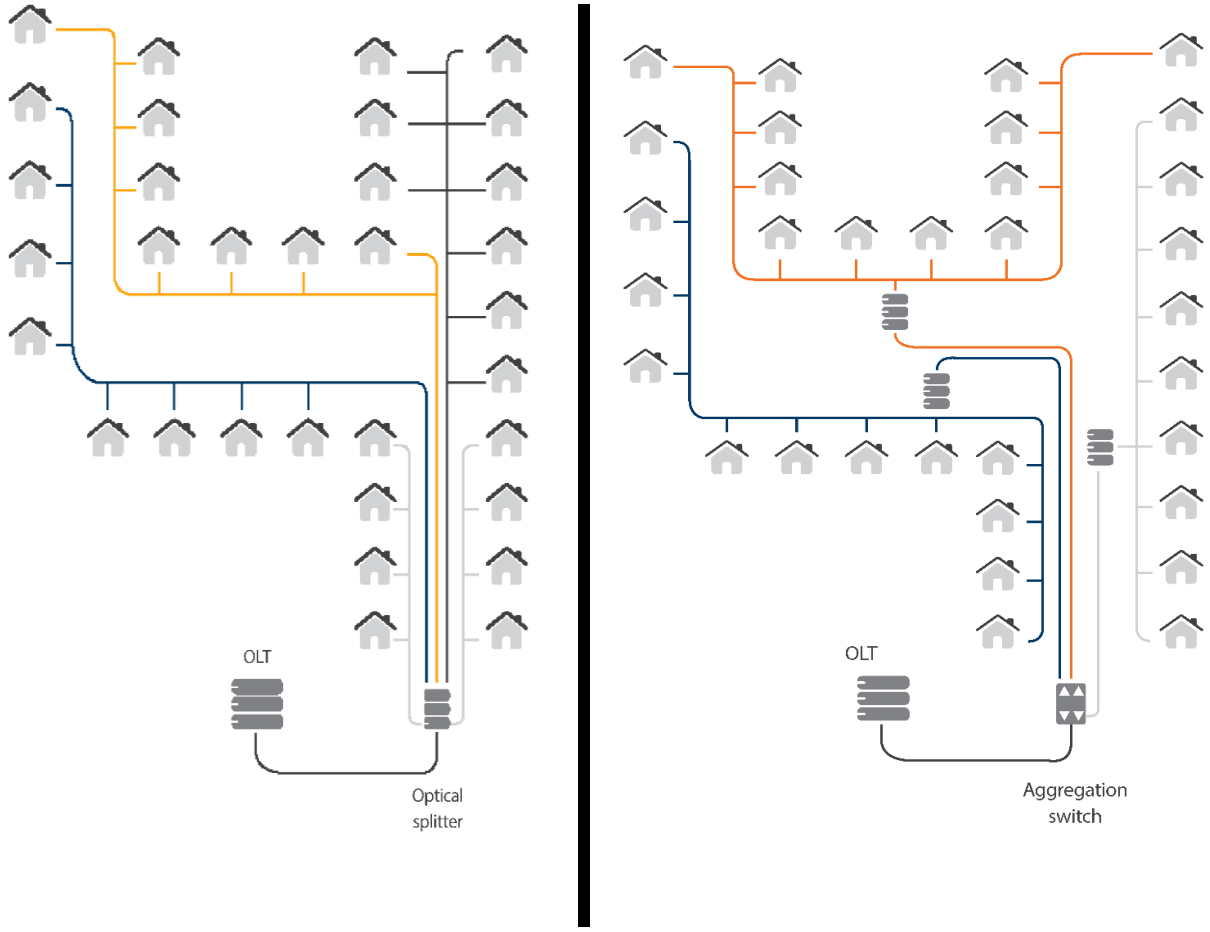

(a) (b)

Figure 2-8: Architectures of (a) Passive optical network (PON). (b) Point-to-point network (P2P) [44].

Table 2-1: strengths and Weaknesses of P2P and PON architectures [44].

P2P	PON
Strengths • Provides balanced bandwidth; • No sharing – individually aggregation switch port is connected to separate premises. • Easy to examine and maintains. • Flexibility – it is able to raise with capacity and bandwidth needs.	Strengths • Less expensive to design and maintain because it uses less fiber cables and ports to terminate the fiber. • Can be placed everywhere as the fiber slitters do not need any power supply. • higher complex than P2P and with faster deployment rate.
Weaknesses • Quite pricey, as it requires the involvement of multiple components; • Longer rollout time.	Weaknesses • Partial level of bandwidth; • The download capacity is well than the upload. • Quite hard to update, mainly when the bandwidth requirements change.

B- Point-to-Multipoint (P2MP) Optical Network

In general, the first section of the first route uses an optical fiber acting as a shared medium for several OLTs. The primary (common) section is connected to a photonic device (or subsystem) to divide the data to individual ONT connections. Each ONT is connected with one of the outputs of the photonic device with an optical fiber having its own length. This connection forms as a secondary link acting as a second part of the route assigned to that ONT. Thus, P2MP may use a single optical carrier that embedded with large data and used to serve many lower-data ONTs [7]. This is to be compared with a conventional PON where all ONTs get the same data as that of the OLT.

Different P2MP architectures have been proposed in the literature to support optical transport network [23]. Most of these architectures are based or using multi-RF subcarriers, each modulated in the central office by one data source and then forwarded optically to one of the ONTs. Figure. 2-9 shows a schematic of a digital (MSC)-based P2MP optical network. To serve N_{sc} ONTs, the uses N_{sc} RF subcarriers. In the central office, each subcarrier is digitally modulated by the data source to be transmitted to one of spectral the ONTs. The pulse spectral shaper bank at the transmitter side is used to produce raised-cosine spectrum for the transmitted QAM symbols. This is useful to get zero inter-symbol interference (ISI) at the receiver symbol detection process. Note that each ONT has its own optical receiver which consists of an optical -to-electrical convertor (photodetection) followed by a digital electrical RF demodulator.

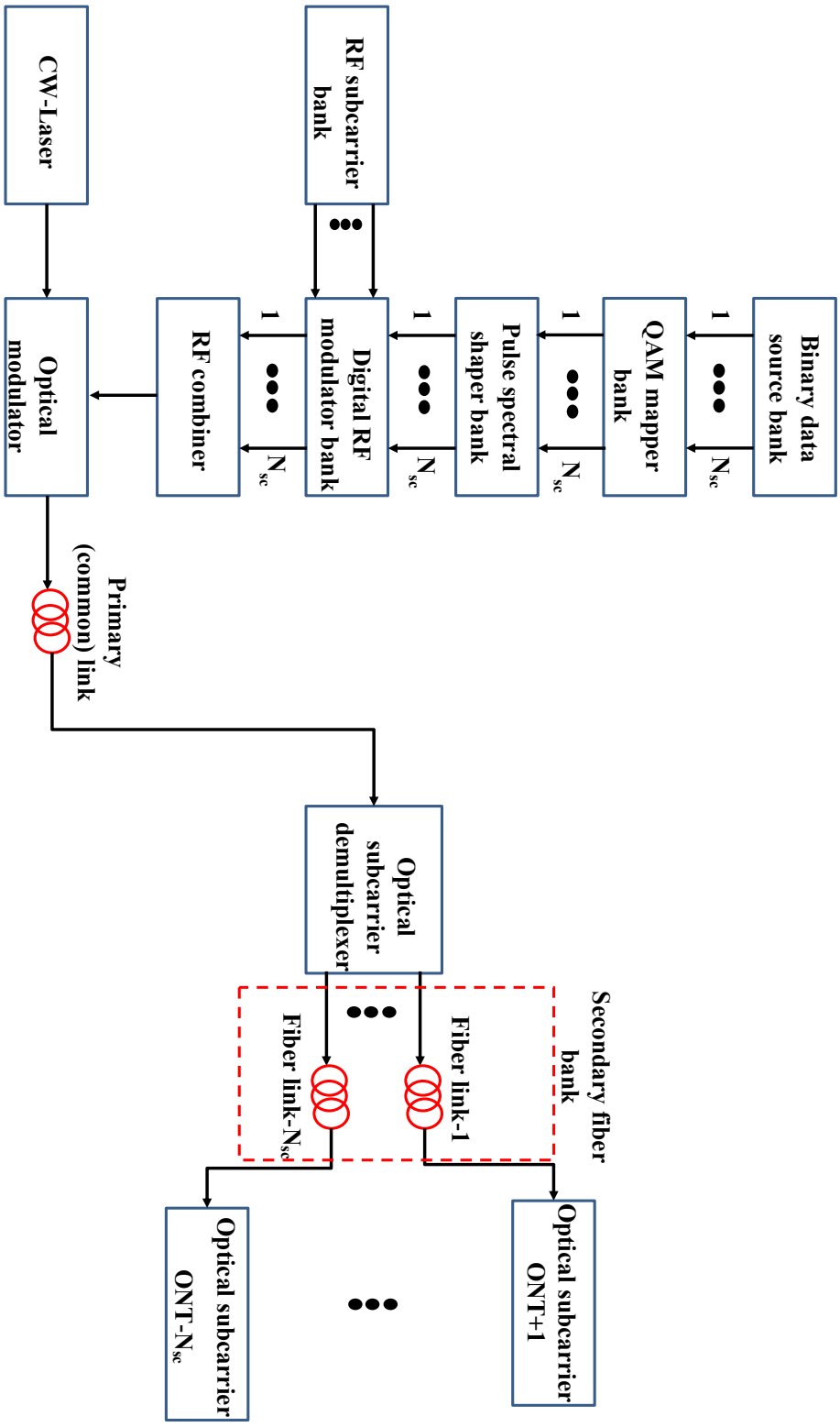

Figure 2-9: Multisubcarrier (MSC)-based P2MP architecture.

CHAPTER THREE

Design Issues and Configurations for P2P and P2MP Optical Networks

3.1 Introduction

This chapter presents the design issues and configurations for point-to-point (P2P) and point-to-multipoint (P2MP) optical networks operating in C or O band. The designs use a single-mode fiber (SMF) route and supported by multisubcarrier (MSC) and wavelength-division multiplexing (WDM) techniques. Both single-polarization (SP) and dual-polarization (DP) WDM architectures are introduced with 16-, 64-, and 128-QAM modulated RF subcarriers. Optical network architecture based on intensity modulation/direct detection (IM/DD) is used for low cost, low power consumption, and small footprint. The P2P and P2MP networks are generally designed with 1-16 WDM channels and with 1-16 subcarriers in each channel. These networks are investigated under the assumption of 25 Gbps per subcarrier data rate. The design implementation and simulation results are obtained using Optisystem version 15 software.

3.2 Design Concepts for P2P and P2MP Optical Networks

The design guidelines give in this section for P2P and P2MP networks under investigation. The networks use digital SCM-WDM with IM/DD scheme and operating either in C- or O-band networks. The group-velocity dispersion (GVD) of a SMF is about 17 and 0 ps/(nm.km) at 1550 nm (C-band networks) and 1310 nm (O-band networks), respectively. Therefore, a dispersion-compensation fiber (DCF) is inserted in each P2P and P2MP route to compensate the GVD of the SMF

when C-band operation is considered. In contrast, no DCF is inserted in the P2P or P2MP route for O-band operation. Additionally, a digital signal processing (DSP) is used in each SC-optical receiver to extract information from the photocurrent to enhance the detection process for that receiver.

If the network transmits N_{ch} identical WDM channels with each channel has N_{sc} subcarriers carrying R_b bit rate per SC, then the total transmitted bit rate R_{bt} through the link is given by

$$R_{bt} = N_{sc}N_{ch}R_b \tag{3.1}$$

The symbol rate R_s corresponds to SP- and DP-WDM channel is given, respectively, by

$$(R_s)_{SP} = R_b/\mathrm{Log}_2\mathrm{M} \tag{3.2}$$

$$(R_s)_{DP} = R_b/2\mathrm{Log}_2\mathrm{M} \tag{3.3}$$

where M-ary quadrature amplitude modulation (M-QAM) format is assumed for the signaling. Note that there is 2 in the denominator of eqn. 3.3 since R_b is the subcarrier bit rate carries by both polarization components. To ensure negligible intersymbol interference (ISI) among the transmitted symbols in each subcarrier, the symbol pulse shape at the input of the receiver decision circuits should have a raised-cosine (RC) spectral profile according to the Nyquist criterion. The electrical bandwidth of the transmitted symbol (message) B_{me} depends on the RC roll-off factor r according to

$$B_{me} = (1 + r)R_s/2 \tag{3.4}$$

The ideal case of r is equal to (0) corresponds to Nyquist filter which has an ideal lowpass spectral characteristics. The other extreme case is when r equal to (1) which gives a full RC spectral shaping and yields a message bandwidth equals R_s.

For multi-RF subcarrier system operating with Δf_{sc} subcarrier frequency spacing, the following condition that illustrated in equ. 3.5 should be satisfied to prevent overlapping between the spectra of neighboring RF subcarriers

$$\Delta f_{sc} \geq 2B_{me} \tag{3.5}$$

The electrical bandwidth of the MSC signal is embedded in one optical channel computed from

$$B_{sc} = \Delta f_{sc} N_{sc} \tag{3.6}$$

If the system contains WDM channels, then the optical channel frequency spacing Δf_{ch} should be chosen to satisfy the following condition

$$\Delta f_{ch} \geq 2B_{sc} \tag{3.7}$$

The condition in equ.3.7 is useful to prevent spectral overlapping between the neighboring optical channels. Then, to find the total link bandwidth B_{ch} the fomulla in 3.8 is used

$$B_{ch} = B_{sc} N_{ch} \tag{3.8}$$

The optical bandwidth of the message (i.e., the bandwidth of the modulated optical carrier) B_{mo} can be estimated as $2B_{me}$ since the QAM modulator produces a double-sideband spectral signal.

The value of subcarrier bit rate R_b considered in this work is 25 Gbps. The corresponding symbol rates Rs are 6.25 Gbaud and 3.125 Gbaud for SP 16-QAM and DP 16-QAM formats, respectively. The International Telecommunication Union-Telecommunication Sector (ITU-T) has issued different wavelength grids for C band WDM networks with a specific channel spacing Δf_{ch}, such as 50, 75 , 100, 125, 200, and 250 GH. These values of Δf_{ch} can be used to implement the WDM systems considered in this work. Table 3-1 lists the total transmission bit rate R_{bt} as a function of number of SCs and number of WDM channels.

In the simulation that presented in this thesis, the frequency of the central C-band WDM channel (i.e., the frequency of the unmodulated central laser) is set to 193.1 THz which approximately corresponds approximately to 1550 nm wavelength. The frequencies of other WDM channels spread above and below the central channel frequency by multiple values of Δf_{ch}.

Table 3-1: Dependance of total transmission bit rate on the number of subcarriers and number of channels.

Number of WDM channel	**Total bit rate (Gbps)**			
	N_{sc} = 1	**N_{sc} = 4**	**N_{sc} = 8**	**N_{sc} = 16**
1	25	100	200	400
4	100	400	800	1600
8	200	800	1600	3200
16	400	1600	3200	6400

3.3 Design of Point-to-Point Optical Network

Figure 3-1 shows a simplified schematic diagram of the C band P2P configuration, while detailed description of the used subsystems are depicted in Figs. 3-2 and 3-3. A DCF is inserted after the SMF section to compensate its dispersion. One optical amplifier (OA) is inserted at the end of the hybrid optical fiber link to compensate partially or completely the link and transmitter insertion losses.

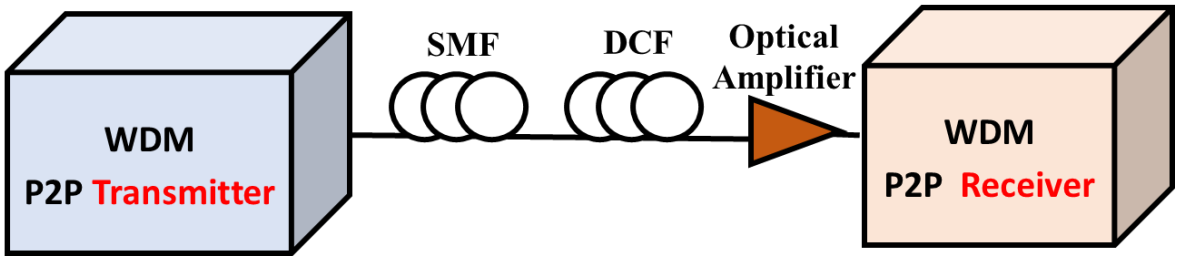

Figure. 3-1: Basic architecture of point-to-point optical network operating in C band.

3.3.1 Transmitter Side

The architecture of P2P transmitter can be explained with the aid of the block diagram depicted in Fig. 3-2a. Here, a continuous-wave (CW) semiconductor lasers are used with each laser acts as a source of unmodulated optical carrier that required for each WDM channel. Fig. 3-2b illustrates the first RF subcarrier modulation subsystem implemented in Optisystem environment. This subsystem consists of quadrature amplitude modulator (QAM) mapper acting as a sequence generator that produces two parallel M-ary symbol sequences from the binary data. The M-ary generates multilevel pulses according to the M-ary signal input. Two lowpass filters having a cosine roll-off frequency transfer function are used

to shape the spectrum of both in-phase (I) and quadrature (Q) component as shown in Fig. 3-4. The RF subcarriers modulation uses a QAM modulator.

All the subcarriers modulators subsystems have identical configuration but each uses its own RF subcarrier as illustrates in Fig. 3-2a. The RF subcarriers frequencies are separated by a subcarrier spacing Δf_{sc} that presents neglectable overlapping between neighboring subcarrier spectra. The multisubcarrier (MSC) electrical signals (modulated RF signals) are combined by using (N_{sc}:1) electrical combiner where the N_{sc} is the number RF subcarriers. The combined signal is then applied to a Mach-Zender optical modulator driven by a CW-Laser. The generated optical signal is forwarded to the WDM multiplexer that multiplexer responsible to gather all channels (each channel has its own wavelength with channel spacing Δf_{ch}). The produced optical signal is forwarded to fiber link.

A QAM modulator is used to modulate the RF subcarrier (electrical subcarrier). The output RF signal is modulated according to

$$v_{out}(t) = G(I(t)\cos(2\pi f_{RF}t) - Q(t)\sin(2\pi f_{RF}t)) \quad (3.9)$$

where I and Q are the input electrical signals, G is the parameter gain, and f_{RF} is the RF subcarrier frequency

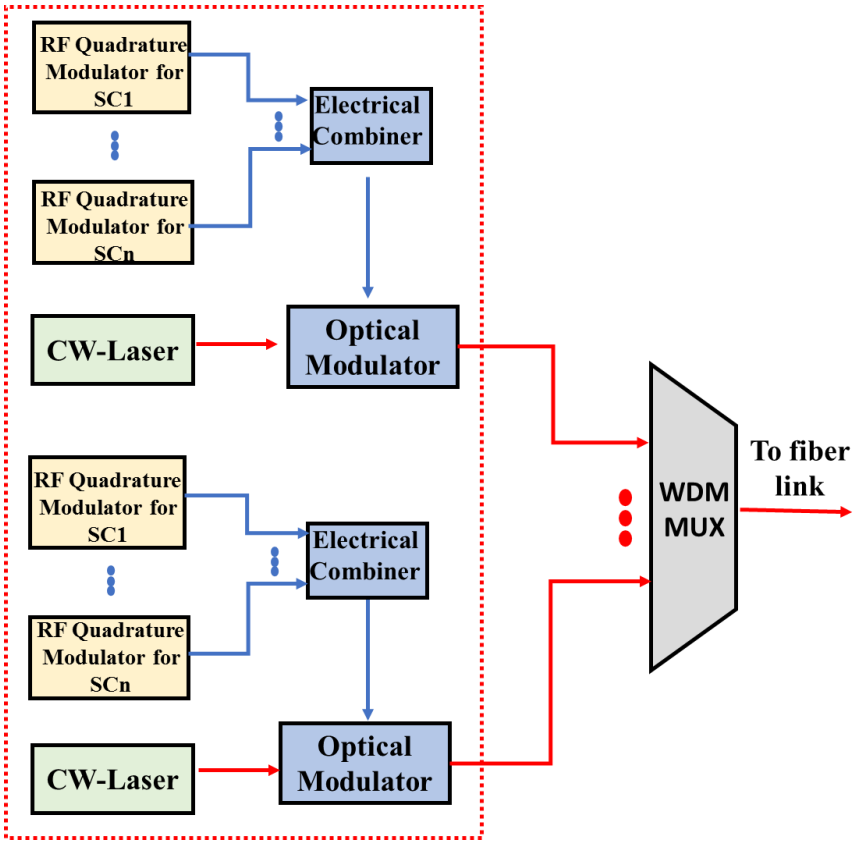

(a)

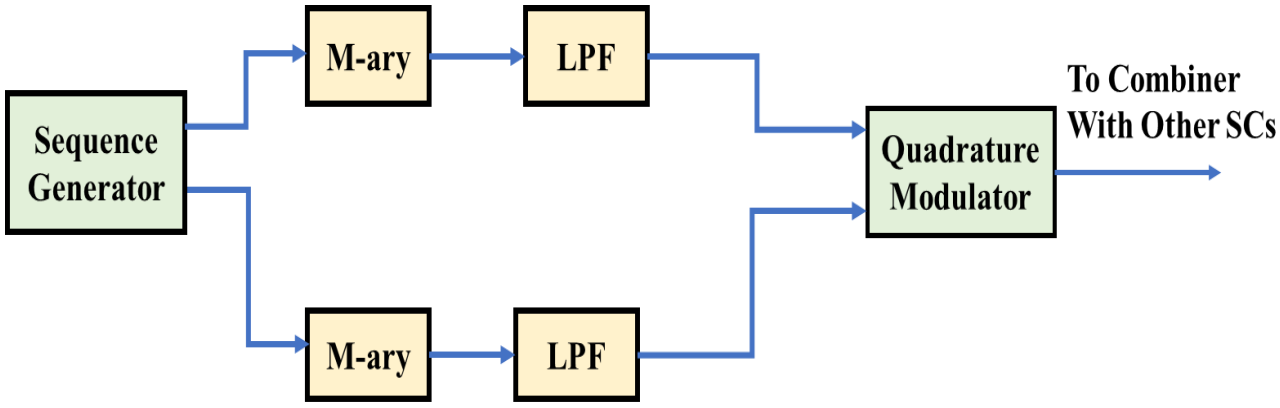

(b)

Figure 3-2: Details architecture for transmitter side P2P network. (a) details block diagram. (b) Single subcarrier architecture.

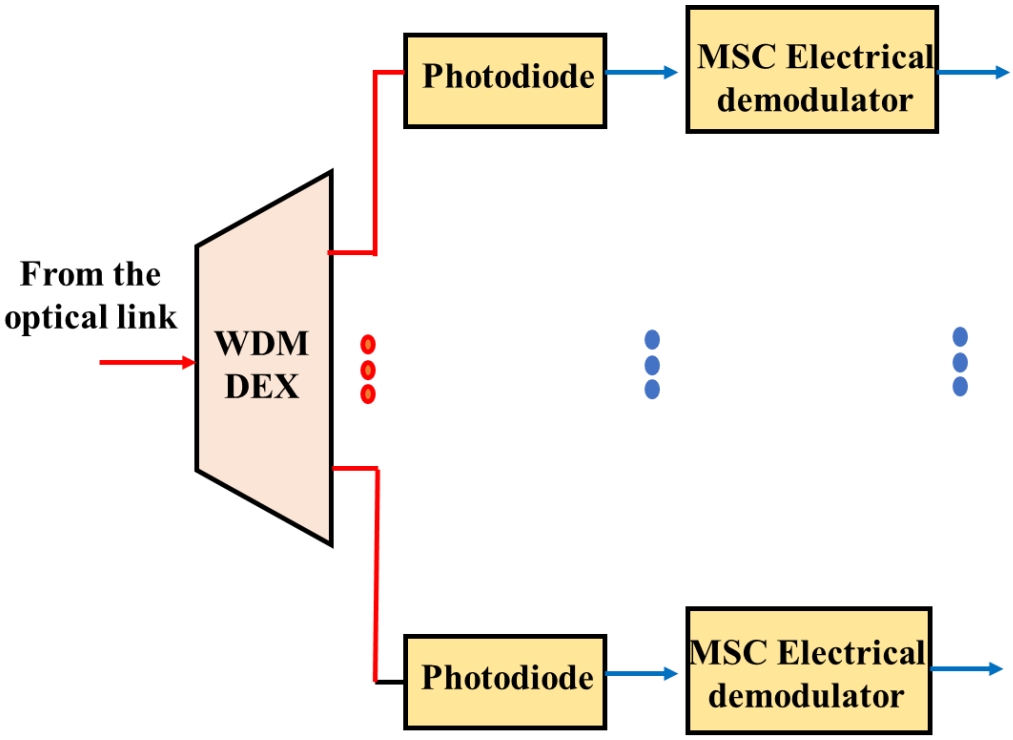

(a) details block diagram.

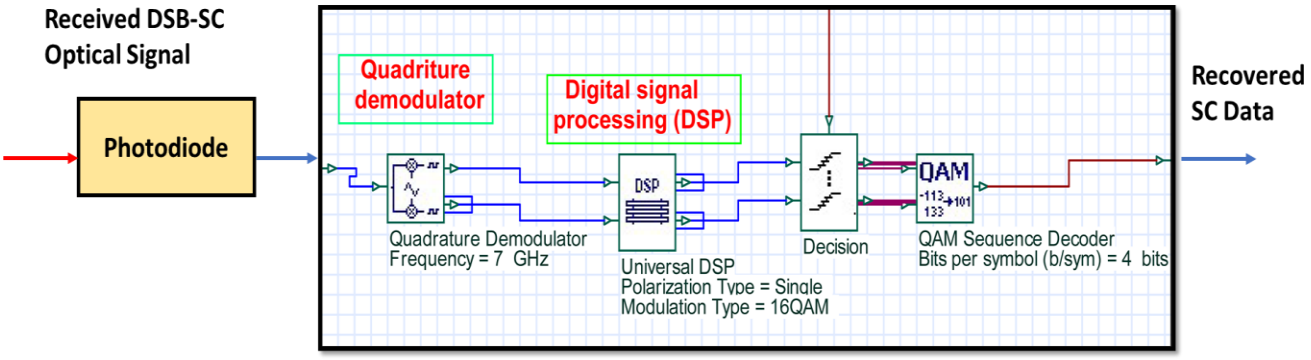

(b) Single subcarrier single-polarization architecture.

Figure 3-3: Details architecture for the receiver side P2P network.

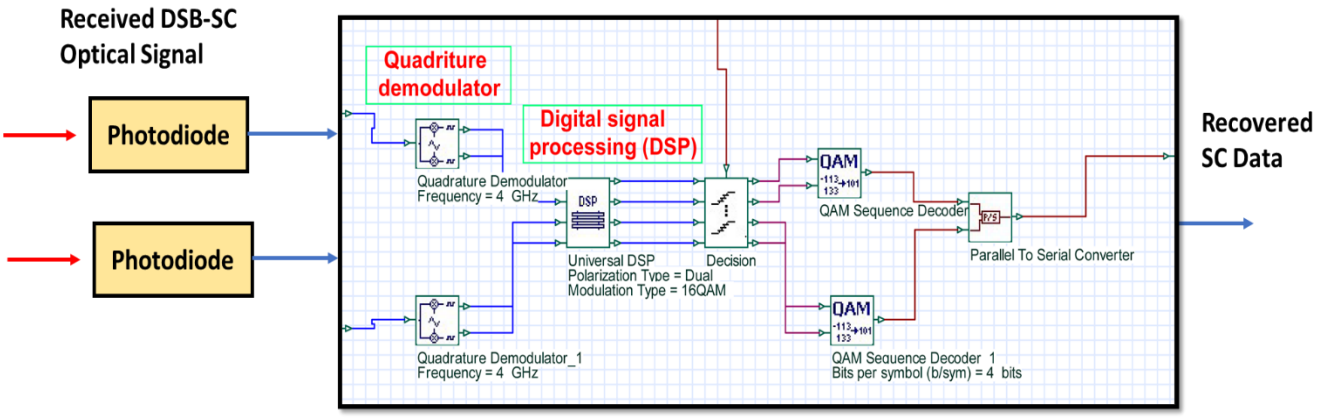

(c) Single subcarrier dual-polarization architecture.

Figure 3-3 (Continued).

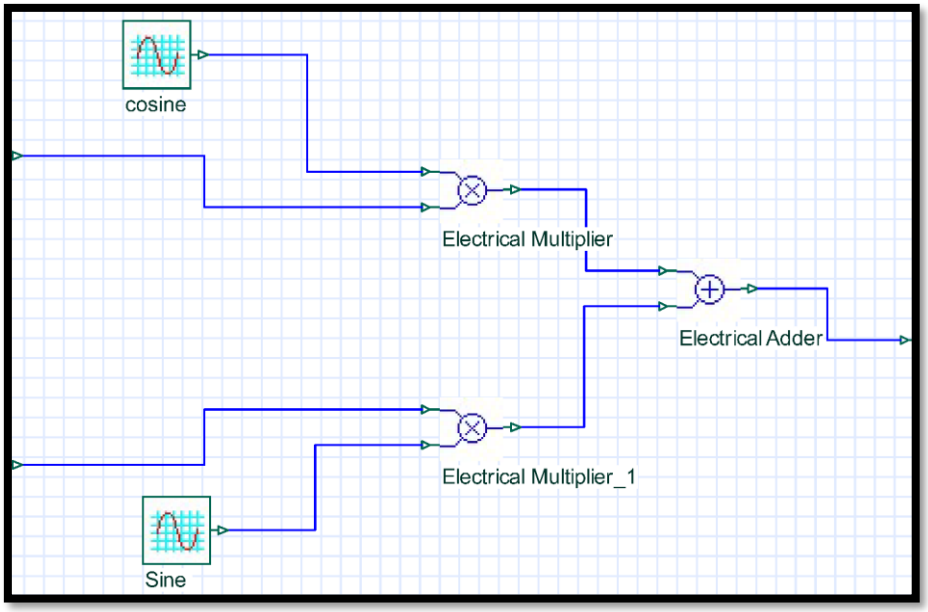

Figure 3-4: Block diagram of the RF QAM modulator.

3.3.2 Transmission Link

In C-band networks the optical link consists of two fiber sections, SMF and DCF. And one OA. The DCF is used to compensate the positive GVD of the

SMF and it is characterized by a relatively high negative GVD. An OA is inserted after the two cascaded fiber sections to compensate their loss. Thus, one can say that the transmission link is both loss and dispersion compensated. Table 3-2 listes the network parameters values used in the simulation.

The maximum reach (i.e., the maximum link length that yields the required receiver quality of service) fiber of the network depends on polarization-state of operation, if its SP or DP, and also depends on number of subcarrier and number of optical channels that are used in the network. The dispersion slop of the fiber is defined as

$$S \equiv dD/d\lambda \tag{3.10}$$

where λ refers to the wavelength. It is worthily to use that dispersion slop of the DCF equal approximately with the reverse sign of the dispersion slop SMF.

The link contains a single OA. If only fiber loss, to be compensated the gain of that amplifier is equal to

$$G_a = \propto_{SMF} L_{SMF} + \propto_{DCF} L_{DCF} \tag{3.11}$$

where G_a is the amplifier gain in dB, α is the loss of each fiber link (in dB/km), and L fiber length in km. The subscript SMF and DCF are used for SMF and DCF, respectively. Note that $\propto$ is about 0.2 and 0.5 dB/km, for SMF and DCF operating in C band, respectively.

3.3.3 Receiver Side

The first stage of the optical receiver is a 1: N_{ch} WDM demultiplexer that produces the N_{ch} modulated channels as shown in Fig. 3-3c with each channel has its own wavelength modulated by RF subcarriers. Figure. 3-3(b and c) show brief schematic for P2P receiver design in SP and DP networks, respectively. However,

the optical signal is applied to photodiode that is used to convert the modulated signal from optical domain to electrical domain. The generated electrical signal is forward to a M-QAM RF demodulator incorporating DSP. The RF QAM demodulator has two modulated inputs, I and Q and uses coherent analog demodulation technique based on an RF local subcarrier generator producing I and Q components. The output signal is demodulated according to

$$v_I(t) = [Gv_{in}(t)\cos(2\pi f_{RF}t)] * h_{low}(t) \quad (3.12)$$

$$v_Q(t) = [-Gv_{in}(t)\sin(2\pi f_{RF}t)] * h_{low}(t) \quad (3.13)$$

where v_{in} is the input electrical signal, G is the parameter gain, f_{RF} is the subcarrier frequency, and h_{low} is the time response of the lowpass filter. The symbol * denote time convolution. Figure. 3-5 shows the entire components of the quadrature demodulator. The filter type is low pass filter (LPF) and its roll-off factor value are (r = 0.5) similar to those in the transmitter side.

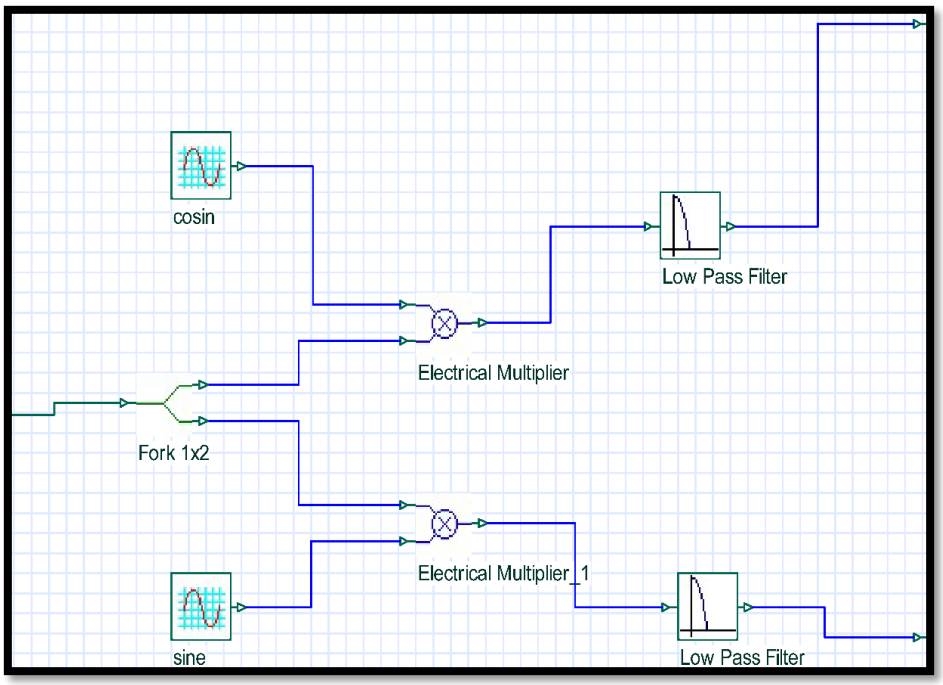

Figure 3-5: Block diagram of the RF QAM demodulator.

It is worthily to note that DSP is used in the receiver side to overcome fiber impairments such as fiber nonlinear and fiber dispersion and to enhance the efficient of detection process. The parameter of DSP with the parameters of the whole design is shown in Table 3-2. DSP unit is used to perform DSP steps required in direct-detection single-carrier communication systems utilizing single-polarization or dual-polarization modulation signaling. The unit is provided with a range of DSP algorithms to perform different actions, such as

i. Compensation of chromatic dispersion (CD) and polarization-mode dispersion (PMD) of the fiber link.

ii. Carrier frequency recovery (CFR) and carrier phase recovery (CPF).

iii. Matched-filter equalization.

3.4 Design of P2MP Optical Network

A- Design Concepts

A block diagram of P2MP network under investigation is shown in Figure 3-6. The transmission side of P2MP network is similar to the transmission side of P2P network which presented in Section (3.3.1).

The transmission link of the P2MP network consists of a primary link (a common link that is shared by all RF subcarrier and all optical channels) and the secondary links with each link provides connection to each subcarrier optical receiver (i.e., user end). A DCF section is cascaded with each SMF section link to compensate its GVD. Also, an OA is inserted after the primary link to amplify the transmitted MSC-WDM signal. The gain of this amplifier is computed by

$$G_a = \propto_{SMF} (L_{SMF1} + L_{SMF2}) + \propto_{DCF} (L_{DCF1} + L_{DCF2}) \quad (3.14)$$

where $\propto_{SMF}$ and $\propto_{DCF}$ is the loss parameter (dB/km) for SMF and DCF, respectively, and the fiber section length is measured in km. The subscript 1 and 2 is used to distinguish the primary link (common link) from the secondary links that connected the WDM demultiplexer to the subcarrier optical receivers.

The first stage of the receiver side is a WDM demultiplexer (WDM DEMUX) that produces 1:N_{ch} output optical signals whose central optical frequencies match that of the transmitter channel frequencies. Each WDM demultiplexer output is connected to an optical sideband demultiplexer (OSD), This demultiplexer is illustrated schematically in Fig. 3-7 and acts as 1: ($2N_{sc}$+1) wavelength selective switch that produces the lower-sideband (LSB) and upper-sideband (USB) of each modulated RF subcarrier beside the optical carrier component. This generated an optical carrier is then applied to 1: Nsc optical splitter to support the N_{sc} optical receivers. The USB and LSB of each subcarrier are combined with one of optical splitter output (optical carrier) to generate the intensity-modulated subcarrier optical signal corresponding to the SC under observation.

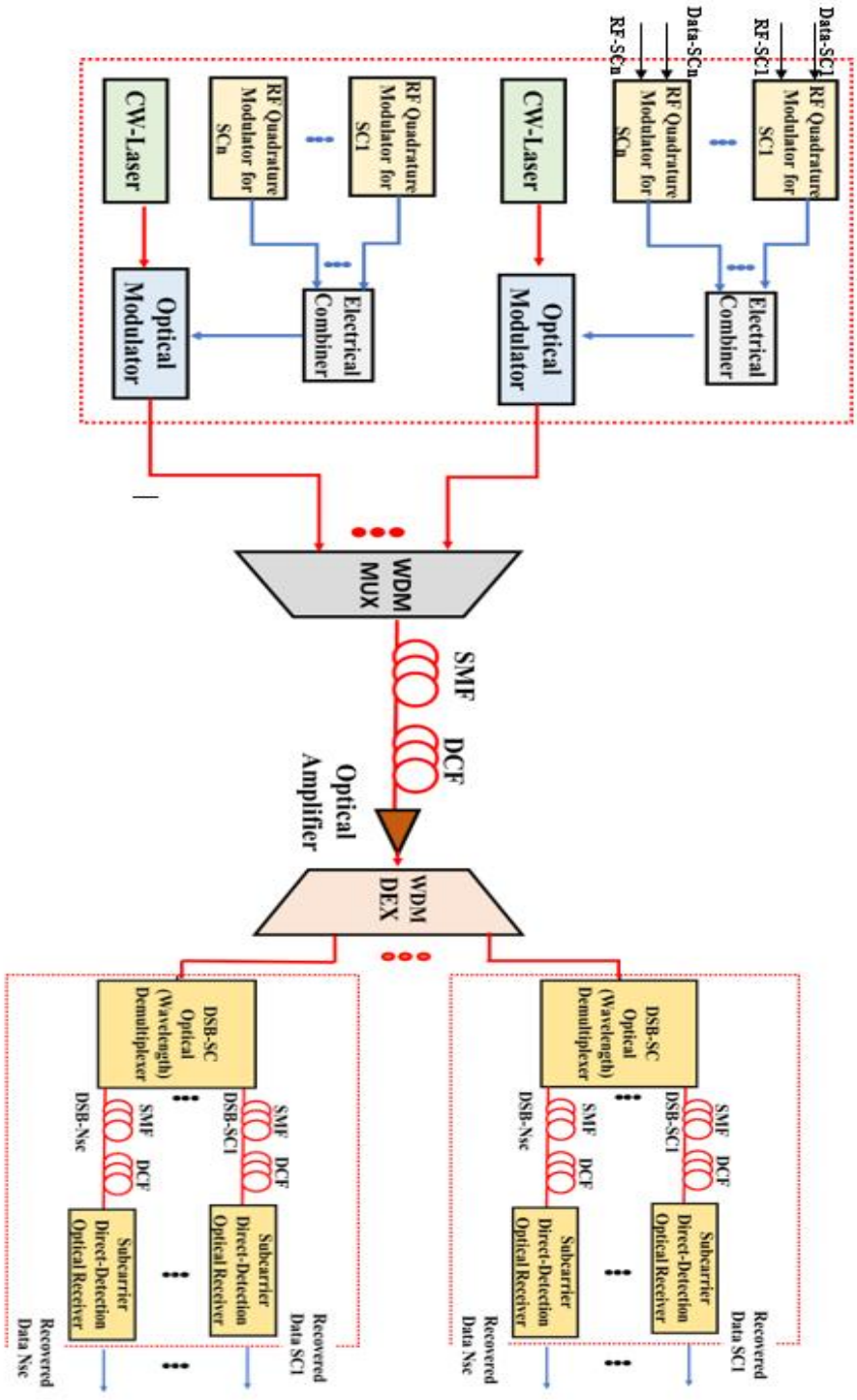

Figure 3-6: Block diagram of the proposed P2MP WDM network incorporating IM/DD scheme.

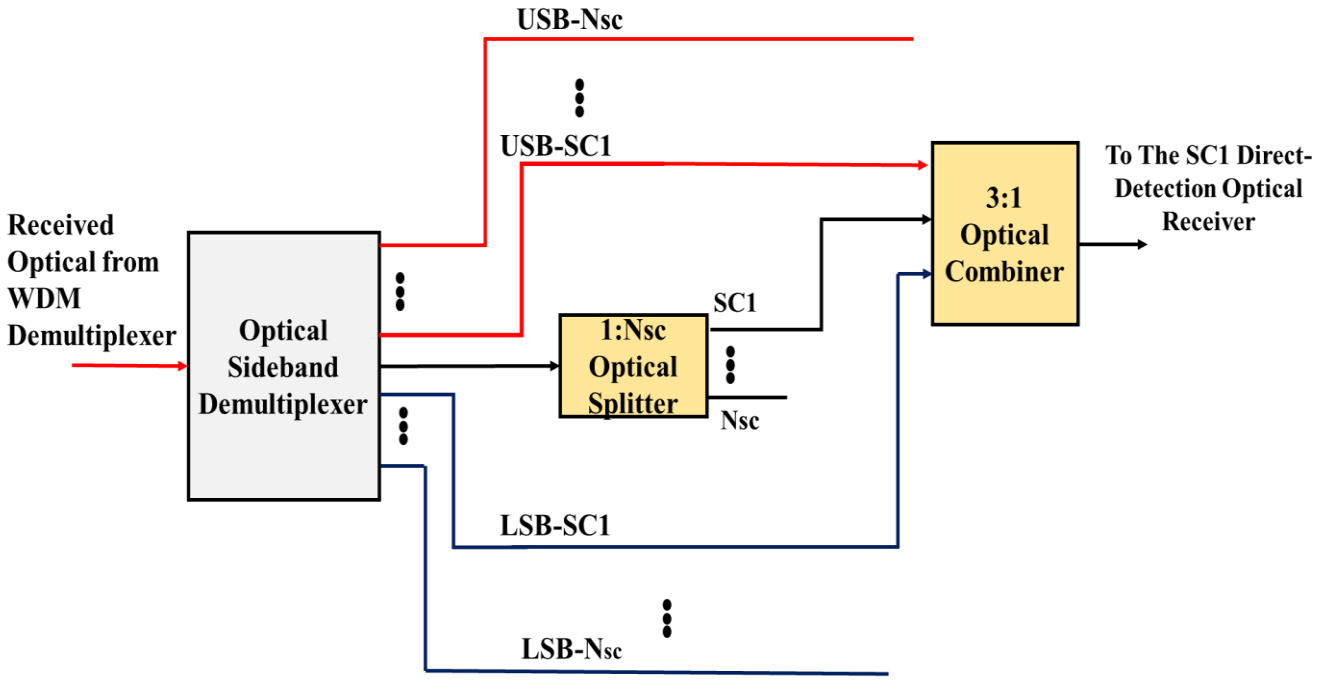

Figure 3-7. Optical sideband demultiplexer.

B- Primary Design Computation

This subsection presents the design computation that related to a DD MSC-P2MP optical networks. The system consists of multi-RF subcarriers embedded in a C-band optical carrier. Both SP and DP configuration are used for 16-QAM and 64-QAM subcarrier modulated formats and DD scheme with assuming 25 Gbps bit rate per subcarrier R_b. The simulation is performed by Optisystem, software using the parameter values listed in Table 3-2.

i- In 16-QAM format, the symbol rate R_s for each subcarrier in DP system is 3.125 Gbaud (= 25 Gbps/(4x2)). This is to be compared with 6.25 Gbaud for the SP counterpart. Therefore, subcarrier spacing Δf is chosen to be 14 GHz and 8 GHz for SP and DP systems, respectively. The first RF subcarrier

frequency for the SP and the DP systems is 7 and 4, respectively. In addition, for the 64-QAM system, the symbol rate R_s for each subcarrier in DP system is 2.083 Gbaud (= 25 Gbps/(6x2)). This is to compared with 4.166 Gbaud for the SP counterpart. Therefore, subcarrier spacing Δf_{sc} is chosen to be 10 GHz and 6 GHz for SP and DP systems, respectively. The first RF subcarrier frequency for the SP and the DP systems is 5 and 3 GHz, respectively the center-channel frequency of the WDM signal is set to 193.1 THz which corresponding to 1553 nm wavelength.

ii. The length of the transmission link between the transmitter and ith subcarrier optical receiver L_i is computed as

$$L_i = L_s + L_{bi} \tag{3.15}$$

where L_s is the lengh of the primary SMF connecting the transmitter to the WDM demultiplexer (common for all subcarrier) while L_{bi} is the length of the secondary SMF that connecting the OSD output to the ith subcarrier receiver. If L_{bi} is assumed the same for all subcarriers, the P2MP network is then denoted by $(L_s + L_{bi})$ network.

iii- The length of DCF is chosen to yield a zero-average GVD over the fiber link

$$D_{SMF}L_{SMF} + D_{DCF}L_{DCF} = 0 \tag{3.16}$$

where D is the GVD, L is the fiber length, and the subscripts SMF and DCF are used to distinguished the two fiber types. From equ. (3.16)

$$L_{DCF} = -\frac{D_{SMF}L_{SMF}}{D_{DCF}} \tag{3.17}$$

iv- The maximum reach of transmission is estimated as the maximum SMF route length that yields a bit error rate BER < BER_{th} for all the subcarriers. Here, BER_{th} denotes the threshold BER which is taken to 3.8×10^{-3} corresponding to 7% hard-decision (HD) forwarded error connection (FEC) code.

Table 3-2: Parameters values used in the simulation.
(a) Transmitter side and transmission link.

Subsystem	Component	parameter	value
P2MP Transmitter	CW-Laser	Power	0 dBm
		Center frequency	193.1 THz @ C band
			228.5 THz @ O band
	RF-Quadrature Modulator	Modulation format	16-QAM
		Frequency spacing	14 GHz for SP
			8 GHz for DP
	optical modulator (MZ-Modulator)	Extinction ratio	30 dB
Transmission Link	Single-Mode-Fiber	Attenuation	0.2 dB/km @ C band
			0.35 dB/km @ O band
		Dispersion	17 ps/nm/km @ λ_{ref} = 1550 nm
			0 @ λ_{ref} = 1310 nm
		Dispersion slop	0.08 ps/nm^2/km @ λ_{ref} = 1550 nm
			0.092 ps/nm^2/km @ λ_{ref} = 1310 nm
		Effective area	80 µm^2
		n2	26×10^{-21} m^2/w
	Dispersion compensation fiber	Attenuation	0.5 dB/km @ λ_{ref} = 1550 nm
		Dispersion	-85 ps/nm/km @ λ_{ref} = 1550 nm
		Dispersion slop	-0.016 ps/nm^2/km @ λ_{ref} = 1550 nm
		Effective area	23 µm^2
		n2	26×10^{-21} m^2/w
	Optical amplifier	Noise figure	4 dB
		Gain	6 dB @ C and O band

Table 3-2: (Continued).

(b) Receiver side.

Component	parameter	value
Wavelength demultiplexer	Filter type	Gaussian
	Filter order	10
	Subcarrier spacing	14 GHz for SP
		8 GHz for DP
	Center frequency	193.1 THz
Photodiode	Responsivity	1 A/W
	Dark current	10 nA
RF-Quadrature demodulator	Modulation format	16-QAM
	frequency spacing	14 GHz for SP
		8 GHz for DP
Digital signal processing (DSP)	Modulation format	16-QAM
	Filter type	Gaussian
	Filter order	10
	Dispersion	17 ps/nm/km @ λ_{ref} = 1550 nm
		0 @ λ_{ref} = 1310 nm
	Dispersion slop	0.08 ps/nm^2/km @ λ_{ref} = 1550 nm
		0.092 ps/nm^2/km @ λ_{ref} = 1310 nm
	Effective area	80 μm^2
	n2	26×10^{-21} m^2/w

CHAPTER FOUR

Results and Discussions

4.1 Introduction

This chapter presents the simulation results to investigate the transmission performance of P2P and P2MP optical networks to support 5G and beyond services. The investigation is performed under various network parameters, namely number of subcarriers N_{sc}, number of WDM channels N_{ch}, modulation format, and fiber length L. The simulation results are reported for C-band network operate with the following number of subcarriers 1, 4, 8, and 16 and numbers of WDM optical channel 1, 4, and 8, and assuming SP and DP for 16-QAM and 64-QAM signaling. The results are extended to include an O-band network with addition results related to 128-QAM. The first scenario of the investigation is based on to be used in the P2P networks and the results are then used as a guideline in the second scenario to design and implement the P2MP optical networks. The simulation is carried out in Optisystem Ver. 15 environment with the parameters values that mentioned in Table 3-2.

4.2 Transmission Performance Results for C-band P2P Optical Networks

This section addresses the effect of various C-band P2P network parameters on the transmission performance.

4.2.1 Effect of Inserting DCF on the Link

The first scenario is to evaluate the fiber link transmission performance when the P2P network operates with and without DCF. This investigation is applied to a C-

band network having one SC and one WDM channel and operating in SP and DP 16-QAM and 64-QAM. Figure 4-1 illustrates the maximum reach for single-subcarrier network operating in different cases. The results reveal that the maximum reach is different for each case because of the link dispersion. In addition, the insertion of the DCF has enhances L_{max} by 7.8 and 5.0 for 15-QAM SP and DP, respectively. These values are to be compared with 5.9 and 2.6 for 64-QAM SP and DP, respectively. Note that the effect of DCF is more pronounced in SP architecture due to its wider bandwidth and therefore, according to this, it be more affected by fiber GVD.

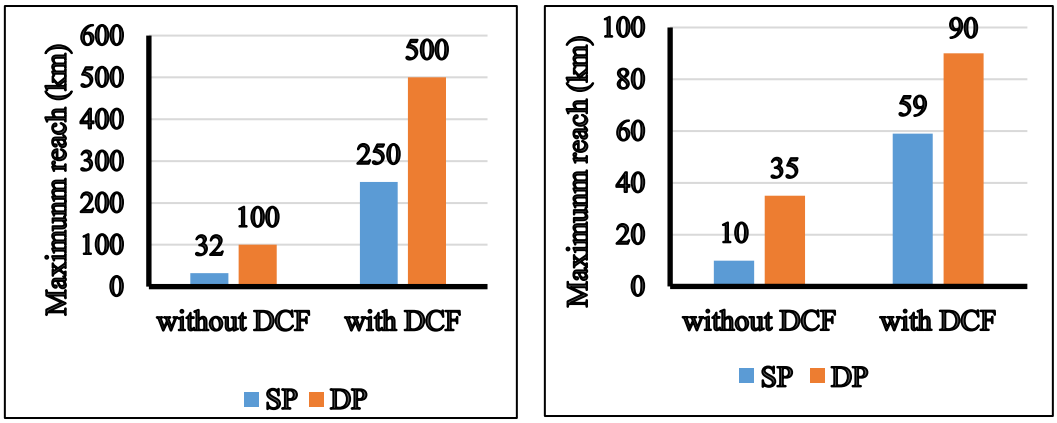

(a) (b)

Figure 4-1: Maximum reach for single-subcarrier and single-channel P2P network operating in C- band in with and without DCF for (a) 16-QAM signaling (b) 64- QAM signaling.

4.2.2 Effect of Polarization, Modulation Format, and Number of Subcarriers

i. Dependance of Transmission on the Number of Subcarriers

The transmission performance of 4-, 8-, 12-, and 16- subcarriers P2P networks is operating with a single-WDM channel and with SP and DP architectures supported by the two modulator formats 16-QAM and 64-QAM, is

investigated and the results are depicted in Fig. 4-2. Here, the longest maximum reach is recorded for the 4-subcarrier network. However, the transmission distance for 8-, 12-, and 16- subcarriers network decreases gradually. In this case, one can say that when both the number of subcarriers and the order of modulation format is increase, the transmission distance decreases. Also, the type of polarization is affects the maximum transmission distance; DP has higher L_{max} than SP counterpart as shown in Fig. 4-2. Note that DP network in some cases has a maximum reach higher than twice maximum reach for SP counterpart.

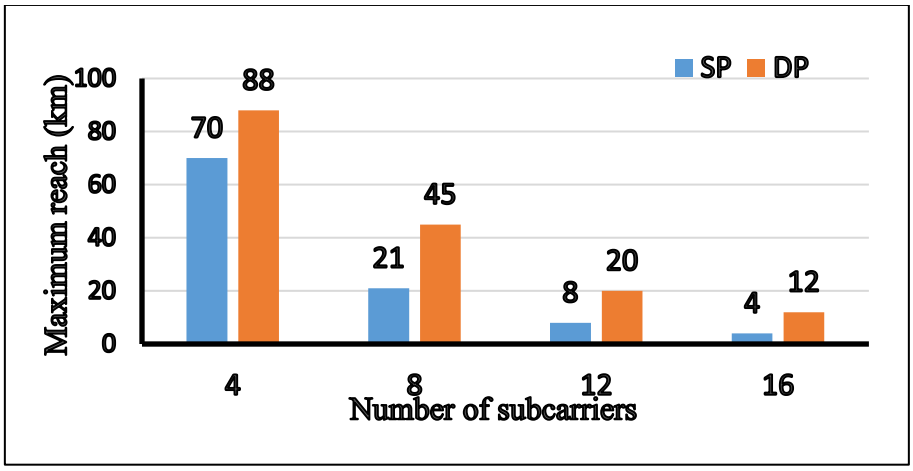

(a)

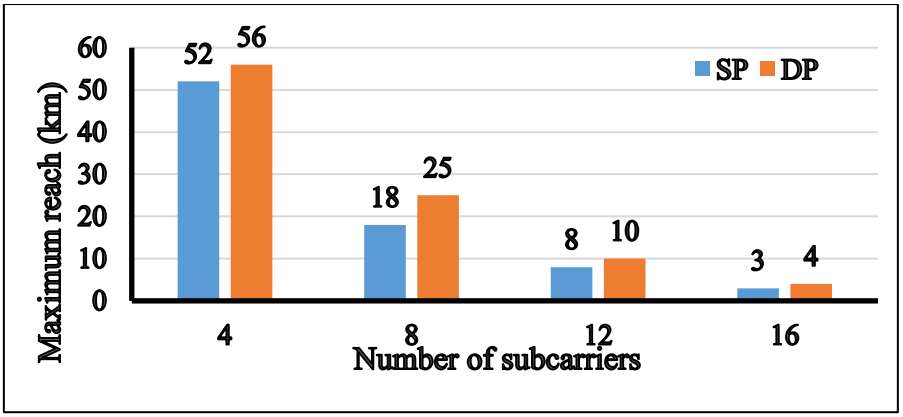

(b)

Figure 4-2: Maximum reach of a single-channel C-band transmission network. (a) 16-QAM signaling. (b) 64-QAM signaling.

ii. Effect of Number of Optical Channels on the Transmission Performance

Figures 4-3 a and b illustrate that number of WDM channels is also affects the transmission performance of the P2P network. The results are reported for C-band network operating with N_{ch} = 4 and 8 and N_{sc} = 4 and 8. Further, both SP and DP architectures are considered with 16-QAM and 64-QAM modulation formats. As shown from the results, the 4-channel WDM network provide longer transmission distance than the 8-channel counterpart.

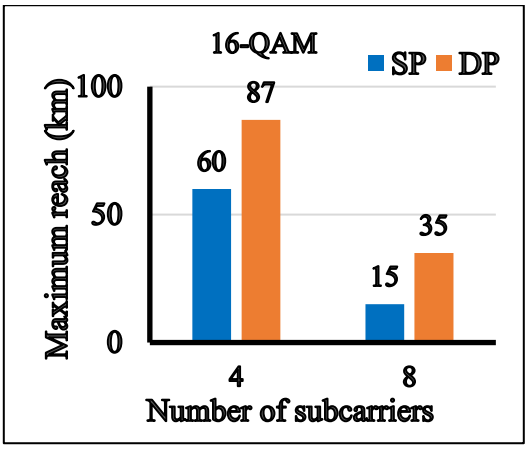

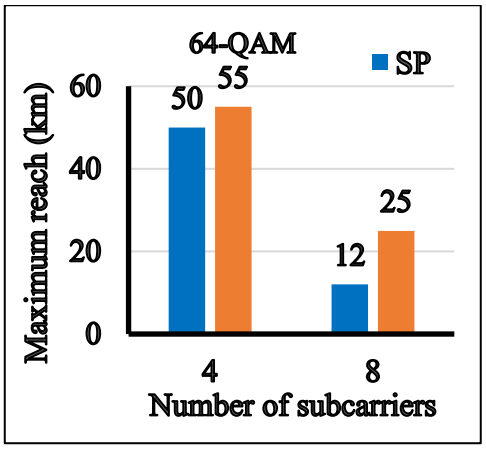

(a) N_{ch} = 4

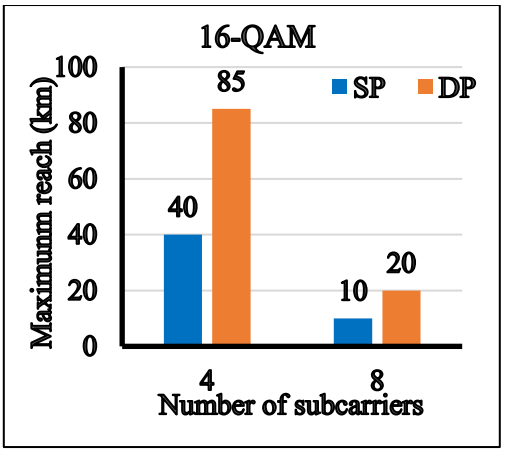

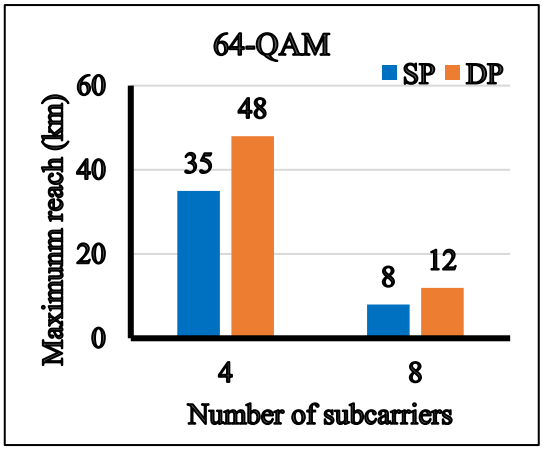

(b) N_{ch} = 8

Figure 4-3: Maximum reach for C- band WDM P2P network.

In summary, it is clear from the results that reported in Section 4.2.2, the maximum reach of P2P networks depends on

i. The number of subcarriers per optical channel.

ii. The number of WDM channels.

iii. The type of polarization architecture.

iv. The order of the QAM modulation format.

v.

4.3 Spectral Simulation Results for C-band P2P Optical Networks

4.3.1 16- and 64-QAM 8-SC networks

The signals spectra at the transmitter side and receiver side with its constellation diagram for SC4 are shown in Figs. 4-4 and 4-5 for SP and DP system, respectively based on 16-QAM signaling. On other hand, for 64-QAM signaling, the signals spectra results for SP and DP system is shown in Figs. 4-6 and 4-7. Note that the spectrum bandwidth of the baseband symbol in 16-QAM network is equal to 4.7 and 2.35 GHz for SP and DP, respectively. These are to be compared with 3.124 and 1.5625 GHz for SP and DP network, respectively, in 64-QAM signaling. These values correspond to ((1+r) Rs)/2 where r is the roll-off factor which is taken to be 0.5 in the simulation.

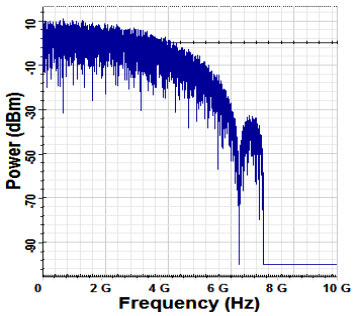

(a) Base band symbol spectrum

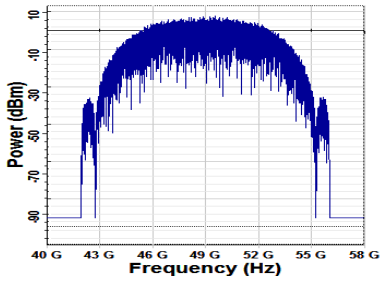

(b) RF quadrature modulator output (SC4).

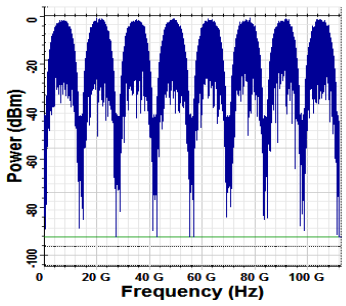

(c) RF MSC combiner output

Figure 4-4: Signals spectra and receiver constellation diagrams for a single-polarization multisubcarrier C-band transmitter operating with 20 km link, 16- QAM, singling optical channel (193.1 THz)

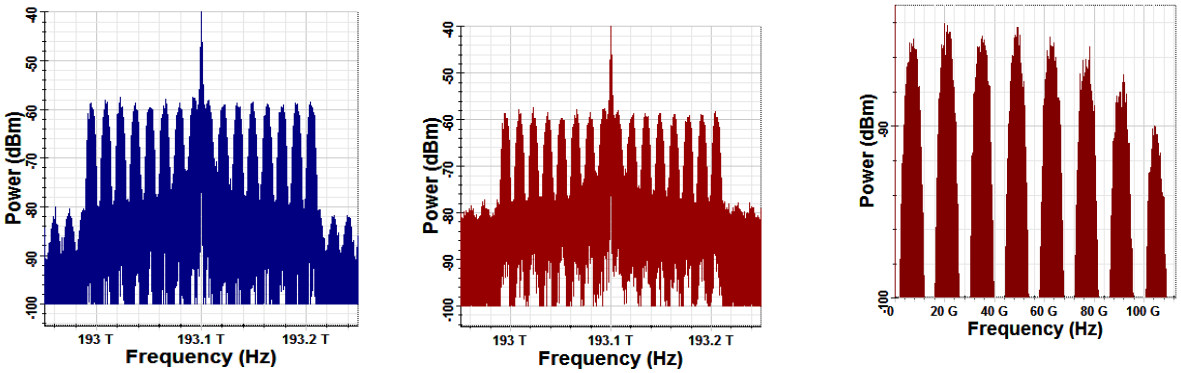

(d) Optical modulator output. (e) Fiber output. (f) photodiode output

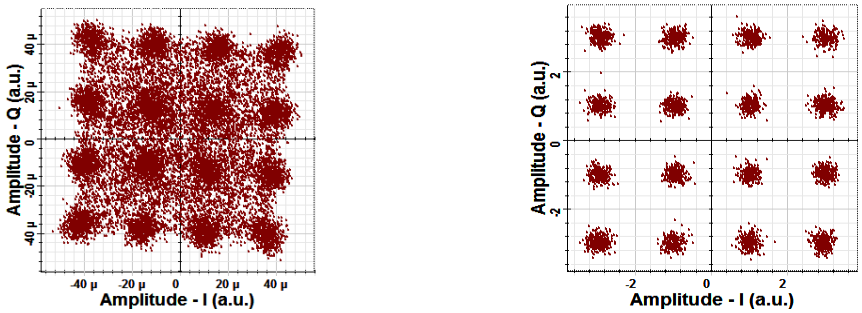

(g) Receiver Constellation diagram before DSP (SC4). (h) Receiver Constellation diagram after DSP(SC4)

Figure 4-4: (Continued).

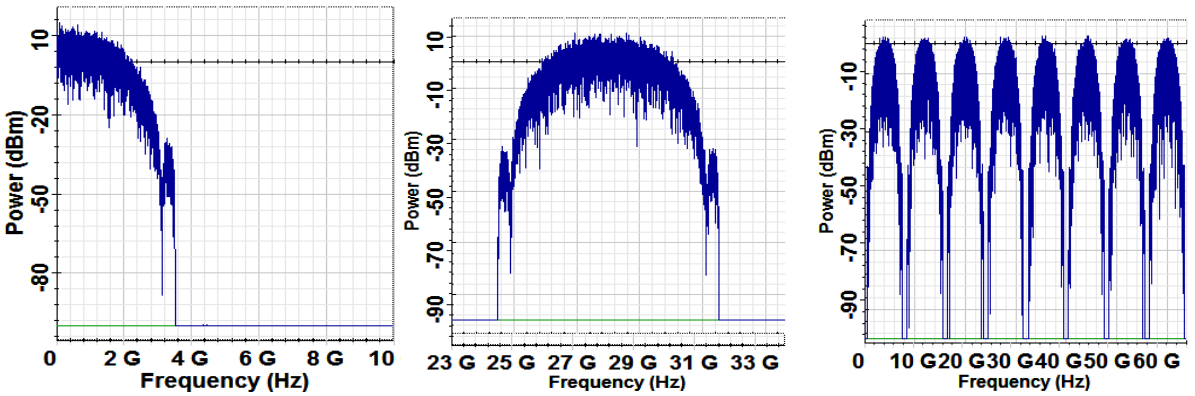

(a) Base band symbol spectrum. (b) RF quadrature modulator output (SC4). (c) RF MSC combiner output.

Figure 4-5: Signals spectra and receiver constellation diagrams for a dual-polarization multisubcarrier C-band transmitter operating with 50 km link, 16- QAM, singling optical channel (193.1 THz).

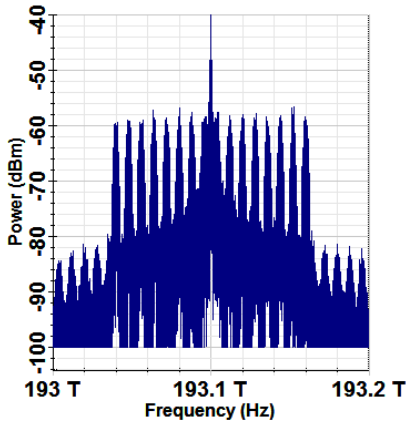

(d) Optical modulator output.

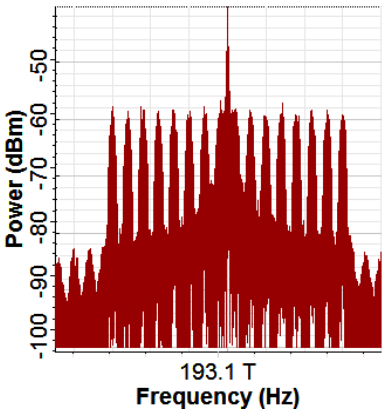

(e) Fiber output.

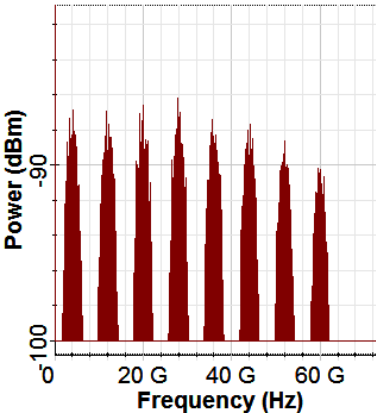

(f) photodiode output.

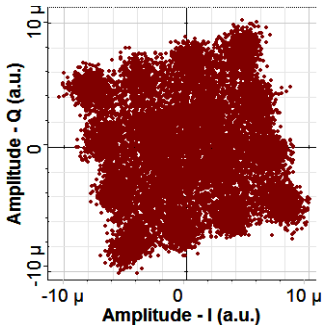

(g) Receiver Constellation diagram before DSP (SC4).

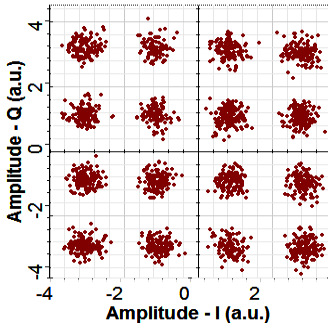

(h) Receiver Constellation diagram after DSP (SC4)

Figure 4-5: (Continued).

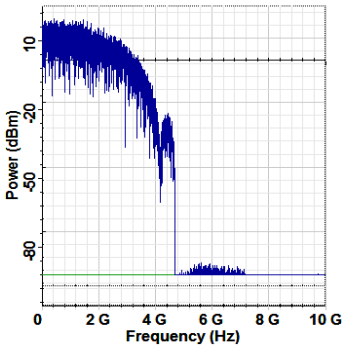

(a) Base band symbol spectrum.

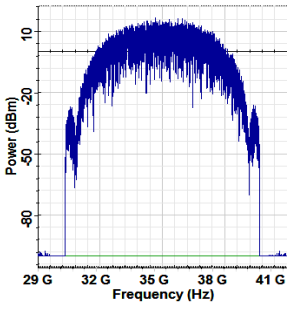

(b) RF quadrature modulator output (SC4).

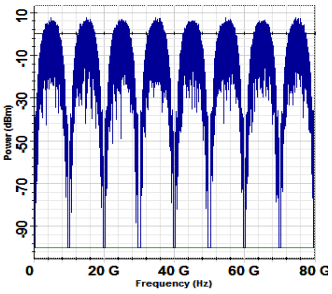

(c) RF MSC combiner output.

Figure 4-6: Signals spectra and receiver constellation diagrams for a single-polarization multisubcarrier C-band transmitter operating with 23 km link, 64- QAM, singling optical channel (193.1 THz).

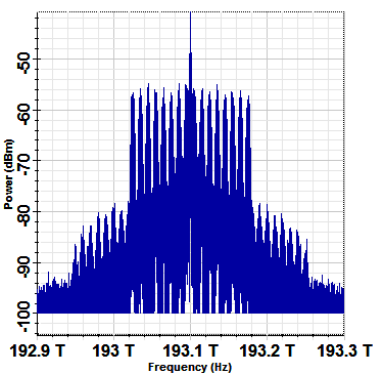

(d) Optical modulator output.

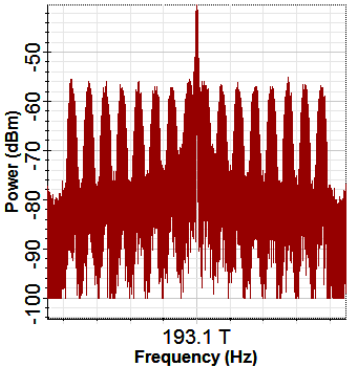

(e) Fiber output.

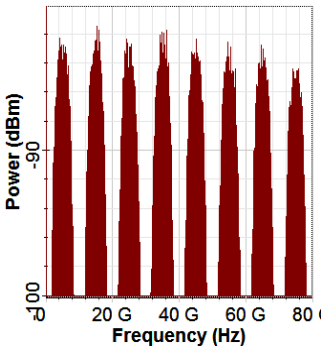

(f) photodiode output.

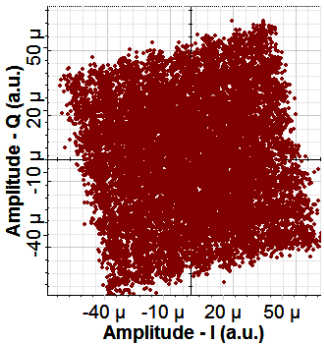

(g) Receiver Constellation diagram before DSP (SC4).

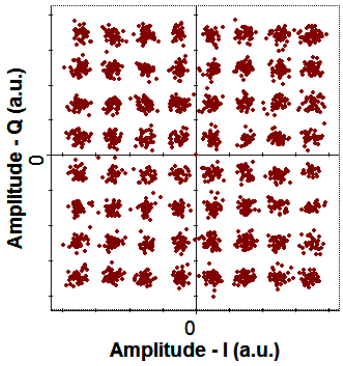

(h) Receiver Constellation diagram after DSP(SC4)

Figure 4-6: (Continued).

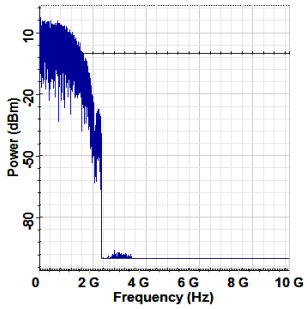

(a) Base band symbol spectrum.

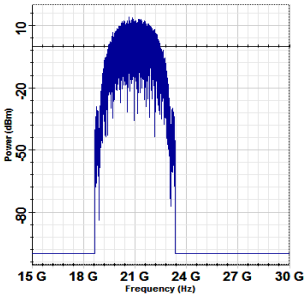

(b) RF quadrature modulator output (SC4).

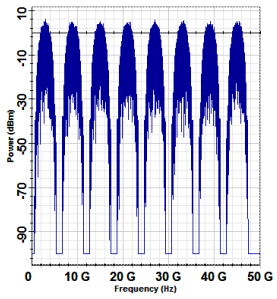

(c) RF MSC combiner output.

Figure. 4-7: Signals spectra and receiver constellation diagrams for a dual-polarization multisubcarrier C-band transmitter operating with 35 km link, 64- QAM, singling optical channel (193.1 THz).

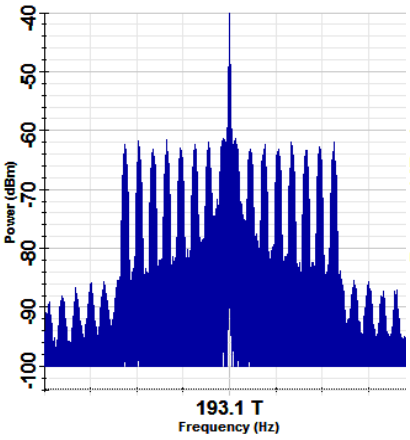

(d) Optical modulator output.

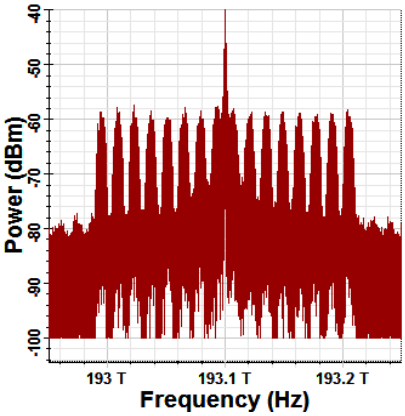

(e) Fiber output.

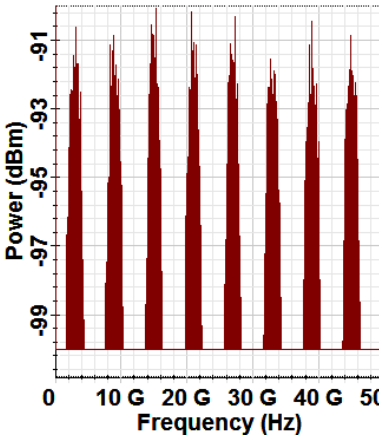

(f) photodiode output.

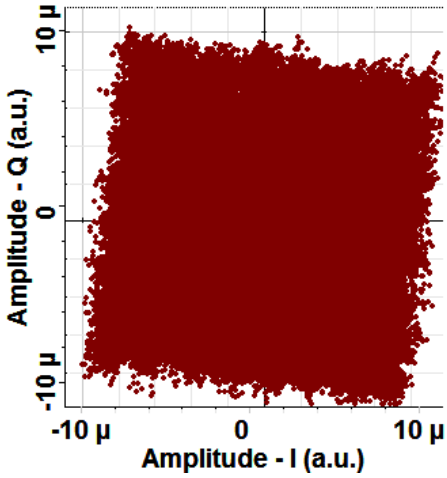

(g) Receiver Constellation diagram before DSP (SC4).

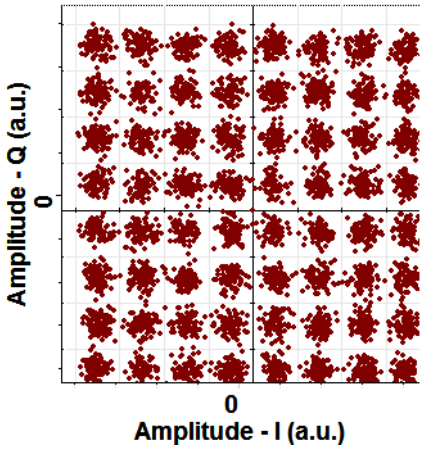

(h) Receiver Constellation diagram after DSP(SC4)

Figure 4-7: (Continued).

4.3.2 Optical Channel Spacing with Different Type of Networks

Table 4-1 lists the suitable values for the optical channel spacing Δf_{ch} that required to design the related WDM network. Note that both number of RF subcarriers and modulation order are affect the bandwidth of the modulated optical

carrier B_{mo}. In addition, Table 4-2 lists total bandwidth of the link with different type of WDM networks.

Table 4-1: WDM Channel spacing for different networks.

Number of subcarriers	**Optical channel spacing Δf_{ch} (GHz)**			
	16-QAM		**64-QAM DP**	
	SP	**DP**	**SP**	**DP**
4	**150**	**75**	**100**	**50**
8	**250**	**150**	**200**	**100**

Table 4-2: Total bandwidth of the link in different networks.

No. subcarriers	**No. WDM channels**	**Total bandwidth (GHz)**			
		16-QAM		**64-QAM**	
		SP	**DP**	**SP**	**DP**
4	4	**600**	**300**	**400**	**200**
	8	**1200**	**600**	**800**	**400**
	16	**2400**	**1200**	**1600**	**800**
8	4	**1000**	**600**	**800**	**400**
	8	**2000**	**1200**	**1600**	**800**

4.3.3 P2P WDM Optical Networks

i. 16-QAM 4-SC WDM Networks

The design of WDM networks uses a WDM multiplexer in the transmitter side and a WDM demultiplexer in the receiver side with optical channel spacing as calculated from equ. 3.7. For 16-QAM 4-SC WDM networks, 150 GHz channel spacing is used (as mentioned in Tabel 4-1). The transmitted and received WDM spectra are illustrated in Fig. 4-8 for N_{ch} = 4, 8, and 16. The receiver spectrum are recorded after maximum reach transmission.

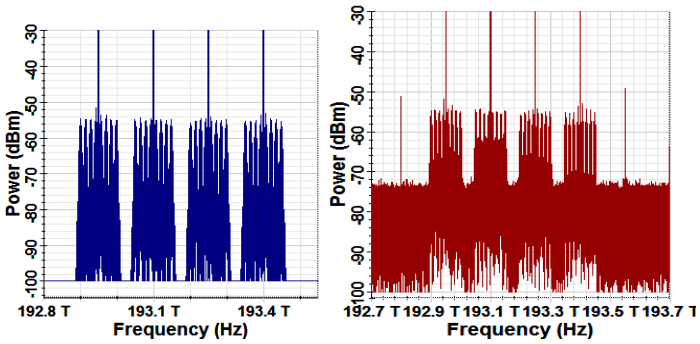

(a) N_{ch}= 4 and L=60 km.

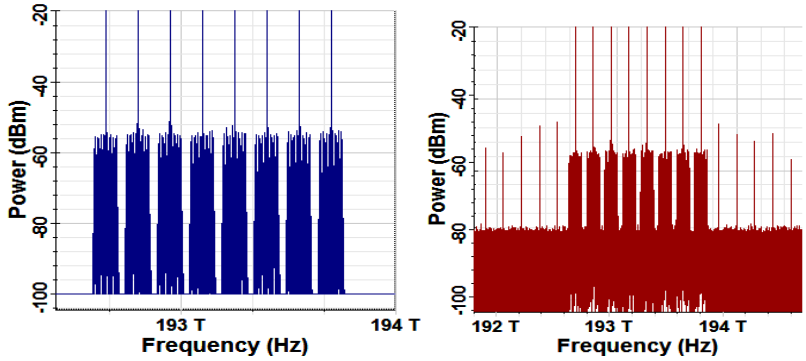

(b) N_{ch}=8 and L= 40km.

Figure 4-8: Transmitted (blue) and received (red) WDM signals for C band system operating with 150 GHz channel spacing and 4 subcarrier per channel.

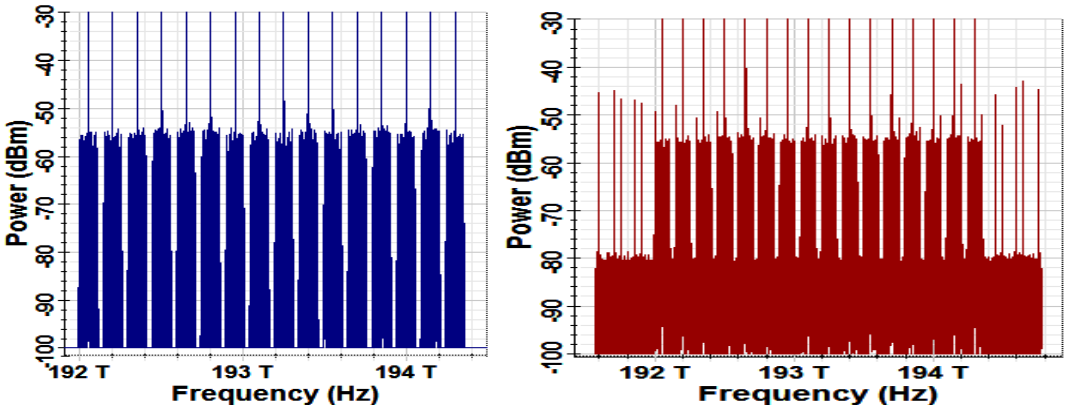

(c) N_{ch}=16 and L=28 km.

Figure 4-7: (Continued).

ii. 16-QAM 8-SC WDM Networks

The channel spacing is set to 250 GHz for 16-QAM signaling. Figure. 4-9 illustrates the optical spectrum at the WDM multiplexer output and WDM demultiplexer output for 4 and 8 optical WDM channels.

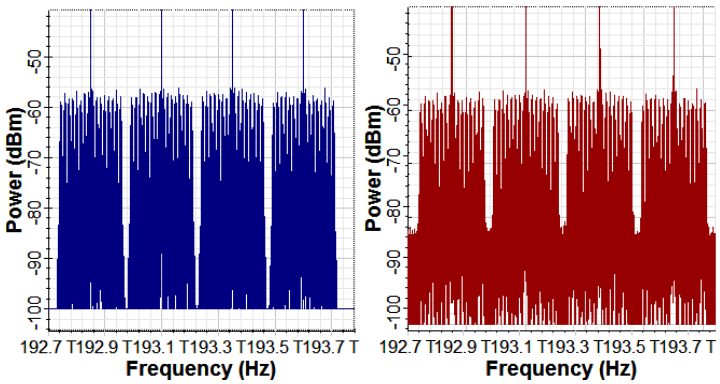

(a) N_{ch}= 4 and L=10 km.

Figure 4-9: Transmitted (blue) and received (red) WDM signals for C band system operating with 250 GHz channel spacing and 8 subcarrier per channel.

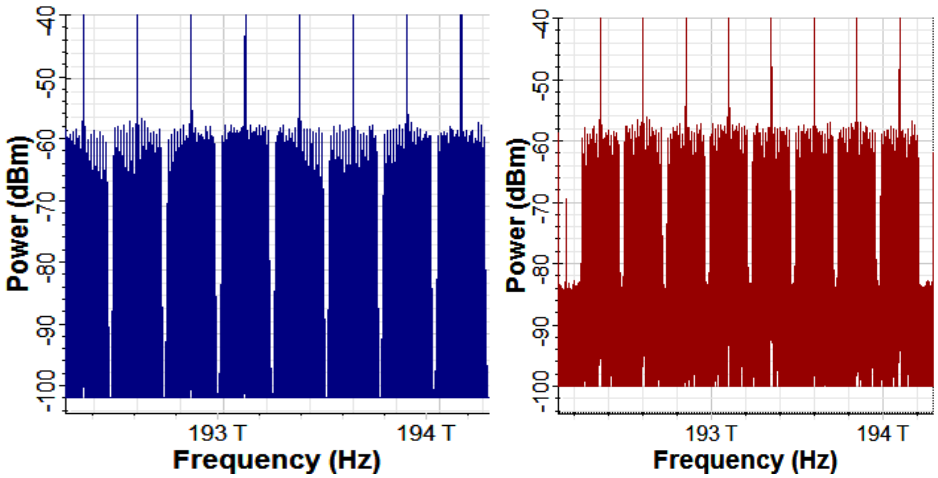

(b) N_{ch}=8 and L= 5 km.

Figure 4-8: (Continued).

iii. 64-QAM 4-SC WDM Networks

Figure. 4-10 displays the transmitted and received WDM signals spectra for 64-QAM 4-SC WDM networks having N_{ch} = 4, 8, and 16 channels. The transmission distance for 4, 8, and 16 channels are 50, 45, and 25, respectively. (See Table 4-1 for channel spacing).

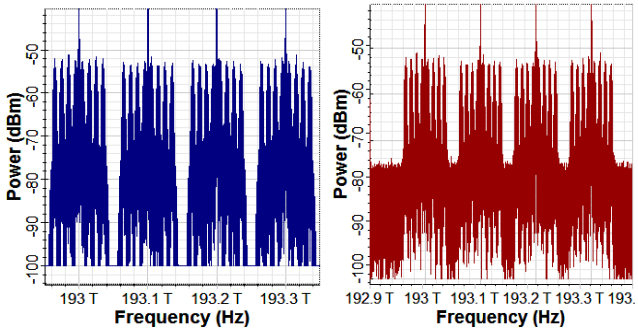

(a) N_{ch}= 4 and L=50 km.

Figure 4-10: Transmitted (blue) and received (red) WDM signals for C band system operating with 100 GHz channel spacing and 4 subcarrier per channel.

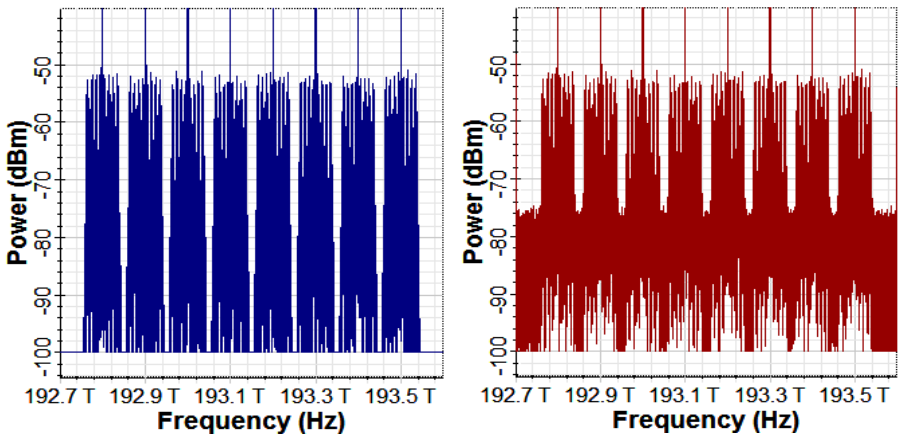

(b) N_{ch}=8 and L= 45 km.

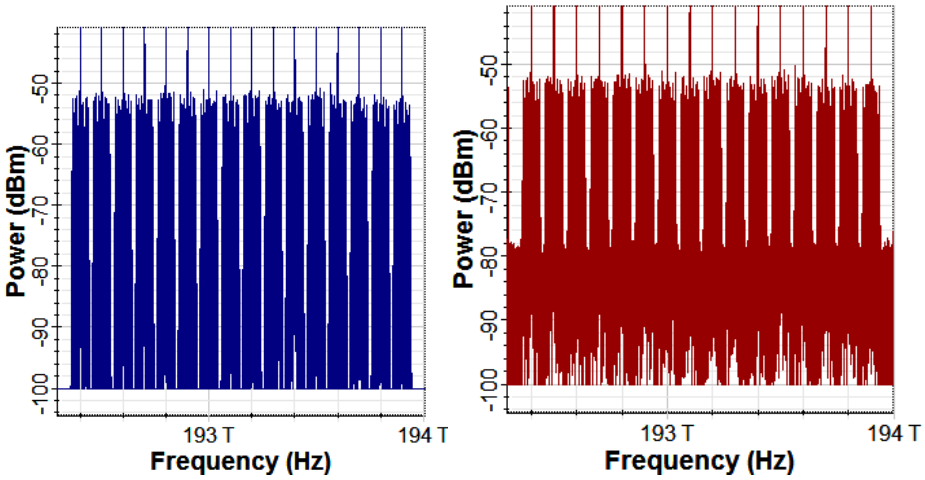

(c) N_{ch}=16 and L=25 km.

Figure 4-9: (Continued).

iv. 64-QAM 8-SC WDM Networks

The simulation performed in part iii is extended for the case of 8-SC WDM networks having N_{ch} = 4 and 8 channels. The transmission distance for 4-, and 8-channel network are 12 and 8 km, respectively. (See Table 4-1 for channel spacing).

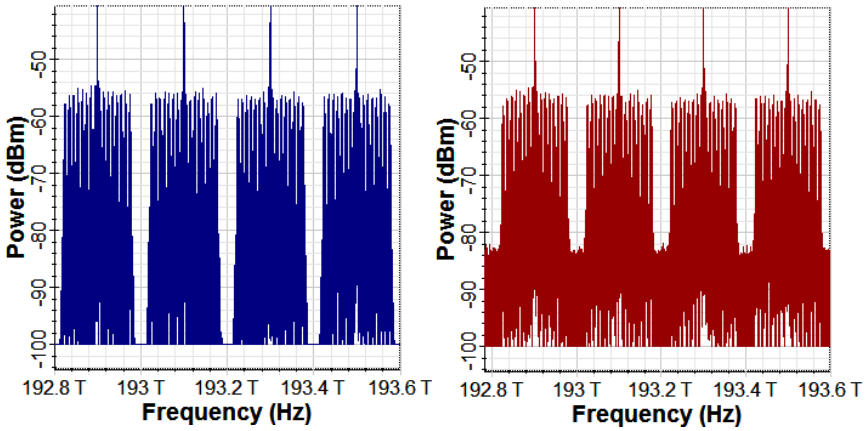

(a) N_{ch}= 4 and L=12 km.

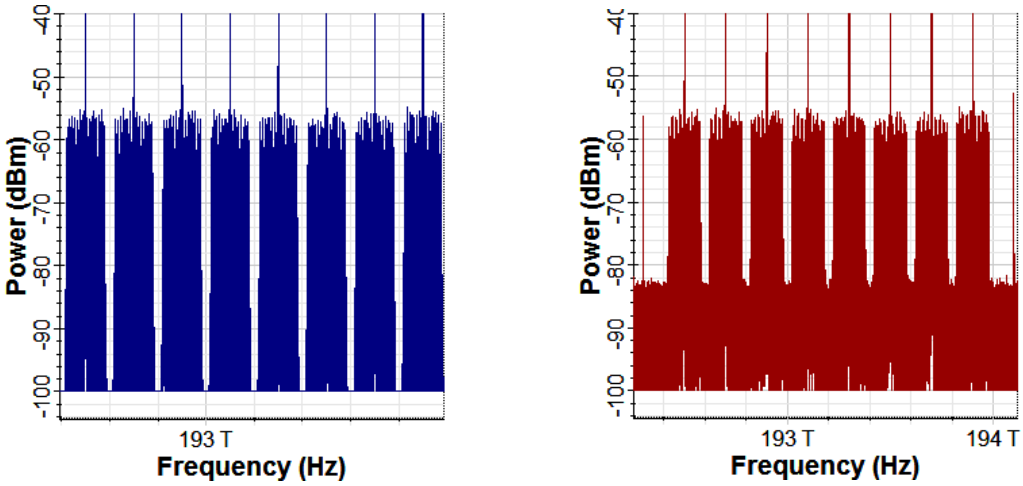

(b) N_{ch}=8 and L= 8km.

Figure 4-11: Transmitted (blue) and received (red) WDM signals for C band system operating with 200 GHz channel spacing and 8 subcarrier per channel.

v. Variation of Bit Error Rate With Transmission Distance for P2P Network

Figure 4-12 shows the variation of BER of the last subcarrier SC4 with transmission distance in 4-SC network and SC8 in 8-SC network. The simulation is performed for both SP and DP single-optical channel operating with C band 16-

QAM signaling. The maximum transmission reaching is estimated as the maximum SMF route length that yields a bit error rate (BER) < $(BER)_{th}$ for all the subcarriers. Here, BER_{th} denotes the threshold BER which is taken to 3.8×10^{-3} corresponding to 7% hard-decision (HD) forward error connection (FEC) code.

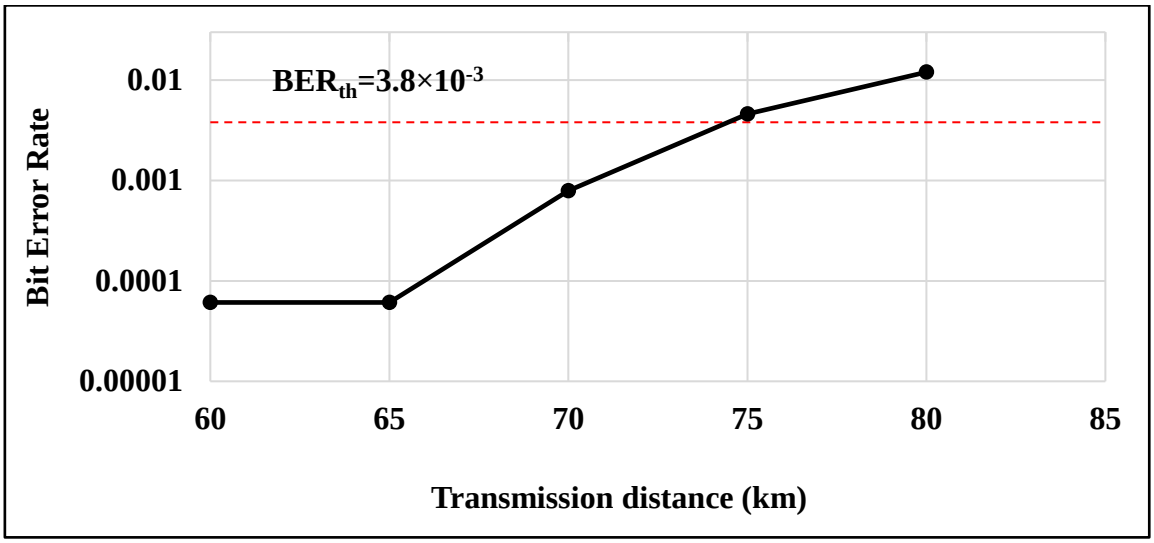

(a) SC4 SP.

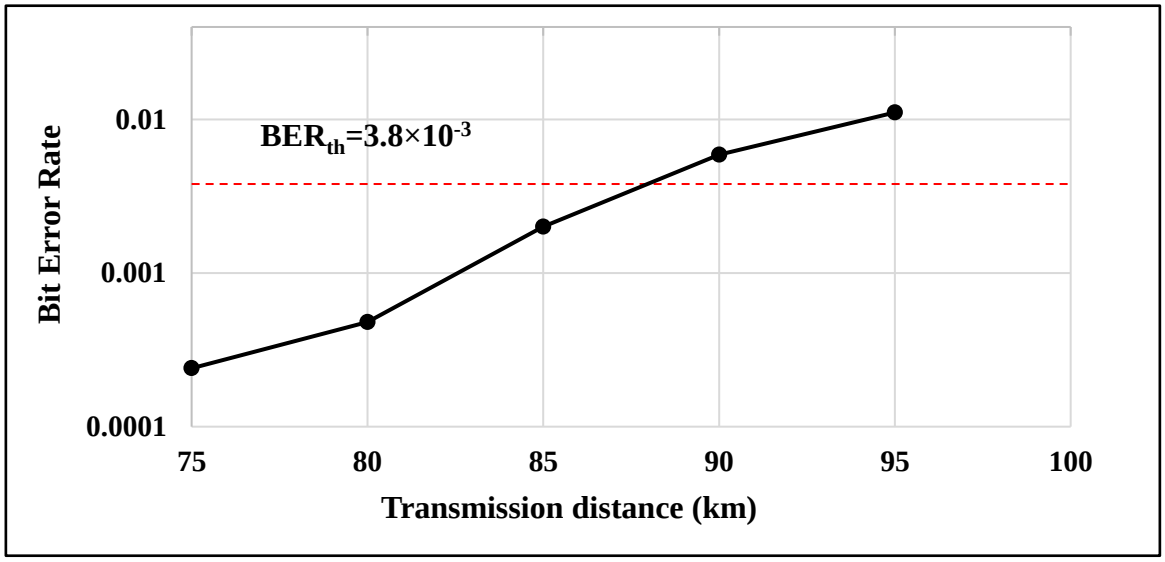

(b) SC4 DP.

Figure 4-12: Variation of BER with transmission length for 193.1 THz system operate with 16 QAM signaling

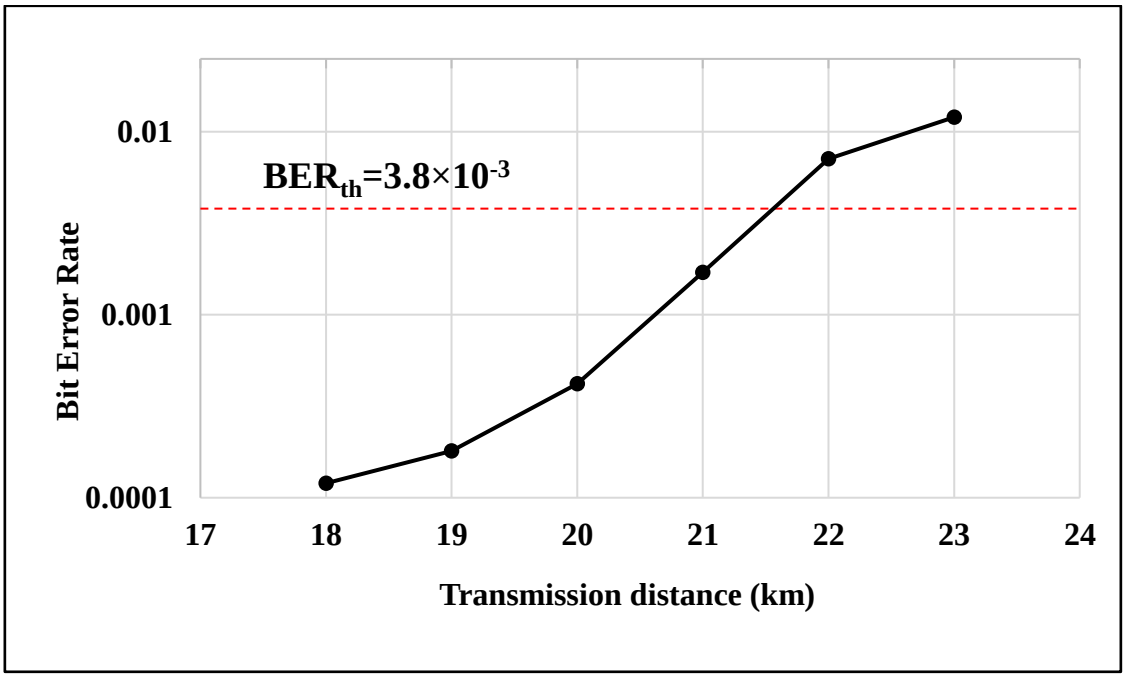

(c) SC8 SP.

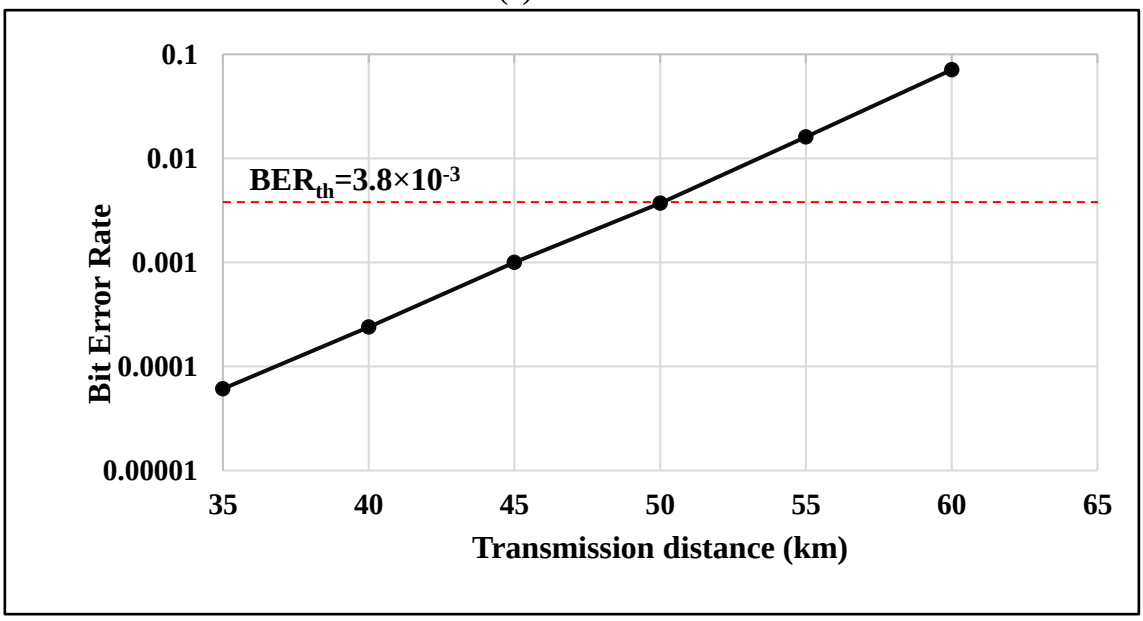

(d) SC8 DP.

Figure 4-12: (Continued).

4.4 Simulation Results for C-band P2MP Optical Networks

The transmitter side spectrum of P2MP network is the same as that of P2P counterpart because both networks use an identical transmitter configration. The tramission link for each user route in P2MP architecture consists of two cascaded parts, a primary part (common) for all users and an individual link (secondary) for each user. The receiver side consists of multiple receiving points each point has its own secondary link whose maximum distance ensuring that the corresponding BER does not exceed the threshold value (3.8×10^{-3}).

4.4.1 8-Subcarrier One-optical Channel P2MP Network

The spectrum of the optical signal for each subcarrier that incidents on its receiver photodiode is illustrated in Fig. 4-13 assuming 16-QAM DP (35km+5km) transmission link. The results indicate that the generated optical modulated RF subcarriers have conventional (IM) spectra sharing the same optical carrier.

Further investigation is carried out to estimate the user maximum reach L_{max} for both SP and DP P2MP network based on 16-QAM signaling. The results reveal that DP network reach longer distance than SP counterpart (L_{max} = 20 km and 40 km for SP and DP networks, respectively). Figures. 4-14 and 4-15, display a detailed investigation reflecting the variation of BER with the rout distance ($L_i = L_s + L_{bi}$) for SP (15km+5km) and DP (35km+5km) P2MP network, respectively. Here, the dependence of BER on the transmission distance L is recorded for each subcarrier.

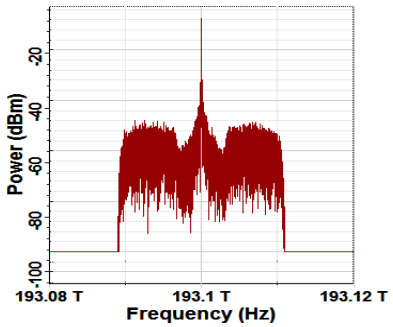

(a) SC1

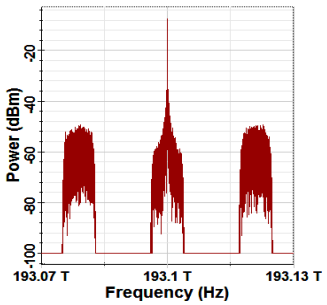

(b) SC2.

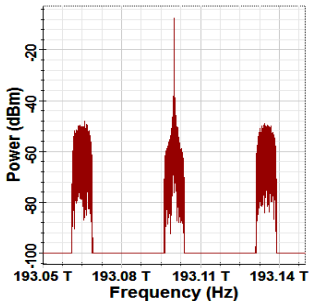

(c) SC3.

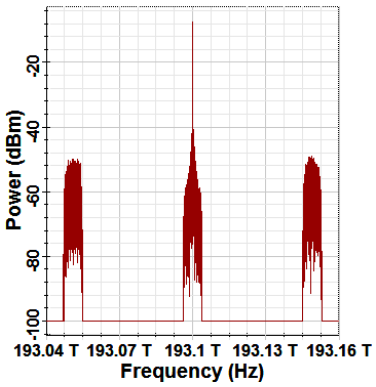

(d) SC4.

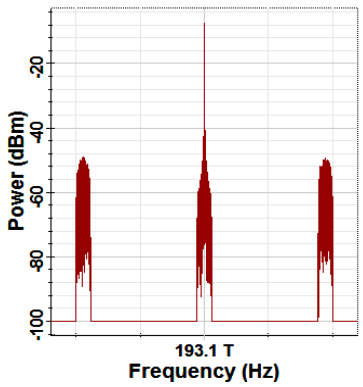

(e) SC5.

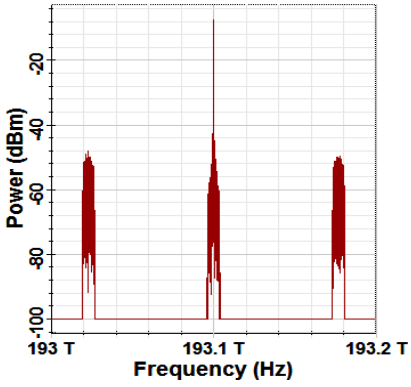

(f) SC6.

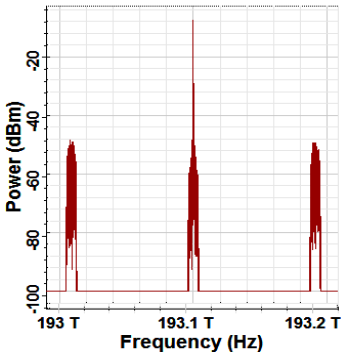

(g) SC7.

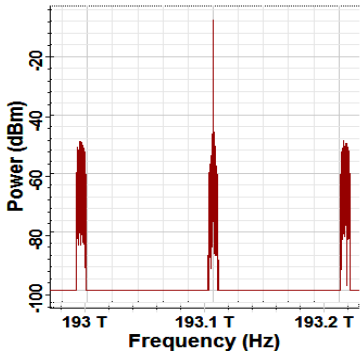

(h) SC8.

Figure 4-13: Received optical modulated subcarriers incident on the photodiodes for 193.1 THz DP 8-sub P2MP system operating with 16-QAM DP signaling and (35km+5km) transmission distance

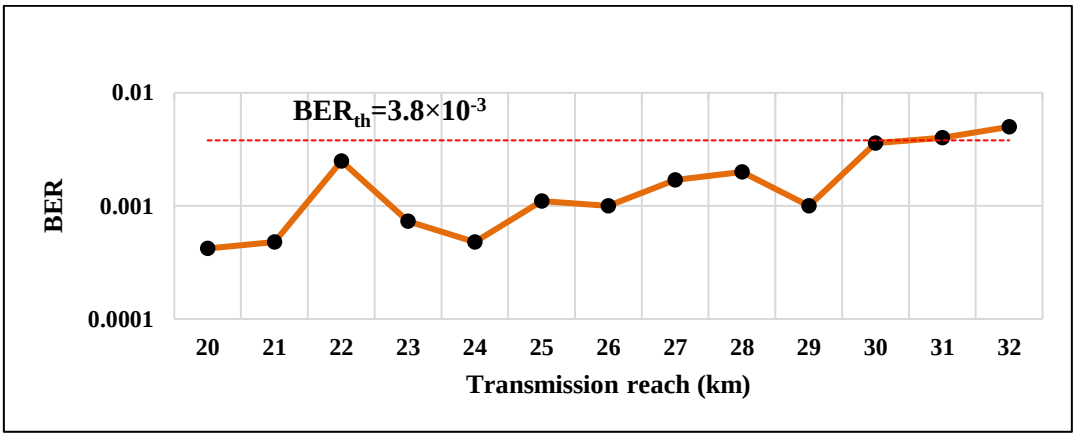

(a) SC1.

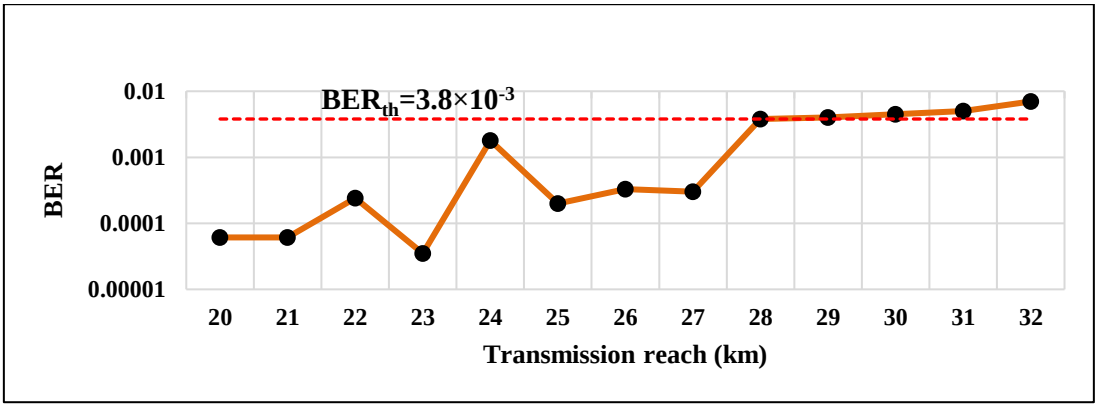

(b) SC2.

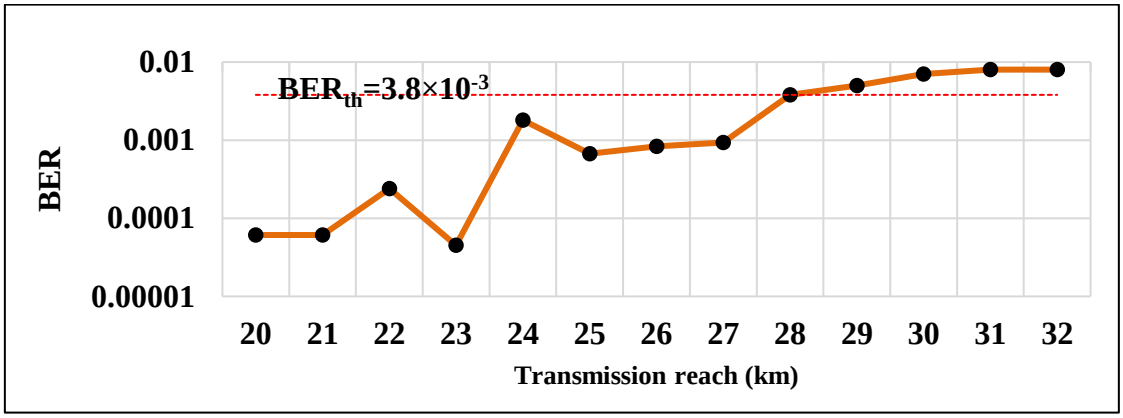

(c) SC3.

Figure. 4-14: Variation of BER of 8-SC SP system with transmission reach.

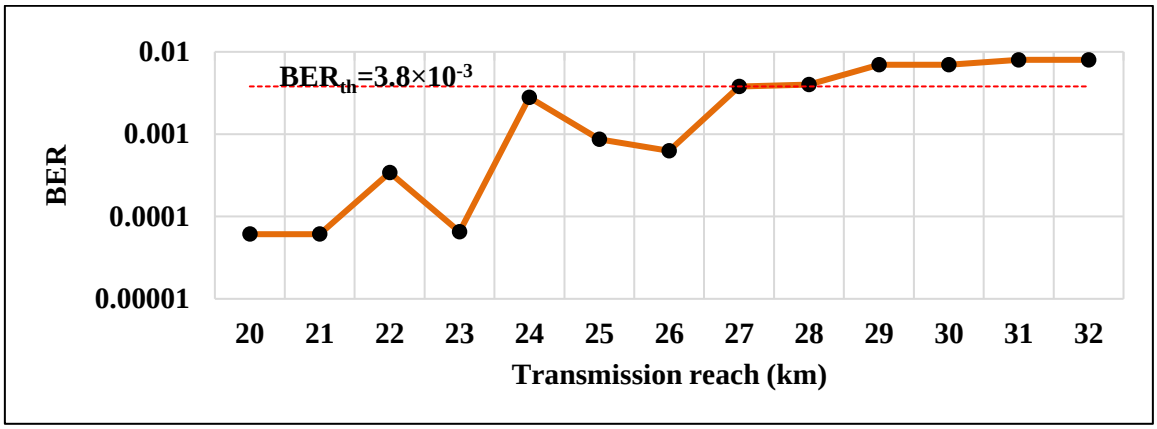

(d) SC4.

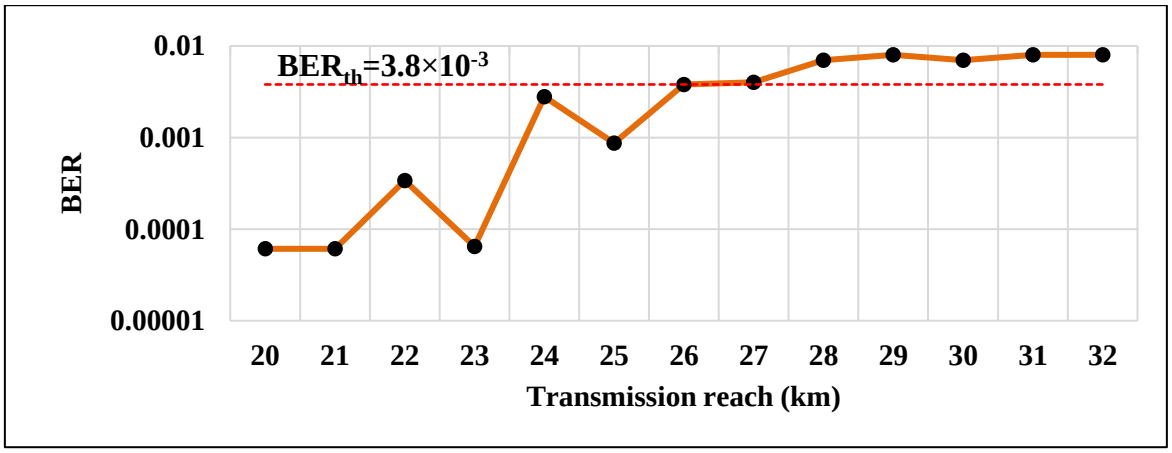

(e) SC5.

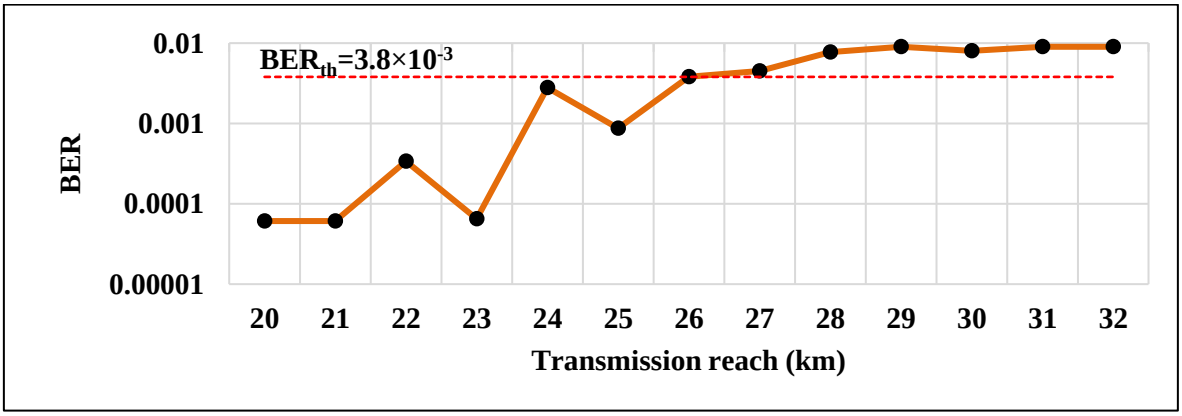

(f) SC6.

Figure 4-14: (Continued).

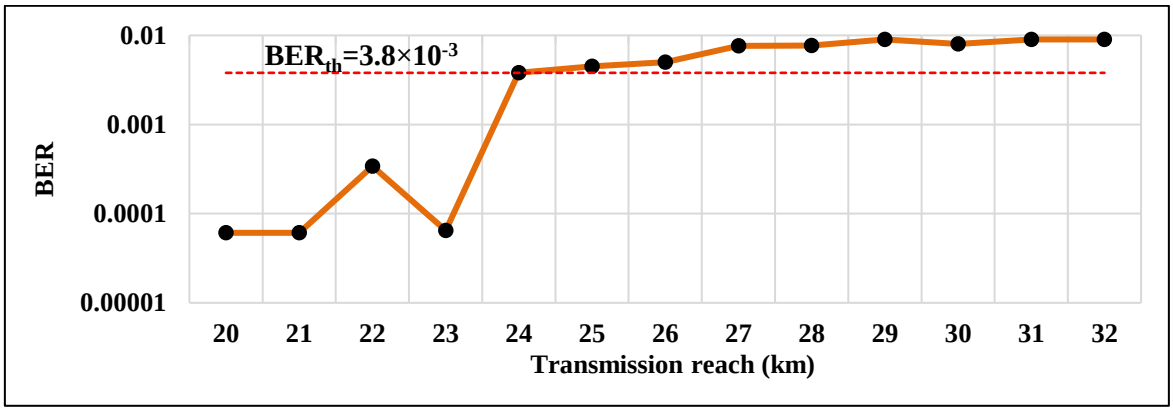

(g) SC7.

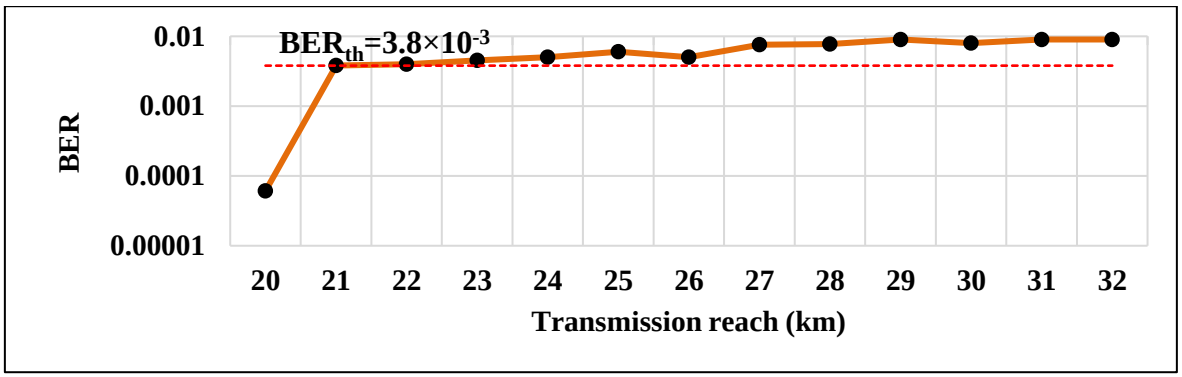

(f) SC8.

Figure 4-14: (Continued).

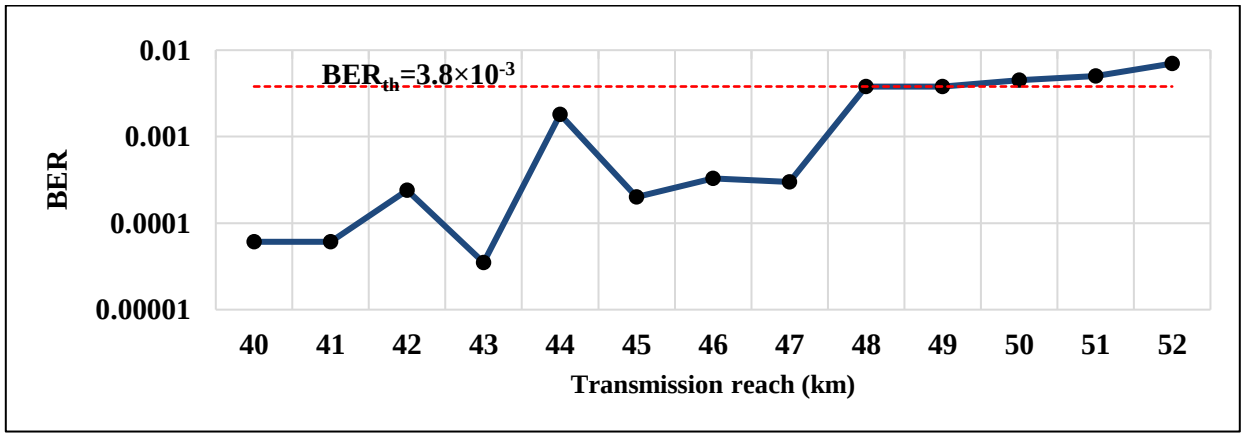

(a) SC1.

Figure 4-15: Variation of BER of 8-SC DP system with transmission reach.

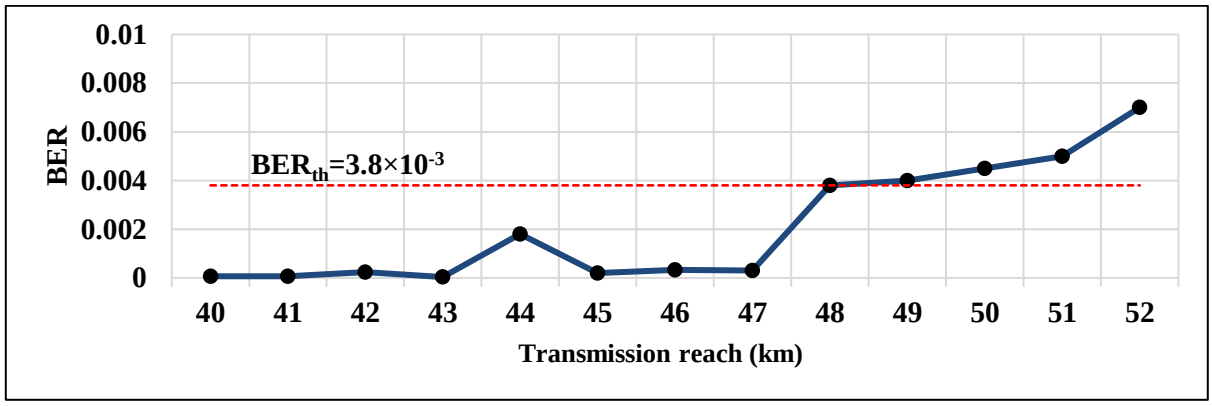

(b) SC2.

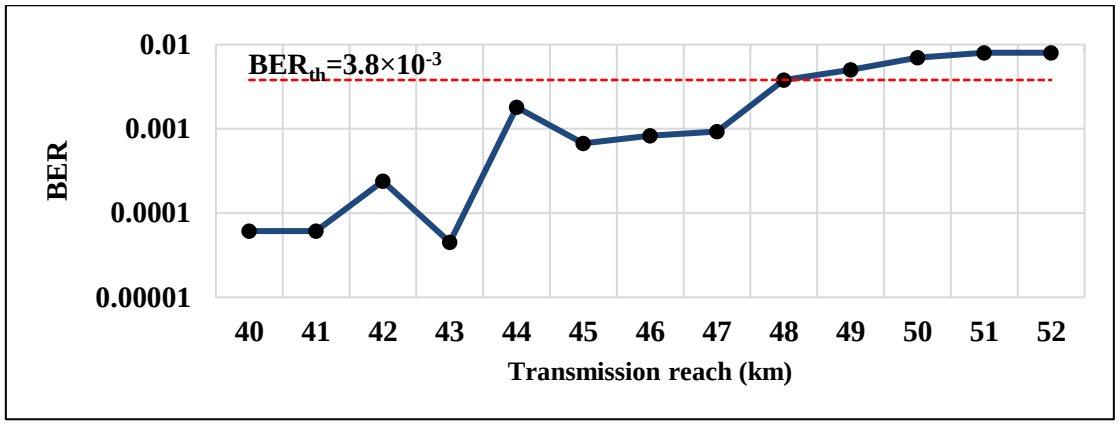

(c) SC3.

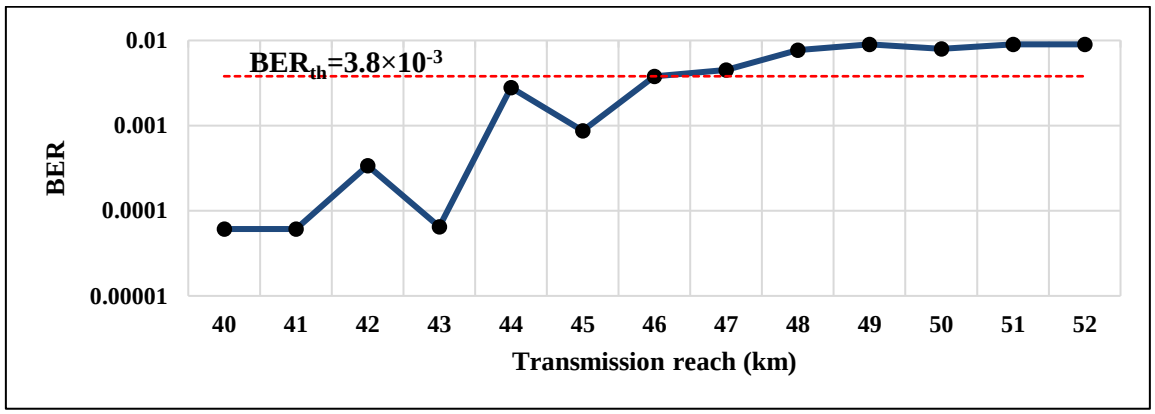

(d) SC4.

Figure 4-15: (Continued).

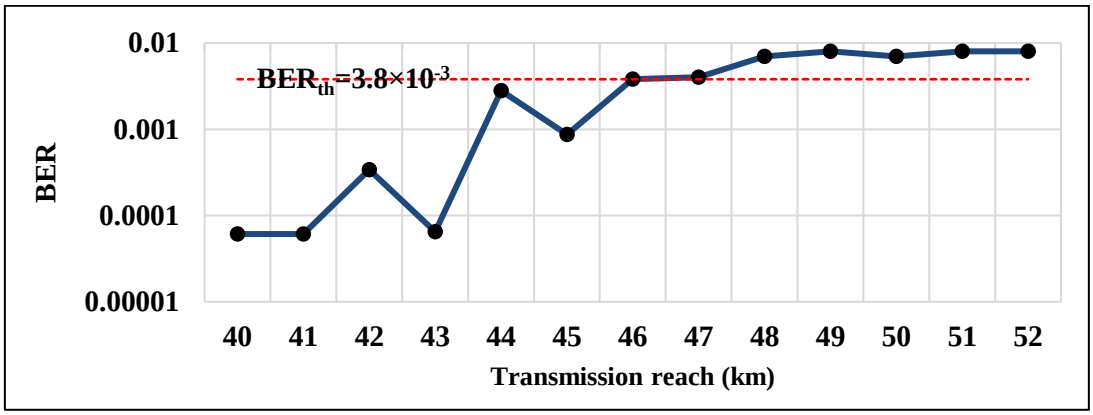

(e) SC5.

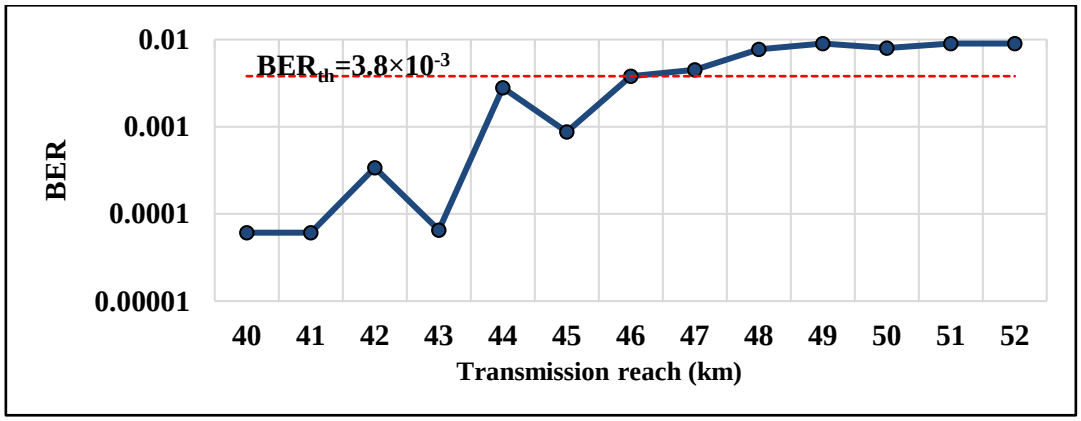

(f) SC6.

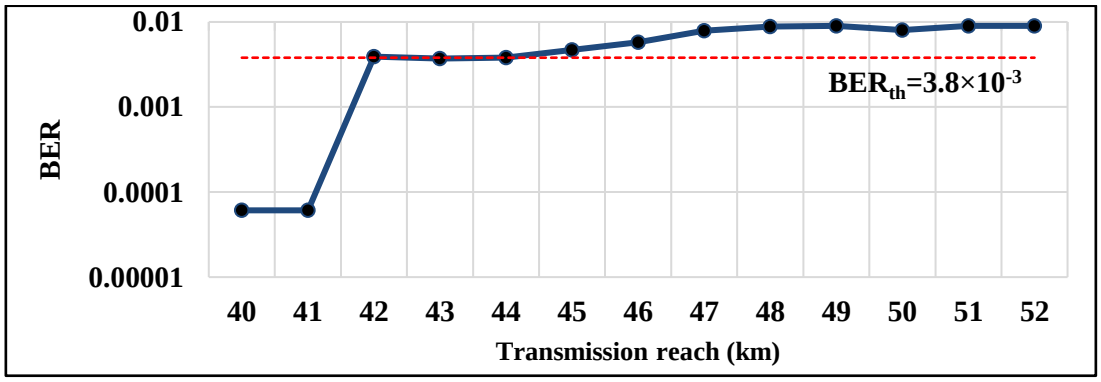

(g)SC7.

Figure 4-15: (Continued).

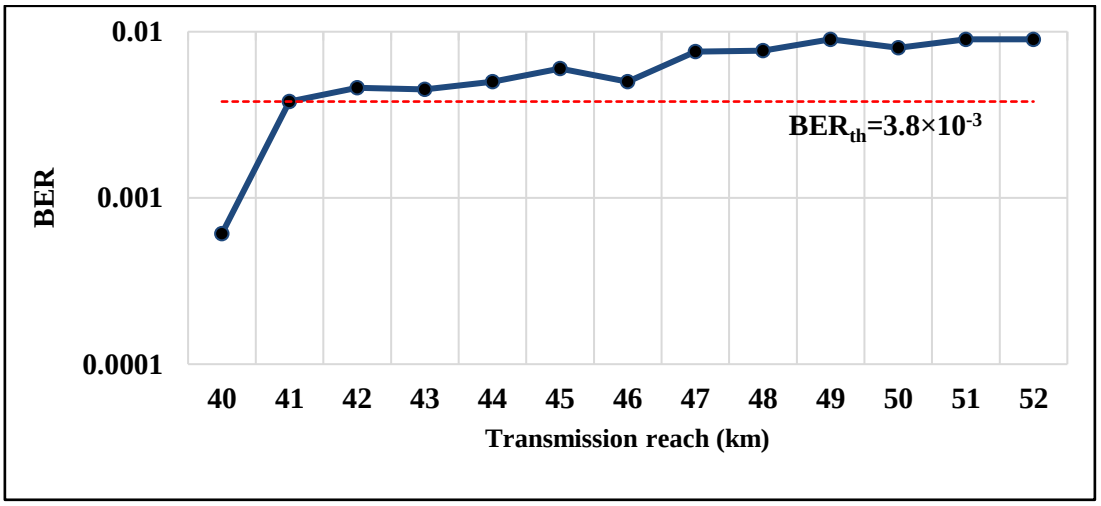

(i) SC8.

Figure 4-15: (Continued).

4.4.2 8-Subcarrier 4-Channel WDM P2MP Network

Like P2P WDM architecture, the P2MP counterpart uses a WDM multiplexer at the transmitter side and WDM demultiplexer at the receiver side. The receiver side of each optical channel also has an optical sideband demultiplexer (OSD) at its starting point that used to separate the spectrum of the upper and lower sidebands for each optically modulated RF subcarrier. These two bands are combined with the optical carrier and forwarded to each user. Figure 4-16 illustrates WDM channels that product from WDM demultiplexer and forward to 4 sides (each side has a OSD that separate optical channel to lower- and upper-sideband), this system operating in DP 16-QAM signaling.

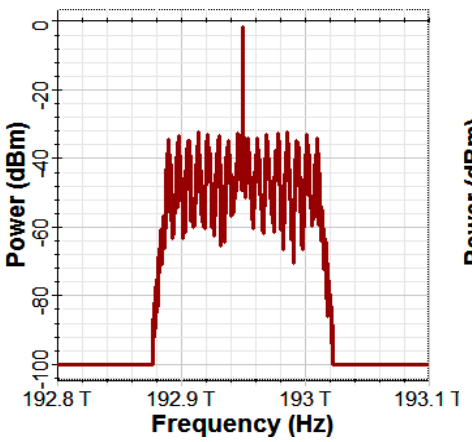

(a) Ch1.

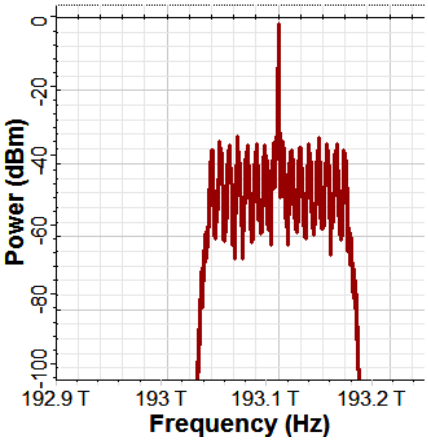

(b) Ch2.

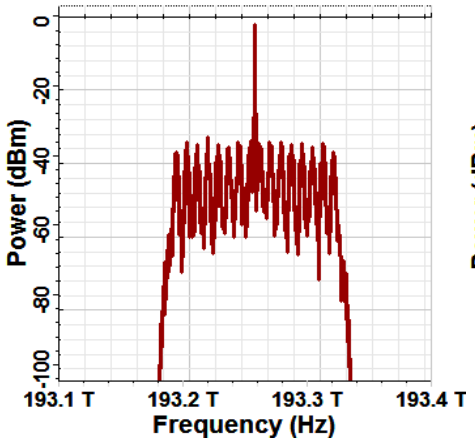

(a) Ch3.

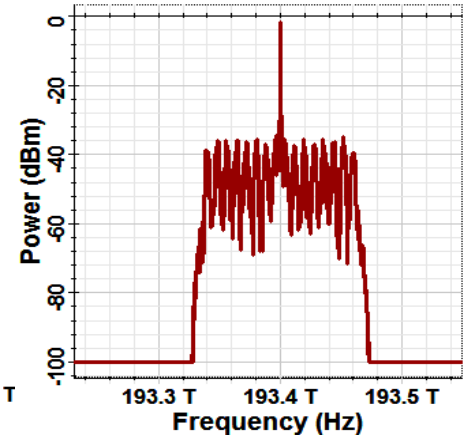

(b) Ch4.

Figure 4-16: Demultiplexing WDM channels

.

i. Transmission distance in 8-SC 4-channel P2MP Network

Figure 4-17 represents the variation of BER with the transmission distance for last subcarrier (SC8) in each optical channel. The investigation reveals that SC8 is the first subcarrier that becomes out of service as the distance increases. In other word, SC8 is the first subcarrier that yield BER > BER_{th} when transmission distance increases.

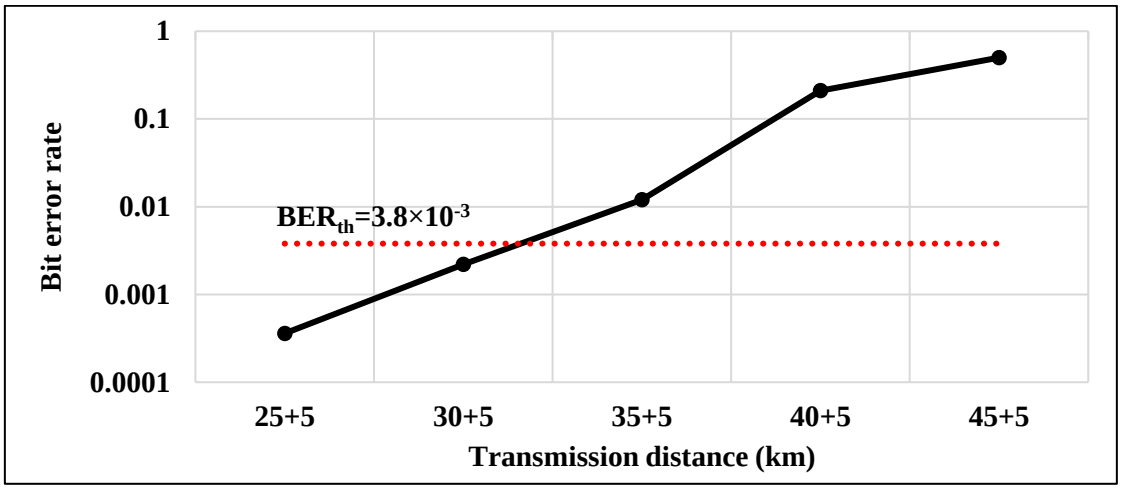

(a) SC8 ch1.

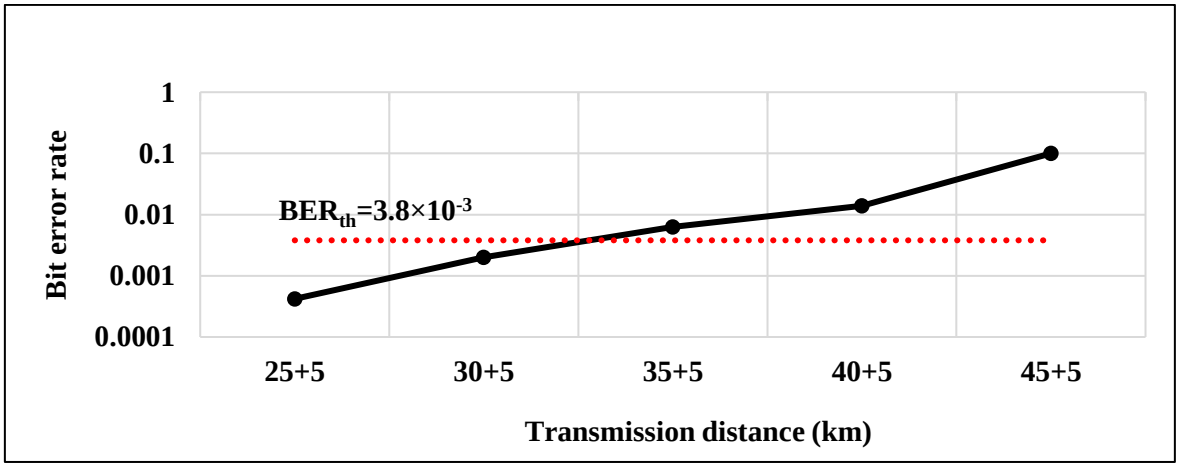

(b) SC8 ch2.

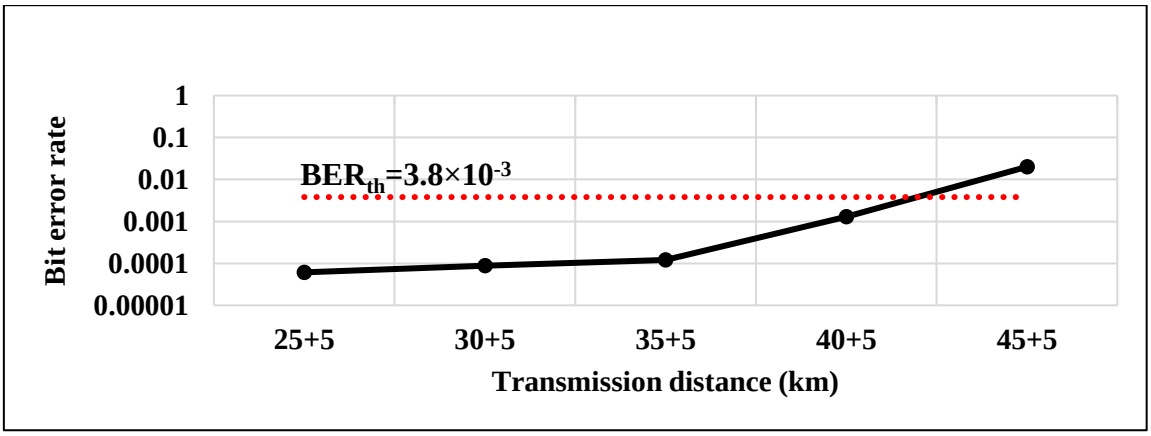

(c) SC8 ch 3.

Figure. 4-17: SC8 in 4 WDM channels operating with DP 16-QAM system.

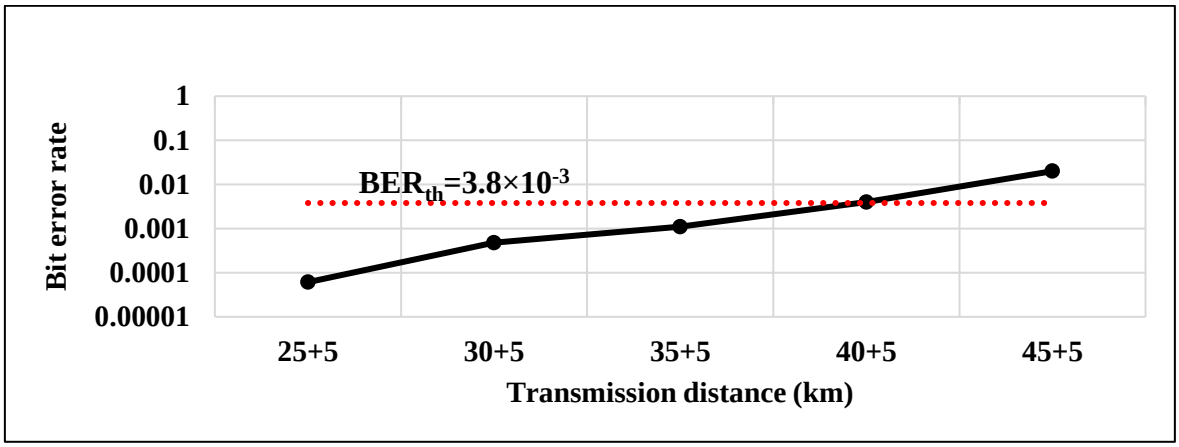

(d) Sub 8 ch 4.

Figure 4-17: (Continued).

4.5 Toward Unamplified C-band P2MP Network

The P2MP networks that simulated in the previous section using a single OA of 5 dB gain that inserted at the end of the primary link and connects the transmitter to the receiver OSD or WDM demultiplexer in cases of single-channel or WDM network, respectively. This OA is common for all subcarriers and WDM channels and can used to compensate, even partially, the link loss between the transmitter and the user. If only fiber link loss is considered, then the gain of the amplifier that used for fiber link loss compensation; can be computed from

$$G_a = \propto_{SMF} (L_{SMF1} + L_{SMF2}) + \propto_{DCF} (L_{DCF1} + L_{DCF2}) \quad (4.1)$$

where $\propto_{SMF}$ and $\propto_{DCF}$ is the loss parameter (dB/km) for SMF and DCF, respectively, and the fiber section length is measured in km. The subscript 1 and 2 is used to distinguish the primary link (common link) from the secondary links that connected the OSD to the subcarrier optical receivers. At 1550 nm wavelength, $\propto_{\mathrm{SMF}} = 0.2$ dB/km, $\propto_{\mathrm{DCF}} = 0.5$ dB/km, D_{SMF}= 17 ps/(nm km), and

D_{DCF} = -85 ps/(nm.km) as given in Table 3-2. From equ. 3.17, $L_{DCF} = -\frac{D_{SMF}L_{SMF}}{D_{DCF}} = 0.2\ L_{SMF}$. For (15km+5km) link used in SP 16-QAM system, G_a = 0.2(15+5) + 0.5×0.2(15 + 5) = 4+2 = 6 dB. If the length of secondary link is negligible for any rout, then G reduces to 4.5 dB. In the simulation presented in Sections 4.2-4.4, and G_a is set to 5 dB as a balance between the losses of longest and shortest links.

Erbium-doping fiber amplifier (EDFA) is usually used for fiber amplification in C-band optical communication systems and networks. The EDFA is a piece of fiber whose core is doped with erbium (Er) and need an optical pumping at 1480 nm wavelength. Since the required gain is relatively low, one can go to another designed scheme which does not use an OA, but adopting higher laser power. In this case, the scheme is called unamplified P2MP network.

The BER performance of unamplified SP (15km+5km) P2MP networks is investigated as a function of CW-laser power P_L assuming N_{sc} = 8, N_{ch} = 1 and 16=QAM signaling. In this investigation, the received BERs of all 8 subcarriers are kept under observation. The results reveal that P_L = 0 dB can support the operation of this unamplified SP (15km+5km) P2MP as listed in Table 4-3.

The BER performance of unamplified DP (35+5) P2MP network is also simulated as a function of laser power P_L. In this scenario, received BERs of all subcarriers are kept under observation. Figures 4-18 a-d show the variation of BER with P_L for subcarriers 1, 6, 7, and 8, respectively, for N_{sc}=8, N_{ch}=1 and 16-QAM signaling. The results for all subcarriers are listed in Table 4-4. The red-colored numbers indicate that the BER exceeds the threshold BER of 3.8×10^{-3}.

Investigation the results in this table indicates that increasing P_L from 0 to 5 dB will ensure a satisfactory BERs for all the 8 SCs of the unamplified network.

Table 4-3: BER characteristics of unamplified 8-SC SP 16-QAM (15km+5km) P2MP network at P_L = 0 dB.

Subcarrier	BER
1	6.1×10^{-4}
2	1.8×10^{-4}
3	1.2×10^{-4}
4	7.1×10^{-5}
5	6.5×10^{-5}
6	6.6×10^{-5}
7	6.3×10^{-5}
8	9.1×10^{-4}

Table 4-4: Received subcarrier BERs for unamplified (35km+5km) P2MP network operating with DP 16-QAM format.

SC	Laser Power (dB)					
	0	1	2	3	4	5
1	**4×10^{-3}**	2.9×10^{-3}	5.4×10^{-4}	7.9×10^{-4}	2.4×10^{-3}	4.2×10^{-4}
2	1.4×10^{-3}	5.4×10^{-4}	1.8×10^{-4}	3.6×10^{-4}	2.4×10^{-4}	1.2×10^{-4}
3	1.2×10^{-3}	6.7×10^{-4}	6.1×10^{-5}	6.1×10^{-5}	3.6×10^{-4}	6.1×10^{-5}
4	2.4×10^{-3}	6.1×10^{-4}	6.1×10^{-5}	6.1×10^{-5}	1.8×10^{-4}	6.1×10^{-5}
5	1.7×10^{-3}	1.4×10^{-3}	6.1×10^{-4}	6.1×10^{-4}	2.4×10^{-4}	6.1×10^{-5}
6	**2.5×10^{-2}**	**1.3×10^{-2}**	**7.1×10^{-3}**	3.8×10^{-3}	2.5×10^{-4}	7.9×10^{-4}
7	**3.7×10^{-2}**	**2×10^{-2}**	**7.6×10^{-3}**	**5.2×10^{-3}**	3×10^{-3}	2.1×10^{-3}
8	**5.4×10^{-2}**	**3×10^{-2}**	**1.6×10^{-2}**	**1.0×10^{-2}**	**5×10^{-3}**	3.3×10^{-3}

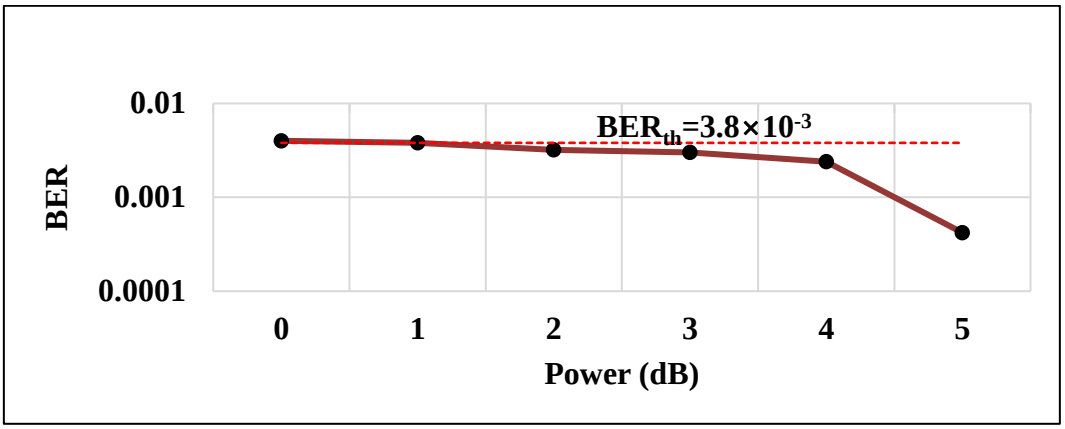

(a) SC1

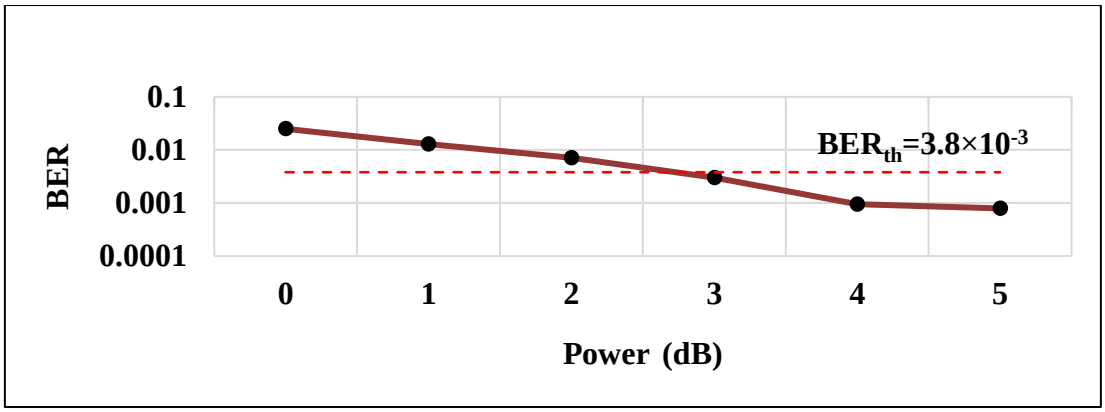

(b) SC6

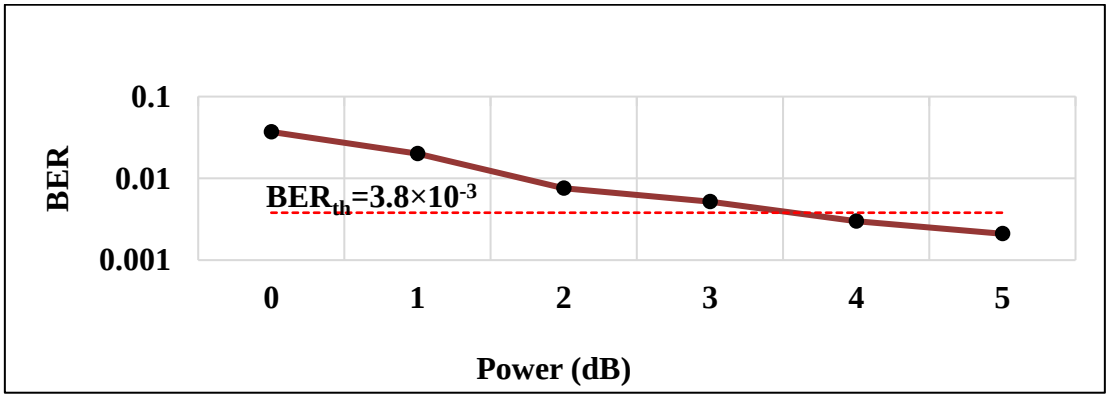

(c) SC7

Figure. 4-18: Variation of BERs of different subcarriers with laser power for DP 16-QAM (35km+5km) P2MP network.

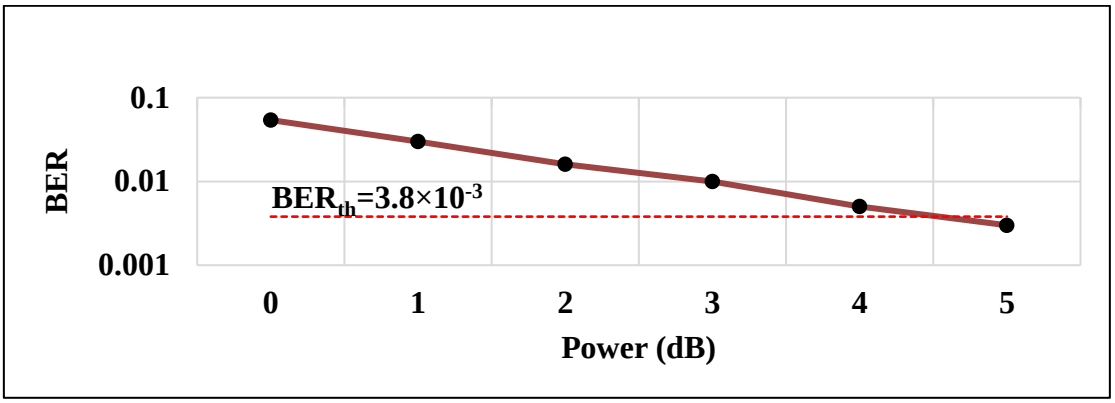

(d) SC8

Figure. 4-18: (Continued).

4.6 Simulation Results for O-Band P2P and P2MP Optical Networks

This section presents simulation results for O-band P2P and P2MP networks incorporating a single optical channel or WDM configuration and supported by digital MSC technique. In O band, the network has maximum reach longer than the C-band counterpart because of the negligible GVD of the fiber in O band. The center frequency in the simulation of O band is set to 228.5 THz (≈1310 nm).

4.6.1 Single Optical Channel O-band Networks

Figure 4-19 illustrates the maximum reach for a single-optical channel networks designed with different values of subcarriers (1, 4, 8, and 16). Results are represented for both 16- and 64-QAM signaling and for both SP and DP architectures. The values display that the 16-QAM has a longer reach than 64-QAM counterpart.

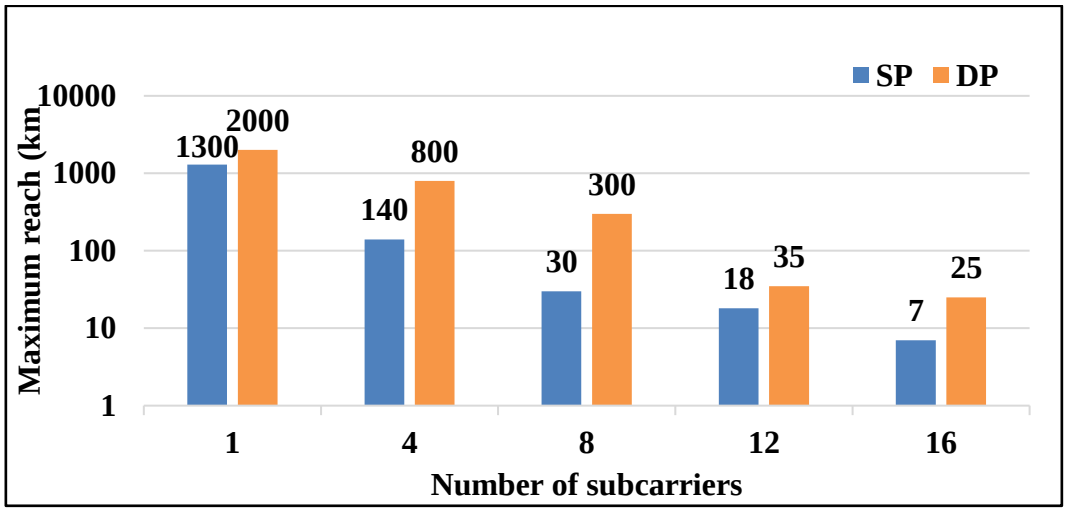

(a)

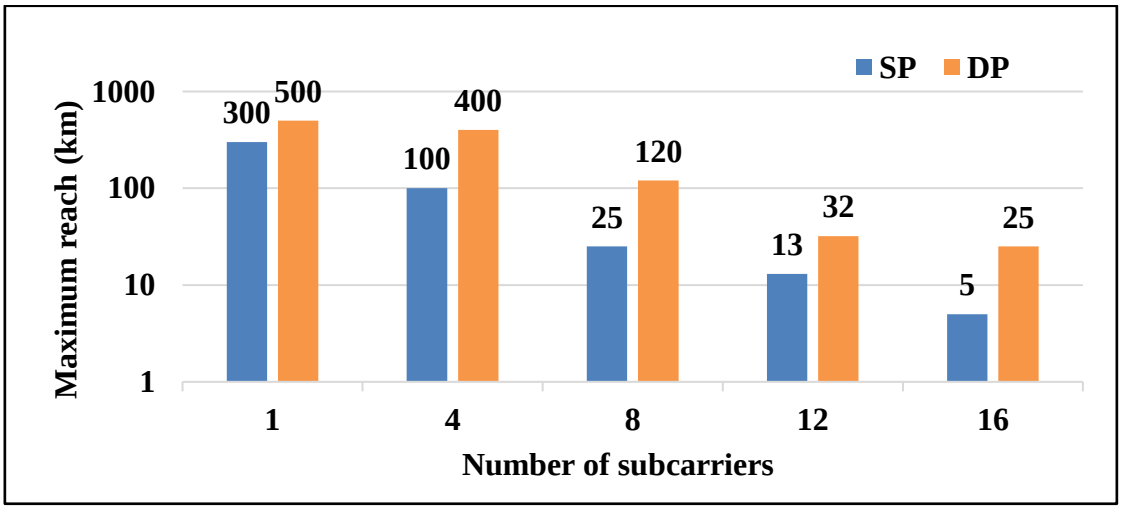

(b)

Figure 4-19: Maximum reach of a single-channel O-band transmission network. (a) 16-QAM signaling. (b) 64-QAM signaling.

4.6.2 O-band WDM Networks

O-band WDM networks are designed and simulated in this section. The designed architectures have 4- and 8-SC 4-Ch WDM and 4- and 8-SC 8-Ch WDM, also 4-SC 16-Ch WDM. The maximum reaches of these WDM networks,

are depicted in Figs. 4.20 1-c for N_{ch} = 4, 8, and 16, respectively. Note that the O-band offers longer maximum reach than the C-band counterpart.

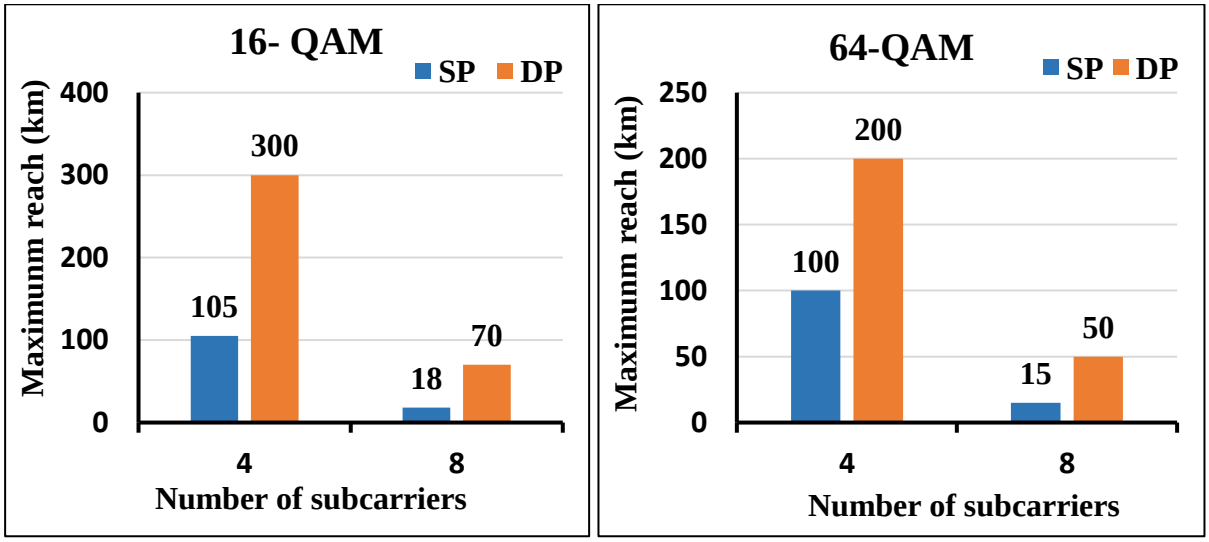

(a) N_{ch} = 4

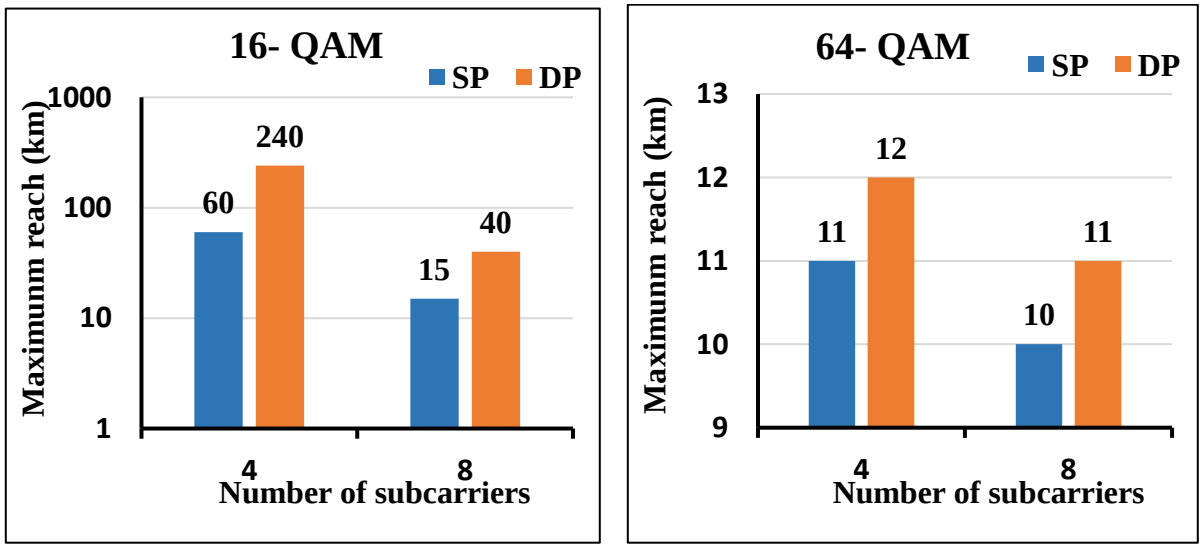

(b) N_{ch} = 8.

Figure 4-20: Maximum reach for O- band WDM transmission system.

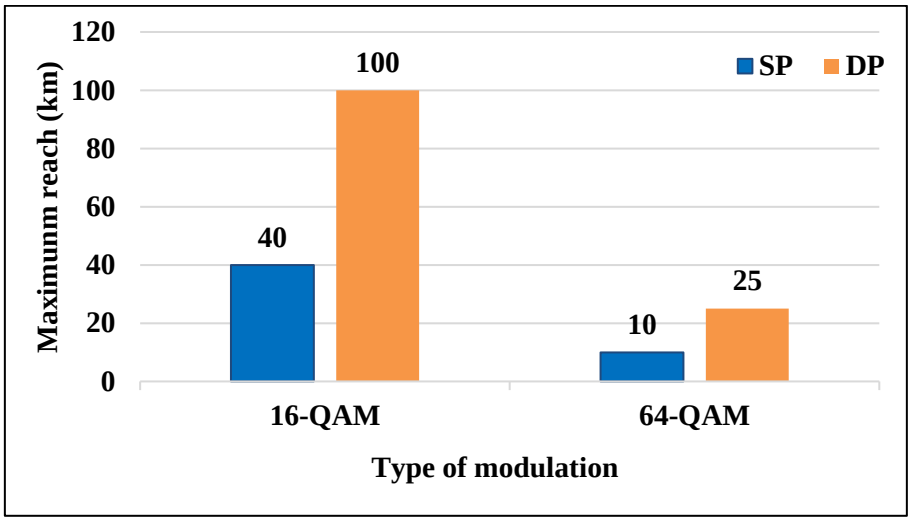

(c) Nch = 16.

Figure 4-19: (Continued).

4.6.3 Going to 128-QAM in O-band Networks

The design of the P2P and P2MP optical networks in the O band can support higher-order modulation such as 128-QAM. This issue is addressed in this subsection. Since the SMF has a negligible GVD at O-band wavelength, a 128-QAM signaling is run successfully on O-band P2P network using N_{sc} = 1, 4, 8, 12, and 16 for both SP and DP architecture. Figure 4-21 shows the maximum transmission distance for 128-QAM SP and DP P2MP networks. Figure 4-22 illustrates the spectra and received constellation diagrams for the 16-SC network; the signals spectra are for transmitter and receiver sides with its constellation diagrams for SC1, SC8, and SC16. Note that the network uses symbol rate of 3.571 and 1.785 Gbaud for SP and DP architecture, respectively. Here the subcarrier spacing is set to 8 and 4 GHz for SP and DP, in consequence.

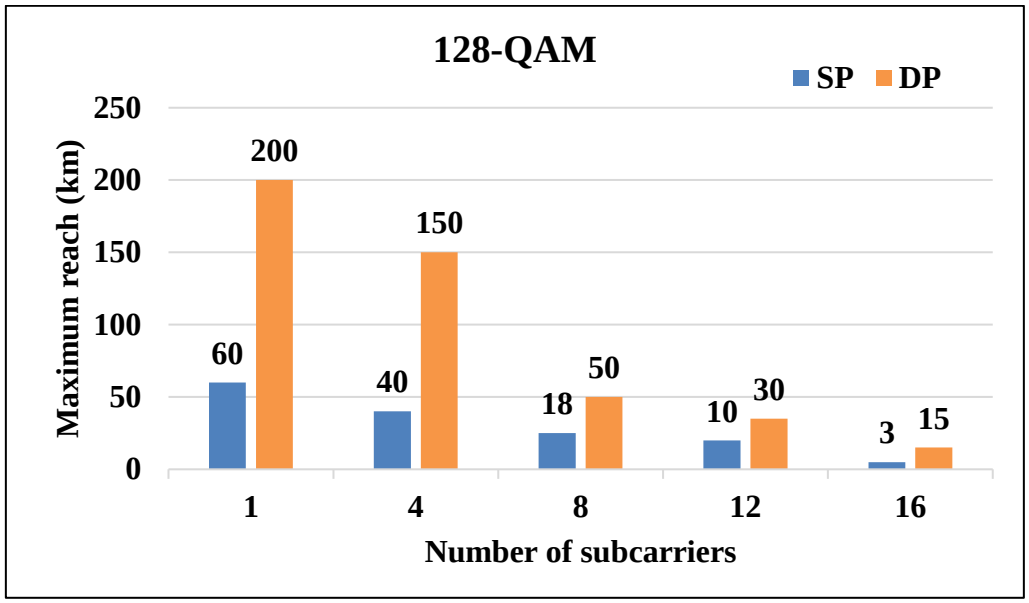

Figure 4-21: Maximum reach of a single-channel O-band P2MP operating in 128-QAM signaling.

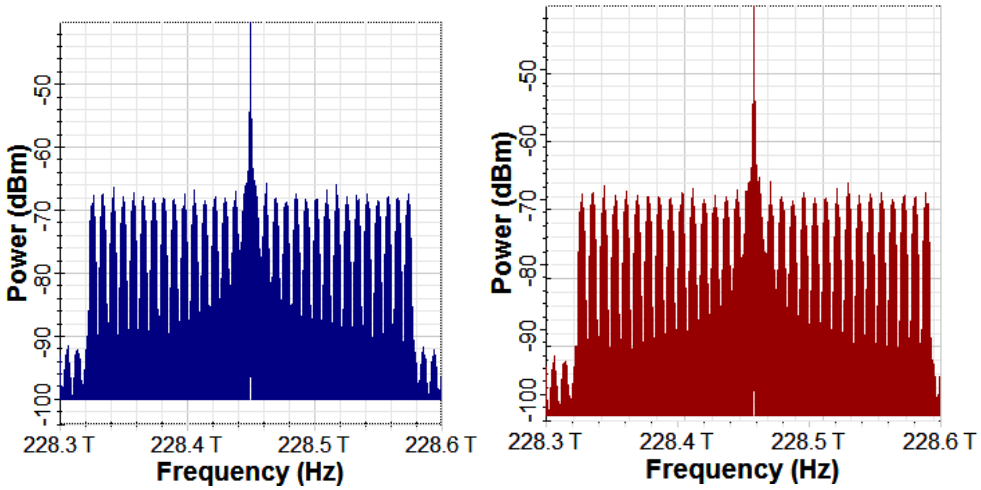

(a) Transmitter signal. (b) Receiver signal.

Figure 4-22: Signals spectra and received constellation diagrams for 128-QAM MSC-based P2MP network formatting.

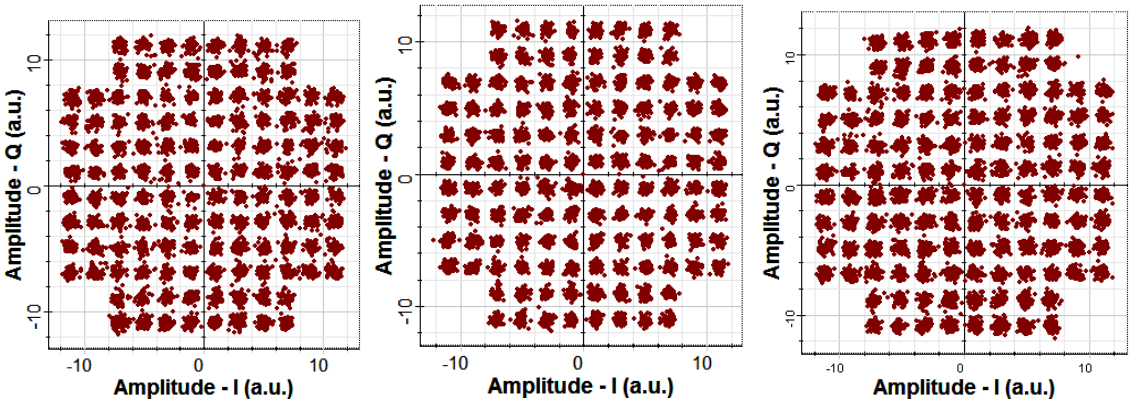

(c) Received constellation diagram for SC1.

(d) Received constellation diagram for SC8.

(e) Received constellation diagram for SC16.

Figure 4-22: (Continued).

4.7 Total Bit Rate-Distance Product (BDP) of C- and O-band P2MP Networks

It is clear that the total bit rate R_{bt} that carried by the P2MP network is increase linearly with the number of WDM channels N_{ch} and number of RF subcarriers per optical channel. This is true when each optical channel is modulated by the same number of RF subcarriers and each subcarrier carriers the same amount of bit rats R_b. Under these conditions, $R_{bt}=N_{sc}N_{ch}R_b$. However, the maximum reach L_{max} of P2MP network does not decreases linearly with increasing N_{sc} and N_{ch} as shown from the simulation results that discussed in this chapter. This leads to an unpredictable behavior describing the dependence of the total bit rate-distance product (BDP) on the number of the WDM channels and number of RF subcarriers per each optical channel. The parameter BDP is a figure-of-merit (FOM) usually used to evaluate the transmission performance of optical network. In this section, the parameter BDP is estimated for different P2MP network

parameter using the relation BDP = $(N_{sc}N_{ch}R_b)L_{max}$. The results are listed in Table 4.5 and 4.6 for C- and O-band networks, respectively. The results are presented for different values of N_{sc} and N_{ch}, and for various modulation formats assuming SP and DP architectures operating with R_b=25Gbps. From the results that introduces in these two tables, one can deduce the maximum BDP obtained when modulation format and polarization type of the architecture are fixed as shown in Table 4-7 and Fig. 4-23. By reviewing these results the following facts can be highlights

i. The DP architectures offer high maximum BDP compared with SP counterpart and this effect is more pronounce in O-band operation. For example, the 16-QAM C-band P2MP network offer 9/6.5=138.5% enhancement in BDP_{max} when the SP architecture is replaced by DP counterpart. This is to be compared with O-band operation where the enhancement archives 80/14 = 571.4%.

ii. The O-band network offers high BDP_{max} compared with C-band network and this is true for any modulation format and polarization architecture. For example, the SP 16-QAM network has BDP_{max} = 6.5 and 14.0 Tbps.km for C- and O-band operation, respectively. These values are to be compared with 9.0 and 80.0 Tbps.km, respectively for DP 16-QAM networks.

Table 4-5: Maximum reach and total bitrate-distance product (BDP) for C-band P2MP network.
(a) Single-polarization network.

Modulation	Number of WDM channels	Number of subcarriers per channel	Maximum reach (km)	BDP (Tbps.km)
16-QAM	1	4	65	6.5
		8	20	4.0
		12	8	2.4
		16	4	1.6
	4	4	60	6.0
		8	10	2.0
	8	4	40	4.0
		8	10	2.0
	16	4	28	2.8
64-QAM	1	4	52	5.2
		8	18	3.6
		12	8	2.4
		16	3	1.2
	4	4	50	5.0
		8	12	2.4
	8	4	35	3.5
		8	8	1.6
	16	4	25	2.5

Table 4-5: (Continued).
(b) Dual-polarization network.

Modulation	Number of WDM channels	Number of subcarriers per channel	Maximum reach (km)	BDP (Tbps.km)
16-QAM	1	4	88	8.8
		8	45	9.0
		12	20	6.0
		16	12	4.8
	4	4	87	8.7
		8	35	7.0
	8	4	85	8.5
		8	20	4.0
	16	4	70	7.0
64-QAM	1	4	56	5.6
		8	25	5.0
		12	10	3.0
		16	4	1.6
	4	4	55	5.5
		8	25	5.0
	8	4	48	4.8
		8	12	2.4
	16	4	35	3.5

Table 4-6: Maximum reach and total bitrate-distance product (BDP) for O-band P2MP network.
(a) Single-polarization network.

Modulation	Number of WDM channels	Number of subcarriers per channel	Maximum reach (km)	BDP (Tbps.km)
16-QAM	1	4	140	14.0
		8	30	6.0
		12	18	5.4
		16	7	2.8
	4	4	105	10.5
		8	18	3.6
	8	4	60	6.0
		8	10	2.0
	16	4	40	4.0
64-QAM	1	4	100	10.0
		8	20	4.0
		12	13	3.9
		16	5	2.0
	4	4	100	10.0
		8	25	5.0
	8	4	11	1.1
		8	10	2.0
128-QAM	1	4	40	4.0
		8	18	3.6
		12	10	3.0
		16	3	1.2

Table 4-6: (Continued).
(b) Dual-polarization network.

Modulation	Number of WDM channels	Number of subcarriers per channel	Maximum reach (km)	BDP (Tbps.km)
16-QAM	1	4	800	80.0
		8	300	60.0
		12	35	10.5
		16	25	10.0
	4	4	300	30.0
		8	70	14.0
	8	4	240	2.4
		8	40	8.0
	16	4	100	10.0
64-QAM	1	4	400	10.0
		8	120	2.4
		12	32	9.6
		16	25	10.0
	4	4	200	20.0
		8	50	10.0
	8	4	12	1.2
		8	11	1.1
128-QAM	1	4	200	20.0
		8	50	10.0
		12	30	9.0
		16	15	6.0

Table 4-7: Dependence of maximum BDP of P2MP network on modulation format and polarization architecture.

(a) C-band network.

Modulation format	Network	Maximum BDP	
		Values (Tbps.km)	Network parameter
16-QAM	SP	6.5	N_{ch} = 1 Nsc = 4
	DP	9.0	N_{ch} = 1 Nsc = 8
64-QAM	SP	5.2	N_{ch} = 1 Nsc = 4
	DP	5.6	N_{ch} = 1 Nsc = 4

(b) O-band network.

Modulation format	Network	Maximum BDP	
		Values (Tbps.km)	Network parameter
16-QAM	SP	14	N_{ch} = 1 Nsc = 4
	DP	80.0	N_{ch} = 1 Nsc = 4
64-QAM	SP	10.0	N_{ch} = 4 Nsc = 4
	DP	20.0	N_{ch} = 4 Nsc = 4
128-QAM	SP	4.0	N_{ch} = 1 Nsc = 4
	DP	20.0	N_{ch} = 1 Nsc = 4

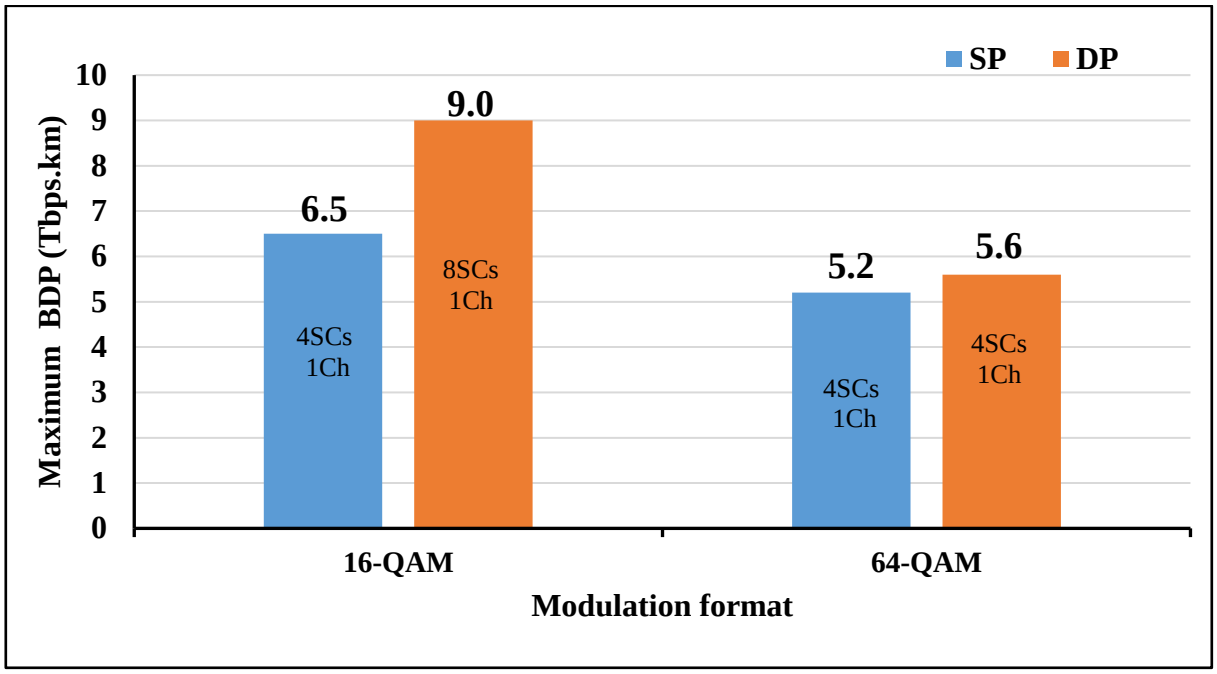

(a)

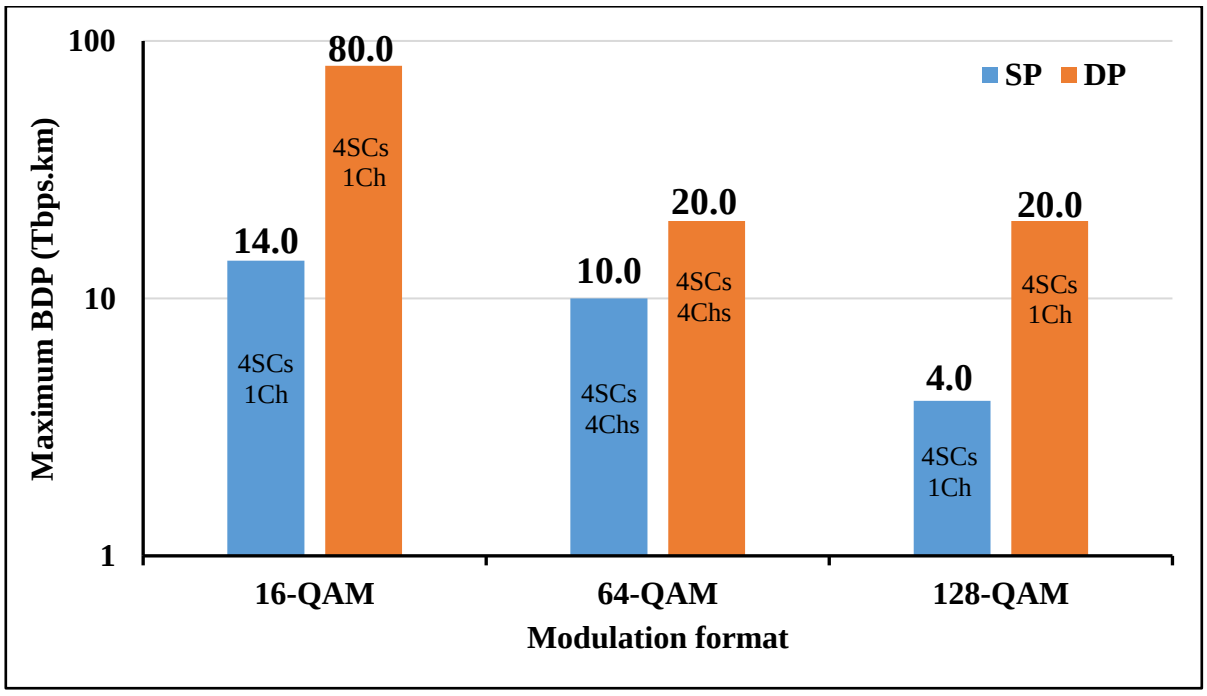

(b)

Figure. 4-23: Variation of maximum bit rate-distance product (BDP_{max}) with modulation format and type of polarization. (a) C-band network. (b) O-band network.

4.8 Comparison with Related Work

Table 4-8 compares the transmission performance of optical network reported in some recent related works with those obtained after simulation them using the methodology adopted in this thesis. The optical networks covered by this comparison are related to a single-optical channel C-band P2P and P2MP operation with 25 Gbps per subcarrier. It is worth to mention here, that the related work uses coherent-detection scheme and supported by experimental results while the results obtained in this thesis are obtained using simulation based on direct-detection scheme.

Table 4-8: Comparison with related work.

Reference	Network parameters			Transmission distance	
	Modulation format	**Number of subcarriers**	**Polarization architecture**	**Reference**	**This work**
Zhang et al. [25] 2020 *	Q-PSK	4	DP	**50 km**	**85 km** (SP: 60 km)
Welch et al. [16] 2021	16-QAM	16	SP	**35 km** (25 km+10 km)	**4 km** (DP: 12 km)
Napoli et al. [27] 2022	16-QAM	4	SP	**55 km** (35 km+20 km)	**70 km** 60 km+5 km (DP: 82 km+5 km)

It is worth to mension that the DP-QPSK of Ref. [25] is also simulated in this work and the result are given in Fig. 4.24.

The results in Table 4-8 reflect the following findings

i. When $N_{sc} = 4$, the DD networks offer a maximum reach longer than the transmission distance used to implement the coherent-detection counterpart. For example, the DP QPSK and SP 16-QAM networks have been

demonstrated over 50 and 35 km, respectively, using coherent-detection scheme. These are to be compared with L_{max} = 85 and 65 km, respectively, when these networks are simulated using DD scheme.

ii. When N_{sc} = 16, the DD network cannot support the transmission distance covered by the implemented coherent-detection counterpart. This network has been demonstrated over 35 km assuming SP 16-QAM while the simulated DD counterpart offers L_{max} = 4 and 12 km for SP and DP version, respectively. Further simulation reveals that L_{max} = 20 and 40 km when the P2MP network is designed with N_{sc} = 8 and using SP and DP architectures, respectively. These values are to be compared with 8 and 20 km for SP and DP, respectively, when N_{sc} increases to 1.

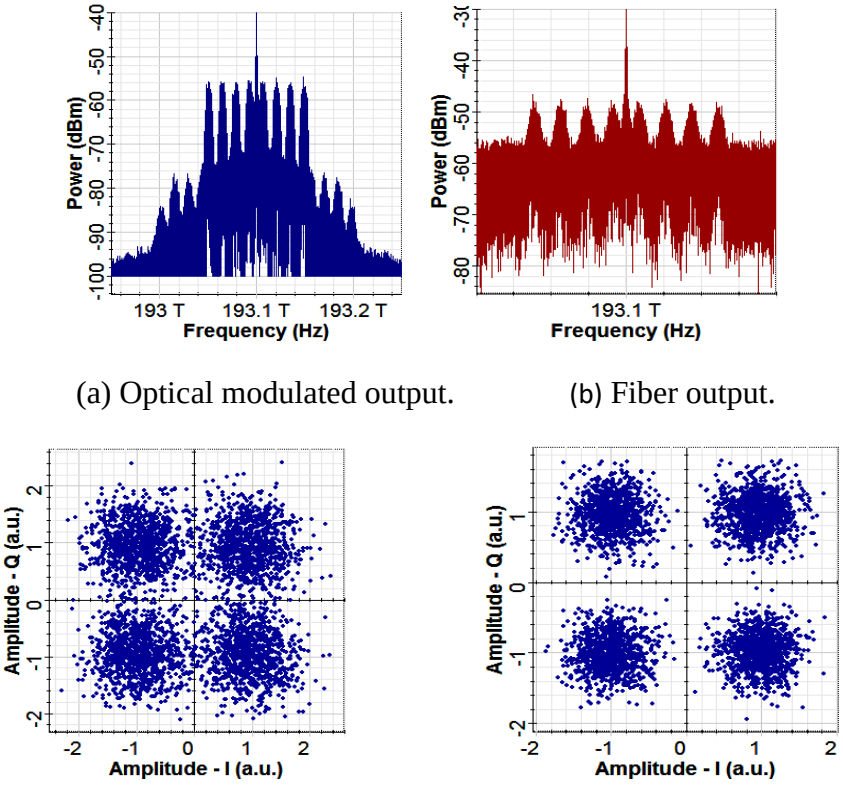

(a) Optical modulated output. (b) Fiber output.

(c) Received constellation diagram for SC2 (d) Received constellation diagram for SC4

Figure 4-24: Simulation results of direct-detection DP-QPSK networks.

CHAPTER FIVE
Conclusions and Suggestions for Future Work

5.1 Conclusions

The transmission performance of IM/DD P2P and P2MP optical networks has been investigated to support 5G and beyond services. These networks have been simulated using MSC/WDM technique and using 4, 8, and 16 SCs with 4, 8, and 16 WDM channels. Results have been reported for both C- and O- band operation. The modulation formats that are used in C-band networks are 16- and 64-QAM, and in O-band networks the modulation formats are 16-, 64-, 128-QAM. The transmission distance for all networks have been recorded in the thesis by using Optisystem ver.15 software simulation. The main conclusions drawn from this work are

i. The maximum reach of optical route in C-band P2MP network is enhanced by using DCF and receiver-side DSP for GVD compensating as illustrated in Fig. 4.1.
ii. The dual-polarization version of P2MP network offers longer route maximum reach (almost double) compared with single-polarization version. This is true for both C- and O-band operation.
iii. Both C- and O-band P2MP networks can be operated without using optical amplification but some time large laser power is required to support the maximum reach of the optically amplified network.
iv. The O-band P2MP network supports longer maximum reach compared with C-band counterpart. For example, 16-SC 16-QAM network has L_{max}=4 and 7 km, for C- and O-band SP network, respectively. These are to be compared with 12 and 25 km, for C- and O-band DP networks, respectively.

v. The DP architectures offer high maximum BDP compared with SP counterpart and this effect is more pronounced in O-band operation. For example, in C-band 16-QAM and N_{sc} = 16, BDP_{max} = 1.6 and 4.8 Tbps.km for SP and DP, respectively. While, in O-band network, BDP_{max} = 2.8 and 10 Tbps.km for SP and DP, respectively.

vi. The O-band network offers higher BDP_{max} compared with C-band network and this is valid for any modulation format and polarization architecture.

For example, O-band 16-QAM network has BDP_{max} of 6.0 and 60.0 Tbps.km for SP and DP, respectively. In addition, the 64-QAM network offers BDP_{max} of 4.0 and 2.4 Tbps.km for SP and DP, respectively. In contrast, in C-band 16-QAM network offer BDP_{max} 4.0 and 9.0 Tbps.km are recoded for SP and DP, respectively. When 64-QAM signaling is used in the C band, BDP_{max} of 3.6 and 5.0 are obtaind for SP and DP, respectively.

5.2 Suggestions for Future Work

The following issues may be addressed in the future as a continuation of the investigation reported in this thesis

(i) Studying the performance of the designed architectures based on bi-direction operation.

(ii) Using other digital modulation formats to support P2MP operation such as orthogonal frequency division multiplexing (OFDM). In this case, the used subcarriers are divided into groups with each group serves one user.

(iii) Investigating the performance of the proposed P2MP architectures when the subcarriers carry different bit rates and different modulation format.

REFERENCES

[1] **X. Liu,** "Enabling optical network technologies for 5G and beyond", J. Light. Technol., vol. 40, no. 2, pp. 358–367, 2022, doi: 10.1109/JLT.2021.3099726.

[2] **E. Hong, I. Lee, B. Shim, Y. Ko, S. Kim, S. Pack, K. Lee, S. Kim, J. Kim, Y. Shin, Y. Kim, and H. Jung,** "6G R&D vision: requirements and candidate technologies", J. Commun. Networks, vol. 24, no. 2, pp. 232–245, 2022, doi: 10.23919/jcn.2022.000015.

[3] **G. Li, J. Deng, S. Xin, and X. Huang,** "A radio over fiber system compatible with 3G/4G/5G for full spectrum access and handover with multi-scenarios", J. Light. Technol., vol. 39, no. 24, pp. 7885–7893, 2021, doi: 10.1109/JLT.2021.3065568.

[4] **C. Ranaweera, J. Kua, I. Dias, E. Wong, C. Lim, and A. Nirmalathas,** "4G to 6G: Disruptions and drivers for optical access", J. Opt. Commun. Netw., vol. 14, no. 2, pp. A143–A153, 2022, doi: 10.1364/JOCN.440798.

[5] **M. Chowdhury, M. Shahjalal, S. Ahmed, and Y. Jang,** "6G Wireless communication systems: applications, requirements, technologies, challenges, and research directions", IEEE Open J. Commun. Soc., vol. 1, pp. 957–975, 2020, doi: 10.1109/ojcoms.2020.3010270.

[6] **S. Noor, P. Assimakopoulos , and N. Gomes**," Flexible subcarrier multiplexing system with analog transport and digital processing for 5g (and beyond) fronthaul", J. Light. Technol, vol. 37, no. 14, pp. 3689-3700, 2019.

[7] **P. Pavon-Marino, N. Skorin-Kapov, M. Bueno-Delgado, J. Back, and A. Napoli,** "On the benefits of point-to-multipoint coherent optics for multilayer capacity planning in ring networks with varying traffic profiles", J. Opt. Commun. Netw, vol. 14, no. 5, pp. B30–B44, 2022, doi: 10.1364/JOCN.448123.

[8] **Y. Fan, M. Fu, X. Liu, Y. Xu, L. Yi, W. Hu, and Q. Zhuge,** "Low-cost asymmetric point-to-multipoint coherent architecture for access networks", Optical Fiber Communication Conference 2022 (OFC 2022), Paper no. Th3E.6, pp. 6–8, 2022.

[9] **N. Skorin-Kapov, F. Muro, M. Delgado, and P. Marino,** "Point-to-Multipoint coherent optics for re-thinking the optical transport: case study in 5G optical metro networks", 25th Int. Conf. Opt. Netw. Des. Model. ONDM 2021, pp. 1–4, 2021, doi: 10.23919/ONDM51796.2021.9492393.

[10] **D. Che , Y. Matsui , R. Schatz , R. Rodes, F. Khan, M. Kwakernaak, and T. Sudo** "200-Gb/s Direct modulation of a 50-GHz Class Laser With Advanced Digital Modulations", J. Light. Technol., vol. 39, no. 3, 2021 doi.org/10.1109/JLT.2020.3043374.

[11] **T. Nakajima, M. Onga, Y. Sekino, A. Nakanishi, N. Sasada, S. Hayakawa, S. Hamada, and K. Naoe** "106-Gb/s PAM4 operation of directly modulated DFB lasers from 25 to 70^{o}C for transmission over 2-km SMF in the CWDM range", Opt. InfoBase Conf., vol. 40, no. 6, pp. 1815–1820, 2021, doi: 10.1364/ofc.2021.tu1d.4.

[12] **X. Li, M. O'Sullivan, Z. Xing, M. Mousa-Pasandi, and D. Plant,** "Asymmetric self-coherent detection based on mach-zehnder interferometers", J. Light. Technol., vol. 40, no. 7, pp. 2023–2032, 2022, doi: 10.1109/JLT.2021.3135000..

[13] **H. Ren, M. Fu, X. Zeng, Z. Zhai, Y. Fan, Q. Liu, L. Yi, W. Hu, and Q. Zhuge,** "Joint power optimization of PTMP coherent architecture for improving link budget in downlink transmission", 2020 Asia Commun. Photonics Conf. ACP 2020 and Int. Conf. Inf. Photonics Opt. Commun. (IPOC 2020), no. 2, pp. 2020–2022, 2020, doi: 10.1364/acpc.2020.m4a.316.

[14] **J. Back, P. Wright, J. Ambrose, A. Chase, M. Jary, F. Masoud, N. Sugden, G. Wardrop, A. Napoli, J. Pedro, M. Iqbal, A. Lord , D. Welch,** "CAPEX savings enabled by point-to-multipoint coherent pluggable optics using digital subcarrier multiplexing in metro aggregation networks", 2020 Eur. Conf. Opt. Commun. ECOC 2020, no. 1, pp. 6–9, 2020, doi: 10.1109/ECOC48923.2020.9333233.

[15] **M. Hosseini, J. Pedro, N. Costa, A. Napoli, J. Prilepsky, and S. Turitsyn,** "Optimized physical design of metro aggregation networks using point to multipoint transceivers", Optical Fiber Communication Conference 2022 (OFC 2022), Paper no. W3F.2, pp. 3–5, 2022.

[16] **D. Welch, A. Napoli , J. Back , W. Sande, J. Pedro, F. Masoud, C. Fludger, T. Duthel , H. Sun, S. Hand , T. Chiang, A. Chase, A. Mathur, T. A.Eriksson , M. Plantare, M. Olson, S. Voll, and K. Wu,** "Point-to-Multipoint optical networks using coherent digital subcarriers", J. Light. Technol., vol. 39, no. 16, pp. 5232–5247, 2021,

doi: 10.1109/JLT.2021.3097163.

[17] **D. Welch, A. Napoli, J. Back, N. Swenson, W. Sande, J. Pedro, F. Masoud, A. Chase, C. Fludger, H. Sun, T. Chiang, A. Mathur, K. Wu,** "Digital subcarriers: a universal technology for next generation optical networks", Optical Fiber Communication Conference 2022 (OFC 2022), Paper no. Tu3H.1, pp. 3–5, 2022.

[18] **B. Hamza, W. Saad, I. Shayea , N. Ahmad, N. Mohamed, D. Nandi, and G. Gholampour**, "Performance enhancement of SCM/WDM-ROF-XGPoN system for bidirectional transmission with square root module", IEEE Access, vol. 9, pp. 49487–49503, 2021, doi: 10.1109/ACCESS.2021.3065285.

[19] **A. Ali, H. Alhamdane, and B. Hassen,** "Design analysis and performance evaluation of the WDM integration with CO-OFDM system for radio over fiber system", Indones. J. Electr. Eng. Comput. Sci., vol. 15, no. 2, pp. 870–878, 2019, doi: 10.11591/ijeecs.v15.i2.pp870-878.

[20] **S. Kumar, S. Sharma, and S. Dahiya,** "WDM-Based 160 Gbps radio over fiber system with the application of dispersion compensation fiber and fiber bragg grating", Front. Phys., vol. 9, pp. 1-3, May 2021, doi: 10.3389/fphy.2021.691387.

[21] **C. Lim and A. Nirmalathas,** "Radio-Over-Fiber technology: present and future", J. Light. Technol., vol. 39, no. 4, pp. 881–888, 2021, doi: 10.1109/JLT.2020.3024916.

[22] **J. He, J. Lee, S. Kandeepan, and K. Wang,** "Machine learning techniques in radio-over-fiber systems and networks", Photonics, vol. 7, no. 4, pp. 1–31, 2020, doi: 10.3390/photonics7040105.

[23] **H. Wang, J. Zhou , J. Wei, D. Guo, Y. Feng, W. Liu, C. Yu, D. Wang , and Z. Li,** "Multi-Rate nyquist-SCM for C-band 100 Gbit/s signal over 50 km dispersion-uncompensated link", J. Light. Technol., vol. 40, no. 7, pp. 1930–1936, 2022, doi: 10.1109/JLT.2021.3131603.

[24] **D, Kraus, A. Awadalla, A. Karar, H. Sun,** "Designe consideration for a digital subcarrier coherent optical modem", Optical Fiber Communication Conference 2017 (OFC 2017), pp. 6–8, 2017.

[25] **J. Zhang, Z. Jia, H. Zhang, M. Xu, J. Zhu, and L. Campos,** "Rate-flexible single-wavelength TFDM 100G coherent PON based on digital subcarrier multiplexing technology", Opt. InfoBase Conf., vol. Part F174-, pp. 2020–2022, 2020, doi: 10.1364/OFC-2020-W1E.5.

[26] **M. Neves, A. Carena, A. Nespola, P. Monteiro, and F. Guiomar,** "Joint carrier-phase estimation for digital subcarrier multiplexing systems with symbol-rate optimization", J. Light. Technol., vol. 39, no. 20, pp. 6403–6412, 2021, doi: 10.1109/JLT.2021.3104523.

[27] **A. Napole, J. Back, N. Swenson, W. Sande, J. Pedro, F. Masoud, A. Chase, C. Fludger, H. Sun, T. Chiang, A. Mathur, K. Wu,** "Enabling router bypass and saving cost using point-to-multipoint transceivers for traffic aggregation", Optical Fiber Communication Conference 2022 (OFC 2022), Paper no. W3F.5, pp. 4–6, 2022.

[28] **Z. Zhou.** "Multipoint-to-point data aggregation using a single receiver and frequency-multiplexed intensity-modulated ONUs", Optical Fiber Communication Conference 2022 (OFC 2022), no. Tu2G.4, pp. 4–6, 2022.

[29] **P. Torres-Ferrera, H. Wang, V. Ferrero**, "100Gbps/λ PON downstream O and C band alternatives using direct-detection and linear-impairment equalization", Journal of Optical Communications and Networking, pp. A111–A123, 2021.

[30] **G. Agrawal,** "Fiberoptic communication systems", Fifth edition, John Wiley, 2021.

[31] **I. Djordjevic,** "Advanced optical and wireless communications systems", Springer International Publishing , 2018.

[32] **L. Binh,** "Optical modulation: advanced techniques and applications in transmission systems and networks", Taylor & Francis Group, 2017.

[33] **L. Binh,** "Advanced digital communications", Taylor & Francis Group, second edition, 2015.

[34] **G. Agrawal**, "Nonlinear fiber optics", Academic Press is an imprint of Elsevier, 2019.

[35] **M. Ferreira** "Optical signal processing in highly nonlinear fibers", Taylor & Francis Group, 2020.

[36] **N. Suzuki, H. Miura, K. Mochizuki, and K. Matsuda,** "Simplified digital coherent-based beyond-100G optical access systems for B5G/6G ", J. Opt. Commun. Netw., vol. 14, no. 1, pp. A1–A10, 2022, doi:

10.1364/JOCN.438884.

[37] **K. Kikuchi,** "Fundamentals of coherent optical fiber communications', J. Light. Technol., vol. 34, no. 1, pp. 157–179, 2016, doi: 10.1109/JLT.2015.2463719.

[38] **R. Borkowski, Y. Lefevre, A. Mahadevan, D. Veen, M. Straub, R. Kaptur, B. Czerwinski, B. Cornaglia, V. Houtsma, W. Coomans, R. Bonk, and J. Maes,** "FLCS-PON an opportunistic 100 Gbit/s flexible PON prototype with probabilistic shaping and soft-input FEC: operator trial and ODN case studies", Journal of Optical Communications and Networking, C82 Vol. 14, No. 6, pp. C82-C91, 2022.

[39] **D. Datta,** "Optical networks", Oxford University Press, 2021

[40] **O. Strobel,** "Optical and microwave technologies for telecommunication networks', Jhon Wiley, 2016.

[41] **P. Torres-Ferrera , G. Rizzelli , H. Wang , V. Ferrero, and R. Gaudino,** "Experimental demonstration of 100 gbps/λ c-band direct-detection downstream pon using non-linear and cd compensation with 29 db + opl over 0 km–100 km', J. Light. Technol. vol. 40, no. 2, 2022

[42] **J. Segarra, V. Sales, V. Polo, J. Tabares, and J. Prat,** "Flexible coherent UDWDM-PON with dynamic user allocation based on limited-tunability lasers", J. Opt. Commun. Netw, vol. 12, no. 9, pp. D27–D35, 2020, doi: 10.1364/JOCN.391023.

[43] **N. Suzuki, H. Miura, K. Matsuda, R. Matsumoto, and K. Motoshima,** "100 Gb/s to 1 Tb/s Based coherent passive optical network technology", J.

Light. Technol., vol. 36, no. 8, pp. 1485–1491, 2018, doi: 10.1109/JLT.2017.2785341.

[44] **PPC Broadband,** "The complete guide to fiber to the premises deployment options for the network operator-option for the network operator", 2020.

[45] **T. Tochino, K. Nishimoto, K. Asaka, J. Kani, and J. Terada,** "Redesigned TDM-PON system architecture based on point-to-point ethernet transmission and software processing with general-purpose hardware", J. Light. Technol., vol. 39, no. 2, pp. 448–457, 2021, doi: 10.1109/JLT.2020.3

شكر وتقدير

اللهم لك الحمد حمداً أبلغ به رضاك وأودي به شكرك وأستوجب به المزيد من فضلك

وانا أضع يدي على اللمسات الأخيرة في كتابة رسالتي هذه أرى من الوفاء أن أتقدم بجزيل الشكر والامتنان الى أستاذي المربي الفاضل الاستاذ الدكتور رعد سامي فياض لما بذله من جهد متواصل ونصح وتوجيه مستمر من بداية مرحلة البحث وحتى اتمام هذه الرسالة. ومن الواجب والعرفان أن أتقدم بشكري وتقديري لعميد كلية الهندسة ورئيس قسم هندسة الحاسوب وجميع اعضاء الهيئة التدريسية في قسم هندسة الحاسوب المحترمين لما قدموه من توجيهات سديدة واراء أغنت البحث.

كما واتقدم بالشكر الى من دفعني الى العلم وبه ازداد أفتخاراً قدوتي ومثلي الأعلى والدي العزيز, ولوالدتي التي بوجودها اكسبتني قوة و بثت في روحي الامل وزرعت في نفسي الثقة عند كل خطوة.

ثم اتوجه بالشكر الى اخواني واخواتي لما قدموه من دعم وتشجيع طيلة فترة دراستي.

والشكرموصول الى كل زملائي وزميلاتي وكل من قدم النصح والمساعدة وكان معي سندا وعون خلال انجاز هذا البحث.

الخلاصة

يدعم الجيل الخامس (5G) وما بعده شبكات الهاتف المحمول عددًا متزايدًا من المستخدمين مع زيادة معدل البت لكل مستخدم. يشجع الباحثين على اقتراح هندسة تعدد إرسال حوامل فرعية رقمية متماسكة من نقطة إلى عدة نقاط (P2MP) لتقليل تكلفة شبكة النقل الضوئية وتعقيدها ، لا سيما في سيناريو التجميع. ومع ذلك ، فإن جهاز الاستقبال البصري المتماسك أكثر تكلفة ويمكن الوصول إليه بعيدًا مقارنةً بنظيره للكشف المباشر (DD) بسبب استخدام الليزر المحلي المتزامن. تكمن المشكلة الرئيسية التي تواجه الباحثين في هذا المجال في كيفية إعادة تصميم شبكات P2MP الضوئية باستخدام مفاصل منخفض التعقيد وعالي المرونة. تقترح هذه الرسالة استخدام تقنية تعديل الشدة / الكشف المباشر (IM / DD) لحل المشكلة.

تم تصميم شبكات P2MP المختلفة باستخدام شكل موجي رقمي متعدد الموجات الحاملة (MSC) مدمج في شدة ليزر الموجة المستمرة (CW) بجانب مخطط الكشف المباشر. يغطي التصميم تشغيل النطاقين C و O باستخدام قناة بصرية واحدة ثم يمتد إلى هندسة تعدد الإرسال بتقسيم الطول الموجي (WDM). علاوة على ذلك ، يتم الإبلاغ عن كل من الإصدارات أحادية الاستقطاب ومزدوجة الاستقطاب (SP و DP) لكل نوع من أنواع الشبكات. تسمح معماريات DP بمضاعفة معدل البتات المرسل مقارنةً بنظيرتها SP. تم إنشاء البنى المذكورة أعلاه في بيئة Optisystem ومحاكاة لمعلمات الشبكة المختلفة. من بين هذه المعلمات عدد قنوات MSC Nsc وعدد قنوات WDM وتنسيقات مختلفة لتشكيل اتساع التربيع (QAM) M. بافتراض 25 جيجابت في الثانية لكل معدل بيانات ناقل فرعي. مقاييس الأداء الرئيسية هي الحد الأقصى للوصول إلى المسار Lmax ومنتج مسافة معدل البت (BDP). تشير نتائج المحاكاة إلى أن شبكات DD يمكن أن تحل محل النظير المتماسك عندما تكون Nsc 4. بالإضافة إلى ذلك ، توفر شبكات O-band P2MP قيمًا عالية للوصول الأقصى BDP مقارنة بنظيراتها في النطاق C.

وزارة التعليم العالي والبحث والعلمي
جامعة النهــرين / كلية الهندسـة

تصميم معماريات كفؤة لشبكة ضوئية نقطة–الى–متعددة النقاط لدعم خدمات الجيل الخامس وما بعده

رسالة مقدمة

الى كلية الهندسة في جامعة النهرين

وهي جزء من متطلبات نيل درجة ماجستير علوم

في

هندسة الحاسوب

من قبل

علي سعدي عبد

(بكالوريوس علوم في هندسة الحاسوب2016 م)

صفر 1444هـ

ايلول 2022م